Characterization of Zinc Oxide, Sulfide and Oxysulfide Thin Films Grown By Spatial Atomic Layer Deposition

Ismo T. S. Heikkinen

School of Science

Thesis submitted for examination for the degree of Master of Science in Technology.

Espoo 19.7.2016

Thesis supervisor:

Prof. Hele Savin

Thesis advisor:

M. Sc. Ville Malinen

Aalto University
School of Science

AALTO UNIVERSITY
SCHOOL OF SCIENCE

ABSTRACT OF THE
MASTER'S THESIS

Author: Ismo T. S. Heikkinen

Title: Characterization of Zinc Oxide, Sulfide and Oxysulfide Thin Films Grown By Spatial Atomic Layer Deposition

Date: 19.7.2016 Language: English Number of pages: 9+70

Department of Micro- and Nanosciences

Professorship: Micro- and Nanoelectronics

Supervisor: Prof. Hele Savin

Advisor: M. Sc. Ville Malinen

In this thesis Spatial Atomic Layer Deposition (SALD) of ZnO, ZnS and Zn(O,S) thin films using a pilot SALD reactor was studied. The films were grown on Si wafers and glass substrates using common ALD precursors DEZ, DI H_2O and H_2S at process temperatures ranging from 110 to 150 °C. The industrial applicability of SALD was investigated by studying the effect of increased substrate velocity on the film growth. This led to higher deposition rates but shortened precursor residence times. Also processing in elevated process pressures was studied to gain further understanding on the phenomena which affect SALD processing in atmospheric pressures.

The growth rate, uniformity, optical properties and elemental compositions of the deposited films were studied. The employed SALD tool was confirmed to function in the ALD mode, and good quality films were deposited at all studied process temperatures, substrate velocities and process pressures. However, all process parameters significantly affected film growth and their properties, and further studies are required to optimize the deposition processes. The employed SALD tool SCS 1000 was designed to coat large-area rigid substrates. The application of SALD in the industrial-scale coating of CIGS solar cells, large metal sheets and glass substrates with oxide and sulfide thin films could be realized using similar equipment.

The results presented in this thesis provide an important reference on the development of zinc-containing films deposited by SALD, and this thesis is the first published report on the SALD processing of zinc sulfide.

Keywords: Spatial Atomic Layer Deposition, Thin Films, ZnO, ZnS, Zn(O,S), CIGS Photovoltaics, Industrial-Scale Processing

AALTO-YLIOPISTO
PERUSTIETEIDEN KORKEAKOULU

DIPLOMITYÖN
TIIVISTELMÄ

Tekijä: Ismo T. S. Heikkinen

Työn nimi: Spatiaalisella atomikerroskasvatuksella valmistettujen sinkkioksidi-, -sulfidi ja -oksisulfidiohutkalvojen karakterisointi

Päivämäärä: 19.7.2016 Kieli: Englanti Sivumäärä: 9+70

Mikro- ja nanotieteiden laitos

Professuuri: Mikro- ja nanoelektroniikka

Työn valvoja: Prof. Hele Savin

Työn ohjaaja: FM Ville Malinen

Tässä diplomityössä tutkittiin spatiaalisella atomikerroskasvatuksella (SALD) valmistettujen ZnO-, ZnS- ja Zn(O,S)-ohutkalvojen kasvatusprosesseja sekä ominaisuuksia. Kalvot valmistettiin pilottireaktorilla Si- ja lasisubstraattien päälle käyttämällä lähtöaineina dietyylisinkkiä, ionivaihdettua vettä sekä rikkivetyä, jotka ovat hyvin tunnettuja ALD-kemikaaleja. Kasvatuslämpötilat olivat 110-150°C. SALD-menetelmän soveltuvuutta teolliseen prosessointiin tarkasteltiin kasvattamalla reaktorin linjanopeutta, mikä kasvatti pinnoitusnopeutta mutta lyhensi prekursorin altistusaikaa, ja tutkimalla näin kasvatettujen kalvojen ominaisuuksia. Lisäksi prosessipainetta kasvattamalla tutkittiin ilmiöitä, jotka vaikuttavat oksidi- ja sulfidikalvojen SALD-prosessointiin ilmanpaineessa.

Kasvatettuja kalvoja tutkittiin tarkastelemalla niiden kasvunopeutta, tasaisuutta, optisia ominaisuuksia sekä alkuainekoostumusta. SALD-reaktorin varmistettiin toimivan ALD-moodissa, ja hyvälaatuisia kalvoja onnistuttiin valmistamaan kaikissa prosessilämpötiloissa ja -paineissa sekä kaikilla substraatin liikenopeuksilla. Prosessiparametrit kuitenkin vaikuttivat kasvatettujen kalvojen ominaisuuksiin ja laatuun, joten kasvatusprosessien optimointi vaatii lisätutkimusta.

Tässä työssä käytetty SALD-laite, SCS 1000, on suunniteltu jäykkien, pinta-alaltaan suurten substraattien pinnoittamiseen. Samanlaista laitetta voitaisiin soveltaa teollisesti esimerkiksi CIGS-aurinkokennojen, metallilevyjen ja suurten lasisubstraattien pinnoittamiseen erilaisilla oksidi- ja sulfidipinnoitteilla.

Tämä työ on ensimmäinen julkaisu sinkkisulfidin kasvatuksesta SALD-menetelmällä.

Avainsanat: Spatiaalinen atomikerroskasvatus, ohutkalvot, ZnO, ZnS, Zn(O,S), CIGS-aurinkokennot, teollisen mittakaavan prosessointi

Preface

The experimental work conducted in this thesis has been performed at Beneq Oy between January and May 2016. I thank my supervisor Prof. Hele Savin for being an inspiration in science and for all her support in helping me to graduate. I also wholeheartedly thank my advisor M. Sc. Ville Malinen for all the guidance I've received in diving into the depths of spatial ALD but also for all the laughs we've had at work. M. Sc. (Tech.) Sauli Virtanen, the wizard of Vantaa, is thanked for the memorable process development moments in our spatial ALD chamber and M. Sc. (Tech.) Pekka J. Soininen is thanked for all his endless knowledge of ALD. I am very grateful to my superiors M. Sc. (Tech.) Kari Härkönen and Dr. Tommi Vainio for providing me with the possibility to learn the secrets of ALD with some of the most experienced ALD specialists in the world, and to M. Sc. (Tech.) Pekka Soininen and Dr. Mikko Söderlund for their visionary work. Working at Beneq Oy in a warm and welcoming community has been a privilege. Warm thanks to Paula for all the discussions and coffee breaks and to Heli and Kalle for the peer-reviewed emotional support. Also cheers to Juhani for the sumppi moments. The Development Services team at Beneq Oy has been an inspirational community, and I have been proud to be its member during the last months.

My experiences as a research assistant at Aalto University in the group of Optics and Photonics and my visit to the Spectroscopy of Materials group at the University of Montreal are warmly reminisced. I wholeheartedly thank Dr. Jaana Vapaavuori for advising me through the years, but I am also very grateful for her friendship and endless support. I thank Prof. Arri Priimägi as well as Prof. Christian Pellerin for guiding me into the world of scientific research.

The years as a student at Aalto University in Otaniemi were filled with joy, laughter, stress, tough exams, amazing parties, tears, great discussions on life in general, and the most memorable moments of challenging myself to do something that the past me had only dreamt of. I am very happy that I've met and made friends with amazingly clever, warm and lovable people. Thank you for all the support and great conversations during all my years: Santtu, Jari, Eero, Tuuli, Sanja, Ilmi and all my friends at Maltain Ritarikunta and Rissittely.

I thank the Guild of Physics for welcoming me into the Teekkari community and helping me to get to know myself and other fantastic geeks. All the memories from the years as a Freshman Captain and later as a Freshman Major will always be in my heart. Warm thanks to UltrabRaati12: Jori, Milja, Riina, Joonas K., Joonas V., Mariia, Katri, Heikki and my flatmates Antti and Saila. Big thank you and all my hugs to FTMK13: LeMikko, Joni, Norri, Anton, Ilmari, Simo, Sofia, Joonas, Ella, Meri, Milla, Eppu, Nicolas, KeeMikko, Olli and Antti. Teidän majurinanne oleminen oli aivan parasta. I thank all my friends at AYY, Teekkarijaosto and Polytechnical Students' Museum for all the arranged events and memorable moments, especially Jari for the emotional support in the form of crazy workouts during the writing of this thesis. I also thank my friend and mentor M. A. (Hist.) Tiina Metso for all the adventures as well as for great discussions on student history. Big thanks to the Lyseo posse as well.

Being a part of Fyysikkospeksi as an Nth year student was something I will surely remember for the rest of my life – huge thanks to all the Mindblowers, especially to my fellow actors. My brothers and sisters at SiMiLi: thank you for all the support and the ever-so-necessary distraction during these years, luckily we have many more to come. In retrospect, I am rather surprised that all the student activities did not get in the way of successfully finishing my studies. Oh well, it has been a fun ride, and if given the chance, I would do it all again.

Lämpimät kiitokset veljilleni Ilpolle ja Ilarille sekä vanhemmilleni Merjalle ja Tuomolle huimasta määrästä tukea tämän matkan varrella. Suurimmat seikkailuni tosin ovat luultavasti vasta edessä – kohta kai on aika kasvaa aikuiseksi.

Eikä syyttä.

Helsingissä 19.7.2016

Ismo T. S. Heikkinen

"Suomessa kaikki hullut saavat valkoisen lakin.
Kaheleimmat heistä merkitään tupsulla."

Contents

Symbols and Abbreviations

Symbols

α	Absorption coefficient
λ	Wavelength of light
τ	Residence time
ν	Photon frequency
D	Deposition rate
d	Thickness of the deposited film
$d_{\%}$	Non-uniformity of the deposited film
E	Energy
E_g	Optical band gap of a material
h	Planck constant
n	Refractive index
P	Process pressure
$R(\lambda)$	Reflectance spectrum
T	Process temperature
$T(\lambda)$	Transmittance spectrum
x	H_2S concentration in the carrier gas flow

Abbreviations

ALD	Atomic Layer Deposition
ALE	Atomic Layer Epitaxy
Al_2O_3	Aluminum Oxide
Al:ZnO	Aluminum-doped Zinc Oxide
CdS	Cadmium Sulfide
CIGS	Copper Indium Gallium Selenide
CBD	Chemical Bath Deposition
CVD	Chemical Vapor Deposition
DEZ	Diethyl Zinc
DI H_2O	Deionized Water
EDX	Energy-Dispersive X-Ray spectroscopy
EL	Electroluminescent
GPC	Growth Per ALD Cycle
H_2S	Hydrogen Sulfide
HAR	High Aspect Ratio
LC_{50}	Median Lethal Concentration, 50 %
MFC	Mass Flow Controller
ML	Molecular Layering
MPI	Multiple Pulsed Vapor-phase Infiltration
N_2	Nitrogen gas
OLED	Organic Light-Emitting Diode
PECVD	Plasma-Enhanced Chemical Vapor Deposition
PVD	Physical Vapor Deposition
R2R	Roll-To-Roll
SALD	Spatial Atomic Layer Deposition
SCS 1000	Sheet Coating System 1000
SEM	Scanning Electron Microscope
Si	Silicon
TCO	Transparent Conductive Oxide
TFT	Thin Film Transistor
TiO_2	Titanium Dioxide
TMA	Trimethyl Aluminum
TOF-ERDA	Time-Of-Flight Elastic Recoil Detection Analysis
UV-Vis	Ultraviolet and Visible Light
WVTR	Water Vapor Transmission Rate
XPS	X-Ray Photoelectron Spectroscopy
XRD	X-Ray Diffraction analysis
XRF	X-Ray Fluorescence analysis
XRR	X-Ray Reflectivity analysis
$Zn(O,S)_x$	Zinc Oxysulfide deposited with varying H_2S concentration
ZnO	Zinc Oxide
ZnS	Zinc Sulfide

1 Introduction

Atomic Layer Deposition (ALD) is a thin film deposition method with emerging applications in various fields, such as depositing dielectric materials for electronics [1–3], applying optical coatings for complicated geometries [4, 5], fabricating various nanodevices and structures [6], and depositing functional layers on photovoltaic cells and for other energy applications [7–9]. The quality and conformality of ALD thin films often surpasses the properties of films fabricated with other methods, such as CVD or sputtering, but so far the wide-scale industrial application of ALD has been limited [10]. The deposition rate of conventional ALD processing has been "vertically challenged" *i.e.* film deposition rate measured in nm/min has been mere fractions of that obtained with other coating methods due to reasons explained in the later sections. The development of Spatial ALD (SALD) concepts has targeted this issue and broadened the reach of ALD by offering fast, large-area processing while maintaining high film quality [11, 12].

The development of ALD dates back a few decades, and there have been different perceptions regarding where ALD was first invented. A technique called Molecular Layering (ML), which closely resembled modern ALD, was developed in the Soviet Union in the 1960s, but a more credited origin is the introduction of so-called Atomic Layer Epitaxy (ALE) by Dr. Tuomo Suntola for the fabrication of electroluminescent displays in Finland in the early 1970s [13–15]. The first ALD-related patent, which described the structure of an ALD reactor, was issued by Suntola *et al.* in 1974 [16]. The use of the term 'epitaxy' was later changed to 'deposition', as films grown by ALD were rarely epitaxial in relation to the substrate. Since its invention, ALD has been used to deposit a wide range of materials, such as oxides, sulfides, nitrides, and metals, as well as nanolaminates, mixed structures, and hybrid inorganic-organic thin films [10, 17].

The first application of ALD was the fabrication of manganese-doped zinc sulfide (Mn:ZnS) thin films from zinc chloride ($ZnCl_2$) and hydrogen sulfide (H_2S) as light-emitting layers in electroluminescent (EL) displays. EL display production was started by Lohja Oy in Lohja, Finland in 1983, but the production was moved to Olarinluoma, Espoo in 1984. The Olarinluoma EL factory was later run by Planar Inc., and Beneq Oy continued the EL production from 2012 onwards. The Olarinluoma factory still remains one of the world's largest ALD laboratories and production facilities. [13–15]

Spatial ALD is a new development direction but definitely not a new invention: even early ALD-related patents described reaction chambers which operated in the same way as modern SALD reactors [16, 18]. However, recent industrial needs for pinhole-free thin films and extreme uniformity combined with fast processing have sparked an interest in the development and application of SALD. Spatial ALD is a very promising method to push the speed of ALD cycling up even further, towards the time scales of the gas-surface chemical reactions [19].

Zinc oxide (ZnO) is an interesting, versatile material with great potential for applications as a transparent conductive oxide (TCO), and its fabrication via ALD has been studied extensively in the recent years [20–33]. Zinc sulfide (ZnS) is a feasible

material for optical applications due to its high refractive index and high growth rate in the ALD mode [34–39]. Dense and conformal zinc oxysulfide (Zn(O,S)) thin films can be fabricated with ALD, and they show great potential for replacing toxic cadmium sulfide (CdS) as buffer layers in copper indium gallium diselenide photovoltaics [40–48]. Depositing all these materials in the SALD mode in continuous operation would reduce processing costs and make their use industrially feasible, which would allow for their use in mass-produced applications.

In this thesis the processing and properties of zinc oxide (ZnO), zinc sulfide (ZnS) and zinc oxysulfide (Zn(O,S)) thin films deposited by a prototype sheet-to-sheet SALD tool SCS 1000 were studied. The main goals of the thesis were to 1) perform a literature survey on the development of SALD processing, 2) prove that ALD-like films can be deposited with the SCS 1000, 3) perform preliminary process tests for zinc oxide and sulfide thin films at various process temperatures, 4) successfully deposit zinc oxide and sulfide thin films with faster line speeds and in elevated pressures, and 5) define a roadmap for further process development.

The properties of the films were investigated by single-wavelength ellipsometry, UV-Vis spectrophotometry, and energy dispersive X-ray (EDX) spectroscopy. The effect of the process parameters on the properties of the deposited materials were investigated by studying the growth rate, refractive index, optical band gap and elemental composition of the films.

First, it was investigated whether the studied processes functioned in the ALD mode. The industrial scalability of the processes was tested by increasing the line speed of the deposition process. In the near future an ambitious target is to apply SALD processing in atmospheric pressures, which would simplify process integration and reduce costs as the need for a vacuum chamber would be eliminated [12,49]. To aim for this target we studied whether SALD processing of ZnO, ZnS and Zn(O,S) with this tool was feasible in higher pressures.

The design, construction and testing of the SALD tool was carried out by Beneq Oy within the PLIANT (Process Line Implementation for Applied Surface Nanotechnologies) project, funded by the European Union [50]. The aim of the project was to develop the fabrication of nanostructured surfaces using atmospheric processes with applications in three focus areas: energy storage, solar power generation, and energy efficient airplanes.

The theoretical background of ALD and SALD is discussed and a literature review of the present state of SALD is presented in Chapter 2. An overview of the process tool and sample fabrication is described in Chapter 3, and characterization methods are described in Chapter 4. In Chapter 5 results of the conducted experiments are presented. Conclusions and future interests regarding the research conducted are discussed in Chapter 6.

2 Background

An overall depiction of ALD is presented in this section. The properties of ZnO, ZnS and Zn(O,S) thin films deposited by ALD are discussed, and spatial ALD along with its recent developments and potential applications are reviewed.

2.1 Atomic Layer Deposition (ALD)

Atomic Layer Deposition (ALD) is a thin film deposition technique which is based on sequential exposure of a substrate to process chemicals, commonly referred to as precursors. A substrate is placed in a vacuum chamber in an inert gas flow, and the first precursor reacts with the substrate surface through a self-saturating gas-solid reaction. Afterwards the excess precursor and reaction byproducts are purged from the reactor. After the purging step the second precursor is introduced to the reaction chamber, and the second gas-solid half-reaction at the surface takes place. After this step the residual gases are, again, purged from the reactor, and process is continued from the application of the first precursor. The principle of ALD cycling is presented in Figure 1. [10, 15, 51]

Commonly used inert gases are nitrogen (N_2), which is affordable and suitable for most applications, and argon (Ar), which is used in special reaction conditions [52–55]. The pulsing routine of conventional ALD, the ALD cycle, is presented in Figure 1. Ideally one full ALD cycle produces a monolayer of material, but due to various reasons such as steric hindrances from the ligands of the precursor, not all reaction sites at the surface can be filled with a single cycle [15].

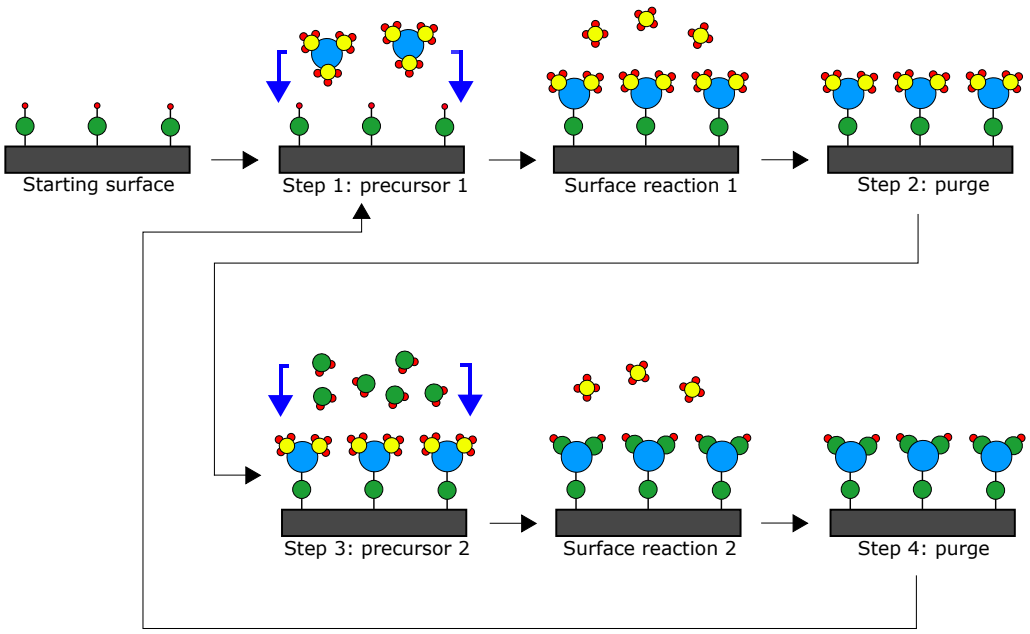

Figure 1: *The ALD cycle consists of four steps: pulsing of the first precursor, first purge step, pulsing of the second precursor, and the second purge step. The sequential pulsing of precursors is characteristic for ALD processing. Adapted from [51].*

This digital application of reactant gases on the substrate is the source of the unique advantages of ALD thin films. The thickness of the deposited film can be controlled in the subnanometer scale only by alternating the number of ALD cycles. Due to the saturating nature of the surface reactions ALD films are highly uniform and conformal, which enables the precise coating of high aspect ratio (HAR) structures and powder materials, such as microchannels and nanoparticles [1,10,56]. Films deposited by ALD are also often pinhole-free, which is a property required in *e.g.* thin film encapsulation applications [57, 58].

ALD has many advantages over other thin film coating methods, but there are also major challenges in the industrial implementation of ALD. The main drawback of ALD is the fact that the purging step between precursor application is often long, from parts of a second up to even tens of minutes. The purging step requires more time to flush the reaction chamber compared to the precursor pulsing, and the purging step is often the limiting factor for the overall time of an ALD process. This means that the growth of ALD thin films is slow measured in nm/s, but this can often be compensated with large batch sizes (nm/m^2) due to the excellent uniformity of ALD [10, 15]. However, many other faster thin film processing methods, such as CVD, have been more feasible and cost-effective for use in industry in the recent years [10,49]. But despite the slowness of the process, many applications have benefited from the high quality and precise thickness control of ALD films. For example, the microelectronics industry has adopted ALD as a means of depositing high-κ gate oxides in transistors [2]. The tunability of ALD films enables the fabrication of optical coatings [4,5] and moisture barrier layers [59–66], and Al_2O_3 films deposited by ALD have been used in the passivation of various types of solar cells [67–70]. ALD is also used in quite exotic applications such as fabricating EL displays and protecting silverware with anti-tarnishing coatings. For example, Beneq Oy manufactures electroluminescent Lumineq® displays [71], in which ALD processing is vital, and has developed the nSILVER® process [72] for protecting silver jewelry from tarnishing. [1]

Many different chemicals can be used as ALD precursors, but often organometallic compounds are used in conjunction with small inorganic molecules, such as water (H_2O), hydrogen sulfide (H_2S) and ozone (O_3) [17]. An ideal example of an ALD process is the sequential pulsing of trimethyl aluminum (TMA) and H_2O, which produces aluminum oxide (Al_2O_3). At suitable process temperatures, up to 300 °C, the half reactions of applying TMA and H_2O are irreversible and saturating, which means that precursors are chemisorbed onto the surface, and that increasing the length of the precursor pulses does not increase the growth rate [10, 15]. This temperature range is called the ALD window, presented in Figure 2.

Below a certain temperature the chemical reactions may lack sufficient activation energy, which is seen as a low GPC value. At low temperatures physisorption of gas molecules on the surface without an actual chemical reaction might also occur, which is a reversible reaction. At too high temperatures the reacted molecules may decompose, which leads to loss of surface species, or the formed chemical bonds

[1] Lumineq® and nSILVER® are registered trademarks of Beneq Oy.

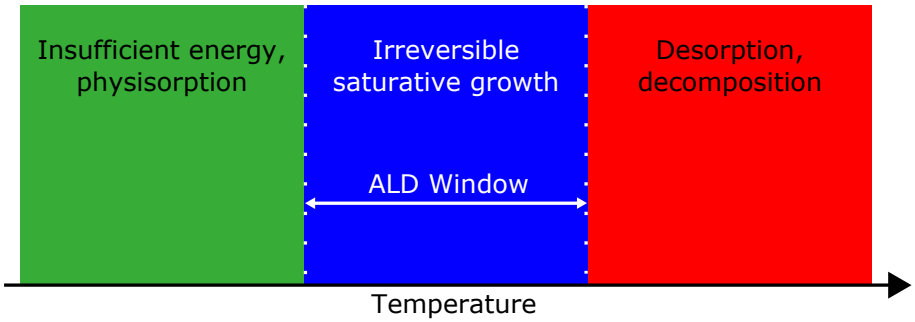

Figure 2: *An ALD window for a specific process is the temperature range in which surface reactions are irreversible and saturating. In reality the growth rate within the window never remains fully constant, but instead it can vary significantly.*

between the surface and the reacted precursor molecules might be broken. [15]

It should be noted that the existence of an ALD window for a specific process is never certain, and that only relatively few processes work in an ideal ALD mode. A common misconception is that the growth rate should be constant in the ALD window. The growth rate can decrease or increase as temperature increases, or there might be sudden discontinuity in an otherwise stable growth rate. It is also possible that the growth rate does not follow a specific trend at all in the ALD window [15]. Finding an ALD process with suitable precursors and an ALD window in a suitable temperature range is vital in applying ALD coatings in industrial use.

2.2 Zinc Oxide, Sulfide and Oxysulfide Thin Films by ALD

In the scope of this thesis, thin zinc-containing films fabricated by fast, large-area spatial ALD were studied. In recent years, ZnO thin films have attracted increasing interest as a potential material in *e.g.* thin film transistors, microelectromechanical systems (MEMS), light-emitting diodes (LEDs), thermoelectric devices, and photovoltaics [20, 21, 24–33]. ZnO is a wide band-gap intrinsic n-type semiconductor material with a direct band gap of 3.37 eV at room temperature [22, 23]. ZnO crystallizes in a polycrystalline hexagonal wurtzite structure. ZnO thin films are highly transparent in the visible spectrum of light and their electrical properties can be easily modified, which means that they are attractive transparent conductive oxide (TCO) materials. Due to the low toxicity, stability, and easy low-cost fabrication of ZnO thin films, they could be used as an alternative for indium tin oxide (ITO). For the industrial-scale deposition of ZnO the most used technology is sputtering, but also chemical vapor deposition (CVD) and plasma-enhaced CVD (PECVD) have been demonstrated to be viable high deposition rate methods. Other methods for the synthesis of ZnO thin films are metal-organic chemical vapor deposition (MOCVD), molecular beam epitaxy (MBE) and pulsed laser deposition (PLD) [26]. The increasing quality demands of microelectronics industry and the need to coat complicated structures have led to an increasing interest for the deposition of ZnO by ALD, which has been studied extensively. In the ALD of ZnO the most used precursors are diethyl zinc (DEZ) and water (H_2O) [17, 34, 73]. A further step for the easily

scalable industrial deposition of high-quality ZnO thin films is the introduction of spatial ALD (SALD) [74].

ZnO can be doped with *e.g.* group III elements B, Al, Ga and In, or with F, a group IV element, to accurately control the charge carrier density. This is vital in optoelectronics and thermoelectric applications. Aluminum-doped zinc oxide (Al:ZnO) has been studied most extensively, as Al-doping offers improved electrical conductivity while maintaining high transparency in the visible spectrum of light [75–78]. Al:ZnO could be used *e.g.* as a front electron in copper indium gallium selenide (CIGS) photovoltaic cells, and it has also been demonstrated as a viable thermoelectric material. ALD processing offers a simple control of layer deposition sequences, which means that the doping of ZnO can be easily and accurately controlled. In addition to ALD, Al- and In-doped ZnO films have also been succesfully deposited by SALD by Illiberi *et al.*, but not on industrially relevant substrate sizes [79–82].

ZnS thin films fabricated by ALD have mainly been used in thin-film electroluminescent display applications and in optical applications [36]. ZnS is a crystalline material which demonstrates cubic zincblende or hexagonal wurtzite structures, depending on the processing temperature and pressure. ZnS is a semiconductor with a direct band gap of 3.65 eV. At low deposition temperatures the cubic crystal structure is dominant. ZnS fabricated by ALD is an interesting material in many ways: it is easy to fabricate from common precursors DEZ and H_2S even at low temperatures, and it has a high refractive index n and growth rate [34–37]. However, sulfur might be a problematic element in components which contain silver, as the formation of dark silver sulfide (AgS) patina is an unwanted process in many applications. Also, the use of highly toxic H_2S might be considered too risky in industrial facilities [38]. Other methods to fabricate ZnS include CVD, chemical bath deposition (CBD), and spray pyrolysis [39].

The deposition of Zn(O,S) by pulsing ALD has been well studied [40–48]. Zn(O,S) is fabricated from the same precursors as ZnO and ZnS by depositing ZnO and ZnS cycles alternatively. For example, 5 ZnO cycles can be followed by 1 ZnS cycle and, therefore, Zn(O,S) can be considered a mixture of ZnO and ZnS. In recent years Zn(O,S) has been proved to be an interesting material as a buffer layer in CIGS photovoltaic cells [9]. The band gap of Zn(O,S) can be modified from 2.6 to 3.8 eV by altering the ratio of O and S in the film, which can be easily done by ALD processing [44, 48, 67]. Other Zn(O,S) deposition methods include chemical bath deposition (CBD), sputtering, spray pyrolysis and molecular beam epitaxy (MBE), but compared to these methods ALD offers the best composition control [44,83]. The most common method in the deposition of Zn(O,S) is CBD, which is the only liquid phase process in the fabrication of CIGS solar cells. Using in-line ALD to deposit buffer layers would be optimal for CIGS processing, as the liquid-phase process step would be eliminated and composition control would be enhanced [84–86]. The ratio of sulfur and oxygen affects the optical and electrical properties of Zn(O,S), and in ALD the ratio can be easily tuned by the number of ZnS cycles [45, 48]. The ALD of Zn(O,S) is often done at relatively low temperatures [48].

2.3 Spatial ALD (SALD)

The main drawback of ALD is that it is a vertically slow process compared to other thin film deposition methods, such as PECVD or sputtering [51]. The length of a purging step in an ALD cycle can be very long at low temperatures, especially in water-based processes due to the high sticking coefficient of the H_2O molecule [87]. Low temperature processing is especially preferred in many industrial applications, such as OLED encapsulation, to lengthen the lifetime of the products by reducing thermal budget of the processing [58]. Low temperature processes also reduce the risk of material interdiffusion in the processed products [10]. To combine the benefits of ALD processing at low temperatures with a high production rate, called throughput, a modification of conventional pulsing ALD, called Spatial ALD (SALD) has been developed [11, 12].

2.3.1 Overview

Spatial ALD is a modification of the conventional pulsing ALD process which facilitates a significant increase in ALD deposition rate, even at low temperatures. In conventional ALD the substrate remains stationary in a reaction chamber, and gases are exchanged in the reactor. In SALD the precursors flow continuously and they are spatially separated by an inert gas purging zone and exhausts to prevent the intermixing of precursors in the gas phase. The substrate is moved between the precursor zones, which replicates the conventional ALD pulsing cycle. [11] The differences of spatial and conventional pulsing ALD are demonstrated in Figure 3. The SALD concept was already invented in the 1970s, and even the first ALD-related patent by Suntola *et al.* described the structure of a reactor which operated in the spatial ALD mode [16]. The concept of SALD did not attract greater interest in 30-40 years, but the need for fast, large-area deposition of ALD-quality thin films sparked the academic interest and industrial development of different SALD concepts.

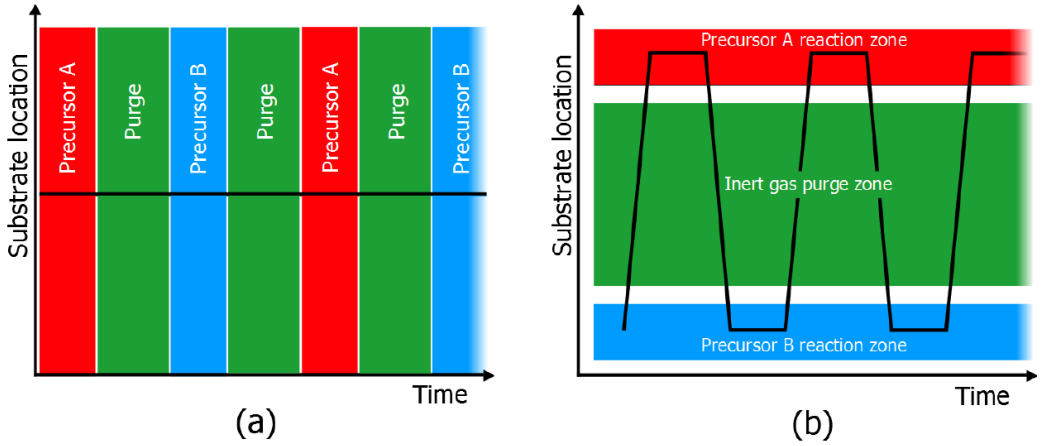

Figure 3: *The differences between conventional and spatial ALD. Figure (a) presents the sequence of conventional ALD, in which the substrate is kept stationary. Figure (b) shows the principle of SALD, in which the substrate is moved between precursor zones that are isolated by inert gas barriers. Adapted from [11].*

In principle an SALD reactor is composed of two main components: a gas distribution system often called the coating head, and a substrate moving system. These components are usually installed inside a vacuum chamber, but the coating area can be isolated from ambient air by effective inert gas zones [88]. The coating head consists of many separate nozzles: precursor nozzles are separated from each other by inert gas zones and exhaust lines, which guarantee that precursors are not mixed with each other in the gas phase. The principle of a coating head structure is presented in Figure 4. Gasses are ejected from the nozzles towards the substrate plate, and the flow through each nozzle is optimized to ensure that the inert gas zones act efficiently as gas shields. It is also important that the exhaust lines have sufficient conductance, so that the excess precursor and reaction products from precursor-surface reactions are ejected before the surface is exposed to the second precursor. When the coating head functions ideally, only the substrate under the nozzles are coated, which means that there is no parasitic growth in reaction chamber walls or the head itself. Coatings fabricated by pulsing ALD usually cover substrates from all sides, and masking is needed if some areas are to be protected from the coating. In SALD there is virtually no growth on the back of the substrate as precursors are injected and ejected on one side of the substrate, which means that SALD is well suited for applications in which one-sided coating of the substrate is beneficial. [11, 12]

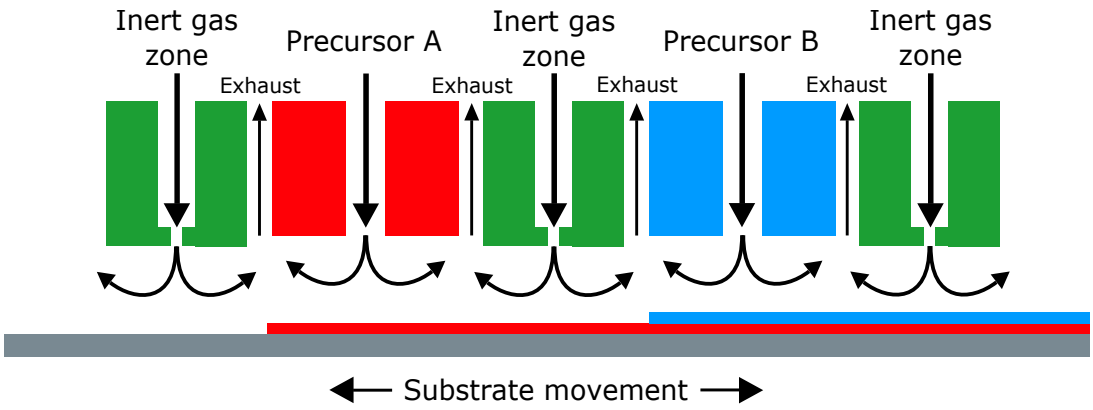

Figure 4: *In spatial ALD precursor flows are kept continuously on, which enables fast in-line processing. Precursor zones are isolated from each other by inert gas zones and exhaust lines. Different areas of the substrate are exposed to the precursors at different times. In the figure the substrate moves from left to right. Adapted from [11].*

Spatial ALD has great potential in extending the range of applying ALD coatings in industrial uses. SALD concept allows the construction of continuous process lines and the implementation of roll-to-roll processing methods. Continuous processing eliminates tool downtime due to heating, cooling, loading, and unloading, which greatly increases the throughput of the process line. Due to the lack of parasitic growth in unwanted areas SALD reactors are, in principle, maintenance-free. Precursor consumption can be optimized in SALD processing, as only the substrate needs to be coated, which further reduces the costs of ALD processing. Using steady continuous flows means that very precise pulsing valves are not needed, which makes

the equipment more reliable and affordable. [11,64,91] SALD technique also reduces the risk of the coating process compared to batch-type pulsing ALD, especially when the coating process is monitored with in-situ characterization methods. With conventional ALD large batch sizes are financially more cost-effective than small ones, as throughput in substrates per time unit can still be very high. However, there is always a possibility of a malfunction in the reactor during the coating process, which means that a notable number of products are scrapped. In SALD substrates are essentially processed one by one, and the process can be immediately stopped if the quality of the coating does not fulfill requirements. In SALD the process speed (the length of the ALD cycle) is not limited by the hydrodynamics of pulsing and purging different gases [19, 87]. SALD can reach deposition rates in the range of nm/s, which is approximately 100 times faster than in pulsing ALD [55]. This is still quite low compared to *e.g.* PECVD, in which the deposition rate can be even tens of nm per second [92], but the superior conformality and uniformity of ALD films can tip the scales in favor of SALD in industrial applications.

Spatial ALD offers fast processing of large area substrates, but it is still quite limited to the coating of planar substrates [12]. This means that SALD cannot replace conventional ALD in all coating applications, but it rather extends the reach of ALD-quality coatings. One of the most important parameters in SALD is the distance of the nozzle to the substrate [88], called the coating head gap, which is almost impossible to control if the substrate does not conform to the surface shape of the relatively large coating head. This shape is usually planar of cylindrical [11]. Due to the requirement for the accurate gap control other process steps should not introduce significant mechanical changes onto the substrate before the SALD step. Controlling the gap is also challenging due to thermal expansion of the moving parts inside the reactor. So far SALD processes have mainly used common precursors, such as TMA, $TiCl_4$, DEZ, and H_2O, which have high vapor pressures [11], but in principle other, more exotic chemistries could be used in the SALD mode too. Expensive precursors could be better utilized in spatial rather than in pulsing mode, as more of the precursor would go where it is needed. However, highly volatile precursors or high temperature sources are needed to ensure that the precursor concentration in the carrier gas remains constant in a continuous flow.

2.3.2 Applications of Spatial ALD

Spatial ALD can be seen as an alternative, high-rate approach to achieving ALD-quality thin films with reduced unit costs. Major applications of SALD include ultra-high barrier coatings in flexible electronics and OLEDs, buffer layers and antireflection coatings for solar cells, polymer sheet and textile functionalization, and barrier coatings for packaging. These applications mainly benefit from roll-to-roll and sheet coating SALD systems, but rotary ALD reactors can also be used for extremely fast processing of optical layers on small-area substrates.

Barrier layers

SALD has great potential in applying gas permeation shields, also called barriers, onto flexible substrates in the roll-to-roll mode or onto rigid substrates in the sheet coating mode. ALD barrier films are dense and pinhole free, which enables them to block atmospheric gases, such as H_2O vapor and O_2, from reaching the shielded components. One of the simplest methods for measuring the barrier performance of coated polymer films is a quantity called the Water Vapor Transmission Rate (WVTR), which measures the permeation of water through the coated polymer in $g/m^2/day$.

Due to the environmental challenges, there is a growing demand for the replacement of synthetic non-biodegradable polymers with more environmentally-friendly, biodegradable materials in food and pharmaceutical packaging. Biodegradable polymers often have low barrier properties, and in order to make these materials commercially viable alternatives to plastics, their properties need to be enhanced to match those of existing packaging solutions [57]. Previously packaging materials have been coated with metallic aluminum deposited by Physical Vapor Deposition (PVD) methods, such as vacuum evaporation. Metallic aluminum is not, however, transparent, and thus interest regarding certain packaging applications has been directed towards metal oxides. The use of ALD Al_2O_3 as a barrier layer for environmentally-friendly packaging materials has been studied extensively [59–63], and the WVTR requirement for the packaging of sensitive products is in the order of 0.1 to 0.01 $g/m^2/day$ [57]. Hirvikorpi *et al.* have shown that a 25 nm thick Al_2O_3 reduced the WVTR of a biodegradable polymer from 64.4 to 1.4 $g/m^2/day$ [60], and large-scale roll-to-roll SALD tools would be ideal for the coating process to aid the adoption of ALD-coated biopolymers.

Also the electronics industry needs gas permeations barriers in many different applications. For example, organic light-emitting diodes (OLEDs) are extremely sensitive to moisture and oxygen, and they lose their luminence quickly if their structure is exposed to ambient air. Glass is an excellent barrier material, but using glass would restrict the OLED products to rigid structures. One of the greatest interests regarding OLEDs is the possibility to manufacture flexible displays, which means using glass would rule out flexible applications. Metal oxide materials are, when the film is thin enough and an organic protection layer is applied, also capable of withstanding stress and bending, rendering Al_2O_3 deposited by ALD a promising material for the OLED industry. In order to make OLEDs and flexible electronics viable products, a WVTR value in the order of 10^{-6} $g/m^2/day$ should be reached with the barrier layer [64,66]. High-quality films deposited by ALD are a good option for reaching these barrier levels, and scaling up the throughput of film production by SALD would reduce the costs of OLED processing significantly [58]. SALD is also attractive for the processing of OLEDs due to the possibility of fast low temperature processing [53]. In conventional ALD of TMA and H_2O, for example, the purging steps are long at process temperatures below 100 °C. This leads to a large heat load for the substrates, as processing takes a long time. The time required to heat the substrate to the process temperature is significant as well in these processes. In

SALD the processing can be done much faster and one substrate at a time, which reduces the risk associated with a coating batch and minimizes the heat damage for each substrate.

Corrosion of metals is a worldwide economical and environmental challenge, as corroded metal components need to be removed from instruments, replaced and disposed of in an environmentally safe way. ALD and especially large-area spatial ALD have applications in protecting metals from corrosion: *e.g.* Al_2O_3 and TiO_2 can be used as protective coatings [52]. Protection of silver jewelry with invisible anti-tarnishing ALD barrier coatings is already in use, as described earlier [72].

Functionalization of fibers and textiles

In addition to using ALD coatings to modify the gas permeation properties of a material also the mechanical, optical and electrical properties of various materials can be tuned by applying ALD thin films on them. For example, Lee *et al.* have demonstrated that the tensile strength of spider silk can be greatly enhanced by incorporating transition metal atoms into the polymer structure [93], and Gregorczyk *et al.* fabricated toughened cellulose with a similar principle [94]. The enhancement of mechanical properties is enabled by metal atoms which can facilitate cross-linking of polymer backbone structure. This was demonstrated in both studies by using common ALD precursors in the Multiple Pulsed Vapor-phase Infiltration (MPI) method, which is very closely related to ALD [93]. Applying this modification principle in *e.g.* the functionalization of textiles in SALD-mode processing could prove to be an interesting industrial application. Also producing nonwoven textiles with ALD-modified electrical or optical properties would enable technologies such as wearable electronics and biosensors [95].

Photovoltaics

A major application field for ALD and SALD is the photovoltaics industry. Al_2O_3 deposited by ALD has been widely used for the rear surface passivation of photovoltaic materials, but also antireflection coatings, buffer layers and transparent conducting layers grown by ALD have applications in photovoltaics [67]. So far slow ALD processing has not been a financially viable method for the solar cell industry, but the introduction of SALD shows great promise in decreasing the cost of high-quality ALD coatings. A viable application for SALD is the deposition of buffer layers, such as Zn(O,S), on CIGS solar cells [41–48].

The structure of a CIGS solar cell is presented in Figure 5. The substrate can be soda-lime glass or a flexible material, and molybdenum (Mo) is used as a back contact. CIGS layer functions as an absorber, in which photons are converted into electron-hole pairs through the photovoltaic effect and are separated from each other. The buffer layer can be made of various n-type semiconductor materials. The front contact is made of Al:ZnO, which is a TCO material, and an intrinsic zinc oxide (i-ZnO) layer protects the buffer layer in the fabrication process. The structure can additionally be capped with an antireflection (AR) coating. [9, 83–86]

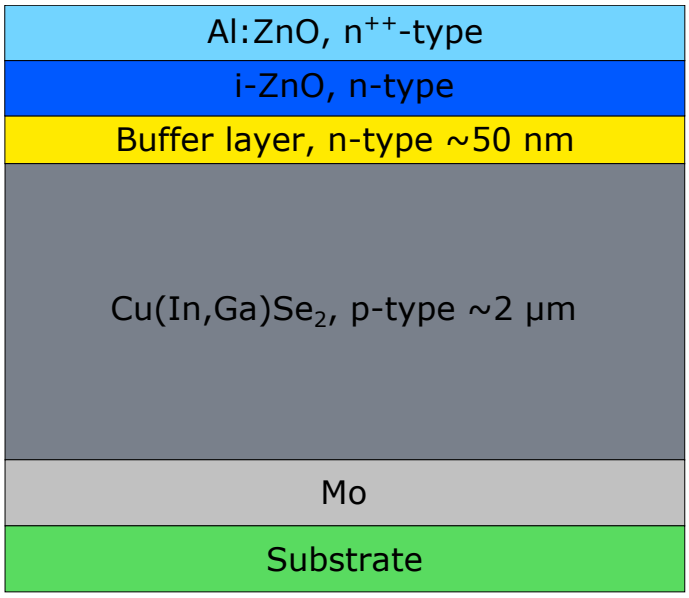

Figure 5: *Schematic of the structure of a CIGS solar cell. Adapted from [9].*

Often cadmium sulfide (CdS) is used as the buffer layer, but it has a low optical band gap of 2.4 eV, which limits light conversion in the UV region of the solar spectrum, as only some of the photons in the blue region of the solar spectrum are collected. Many doped ZnO materials, such as magnesium-doped Mg:ZnO and boron-doped B:ZnO can be used as buffer layers, but Zn(O,S) has emerged as one of the most attractive alternatives due to its facile fabrication and improved efficiency compared to CdS. Zn(O,S) has a high and adjustable band gap and it is significantly less toxic than CdS. [43–48]. CIGS solar cells could be made more efficient and safer and easier to recycle by replacing the cadmium in them. Spatial ALD is the most viable deposition method for the deposition of Zn(O,S) buffer layers, as SALD combines the precise structure control and high quality of ALD films with high deposition rate and fast processing. Roll-to-roll SALD could be used in applying buffer layer coatings on flexible CIGS solar cells.

Spatial ALD is a technique that has enormous potential and many uses in various industrial applications, but so far many SALD tools have been small-scale devices for research use or industrial pilot tools for very specific applications. In the following part we describe different SALD reactor designs.

2.3.3 Development of Spatial ALD Reactors

Despite the fact that the concept of SALD was patented decades ago, SALD processing has started to attract greater interest only in the recent years. T. Suntola and J. Antson described a SALD reactor-like coating device in the first ALD-related patent in 1977 [16]. In a later patent published in 1983 T. Suntola *et al.* described a reactor in which reactive gases were simultaniously inserted into a reaction chamber from inlet and exhaust slits, presented in Figure 6, and these reaction zones were separated by gas diffusion barriers which prevented the intermixing of reactants [18].

The operating principle of many modern SALD coating heads is based on these early patents.

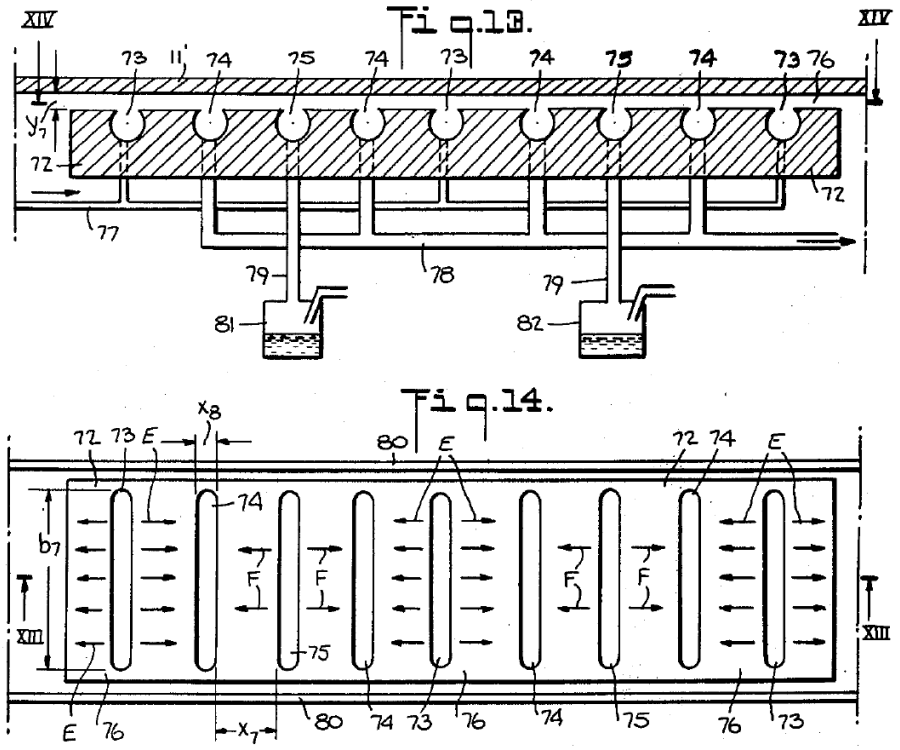

Figure 6: *The original spatial ALD concept patented by T. Suntola et al. in 1983. Reprinted from [18].*

The first peer-reviewed studies that demonstrated the application of SALD were published by Levy *et al.* of Eastman Kodak in 2008 [88]. In the technological solution, presented in Figure 7, the coating head was positioned tens of μm above the substrate. With this concept a line speed of 3 m/min was reached. Their next coating head design, presented in Figure 7b, was based on gas bearings: the sample was positioned face down on a susceptor, and the gas curtain flows supported the sample hydrodynamically at a distance of approximately 30 μm from the coating head. This approach, called close-proximity SALD, had the advantage of simple processing in ambient pressures, as the small gap between the sample and the head provided an efficient gas curtain around the coating area, which isolated the reaction zone from ambient air [11,88]. The device has been used in the study of Al_2O_3, ZnO and Al:ZnO for thin film transistor (TFT) applications, but so far only coating of small-scale samples with dimensions in the order of tens of millimeters have been demonstrated [88–90]. Close-proximity SALD has been realized in many other approaches to spatial and atmospheric deposition, and in addition to Eastman Kodak also ASM International and TNO, both located in the Netherlands, have patented SALD concepts that rely on gas bearings [11].

In close-proximity SALD the precursor zones are very narrow and the gap between the head and the substrate is very small, which means that the systems require

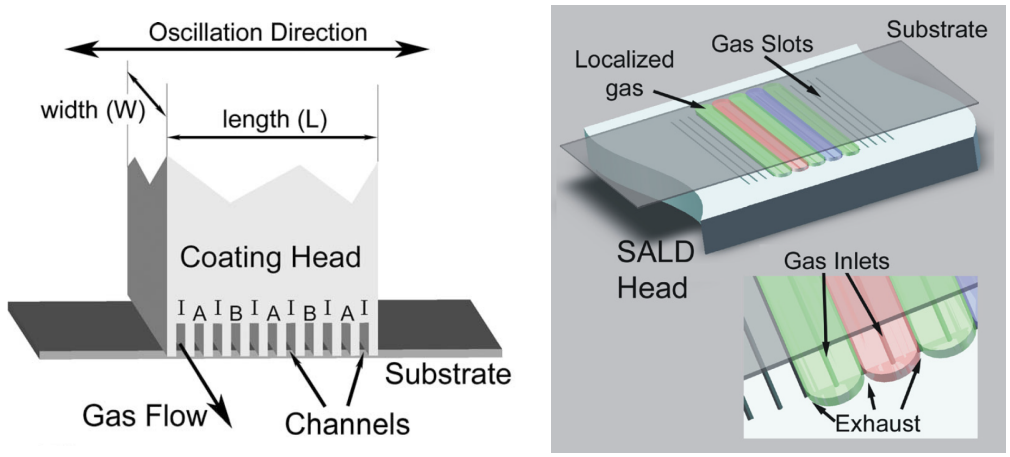

(a) (b)

Figure 7: *Eastman Kodak spatial ALD coating head concepts. (a) Reprinted from [88]. (b) Reprinted from [11].*

extensive optimization and fine-tuning of the process flows. Also, the application of close-proximity SALD is limited to flat substrates. A different approach to spatial ALD is rotary SALD, in which the substrate is placed on a rotating plate and moved under separate precursor zones located in different sectors of a circular area and separated from each other by inert gas barriers [11]. The deposition rate can be controlled by altering the angular frequency of the rotator, enabling high deposition rates of up to nanometers per second. The rotary ALD concept has been proved to function in atmospheric mode by TNO, whose reactor is presented in Figure 8a. Illiberi *et al.* have reported the deposition of Al_2O_3, ZnO, Al:ZnO, Zn(O,S) and even exotic compounds, such as InGaZnO, in atmospheric pressures [74,79,82,96,97]. The deposition of mixed compounds was done by co-injecting two or more different metal or non-metal precursors from the same inlets, and the elemental ratios of the films were controlled by tuning the precursor concentrations in the carrier gas [96, 97].

Another realization of rotary ALD has been built by Lotus Applied Technology, situated in the US. The principle of the Lotus AT Vortex rotary ALD reactor is presented in Figure 8b. The device has been reported to function in medium vacuum conditions, which enabled that the gap between the precursor inlet and the substrates could be made significantly larger than in close-proximity SALD while maintaining gas zone separation. The larger gap allows processing of irregularly shaped substrates, while only planar substrates can be coated with close-proximity SALD. The Vortex reactor relies on the application of plasma, and the processing of TiO_2, SiO_2, Ta_2O_5, HfO_2 and ZrO_2 has been demonstrated [98]. Other industrial suppliers of rotary SALD reactors have emerged as well. For example, the Lotus AT Vortex design has been licensed by Beneq Oy, and Applied Materials in the US has developed their own rotary ALD reactor [99].

Rotary ALD offers an extremely high growth rate for the fast processing of individual samples and small batch sizes, but often only small-area samples can be coated with rotary reactors. Also, continuous in-line operation is often not feasible

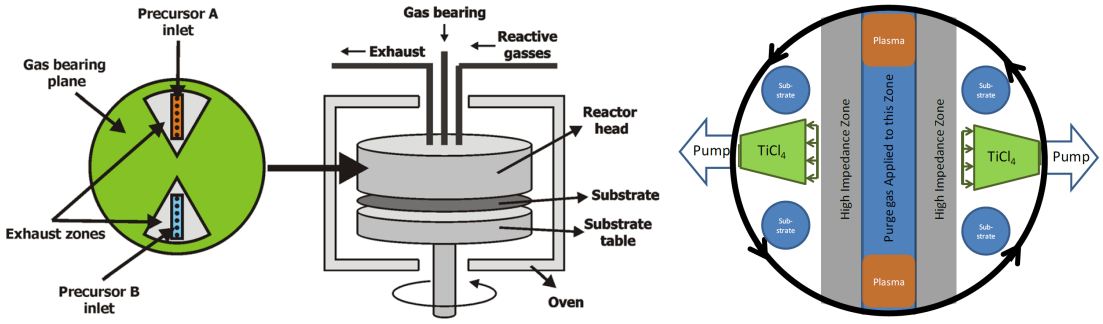

(a) *TNO Atmospheric Rotary SALD reactor [11].* (b) *Lotus AT Vortex [98].*

Figure 8: *Rotary SALD reactor concepts by TNO and Lotus Applied Technology.*

with rotary ALD. In order to coat large area substrates in a continous operation mode, different technological solutions have been presented. Roll-to-roll spatial ALD (R2R SALD) concept aims to coat large area flexible substrates, such as polymer sheets or metal foils, which are unwound from a roll and transported under a SALD coating head. The gap between the flexible substrate and the coating head can be secured to a constant value by applying tension in the substrate. R2R SALD has been studied, for example, by Maydannik *et al.* [64, 100, 101], and many reactor designs have been realized. Beneq Oy has developed the TFS 200R, which is a research-scale tool which has the possibility of coating samples with an area of 300 mm $\times$ 100 mm [11], and WCS 600, a pilot reactor capable of coating 600 mm wide flexible substrates in continuous operation [58, 102]. A schematic of the WCS 600 coating drum is presented in Figure 9c. A different type of R2R SALD tool was developed by TNO in 2012, in which the substrate supported by gas bearings is moved slowly over a rapidly spinning precursor distribution system (Figure 9b) [91]. Lotus AT developed a R2R system, the Transflex Roll to Roll tool presented in Figure 9a, already in 2008 [11], and researchers in Jeju National University in South Korea built a R2R SALD tool for the deposition of gas diffusion barriers on polymer substrates in 2014 [103].

Rearside passivation of solar cells is an application for SALD [55, 104]. To tap into this market, Levitech and SoLayTec, both situated in the Netherlands, have developed fast SALD tools for the passivation of crystalline silicon (c-Si) solar cells. Both companies have employed a double-sided gas bearing system as the susceptor, which enables minimal friction as substrates travel on N_2 beds [105,106]. A schematic of a Levitech SALD reactor is presented in Figure 10a. For these photovoltaics passivation tools throughputs of over 3000 wafers per hour with an Al_2O_3 coating ranging from 5 to 10 nm have been reported. In these in-line SALD tools the film thickness can only be adjusted by changing the hardware, as wafers pass the coating head only once.

However, the use of gas bearings to control the gap between the coating head and the substrate and to facilitate the fast transportation of wafers is difficult when large-area glass or metal substrates need to be coated. In early 2016 Choi *et al.* of Hanyang University and LIG INVENIA Co. Ltd, South Korea, reported of a high-

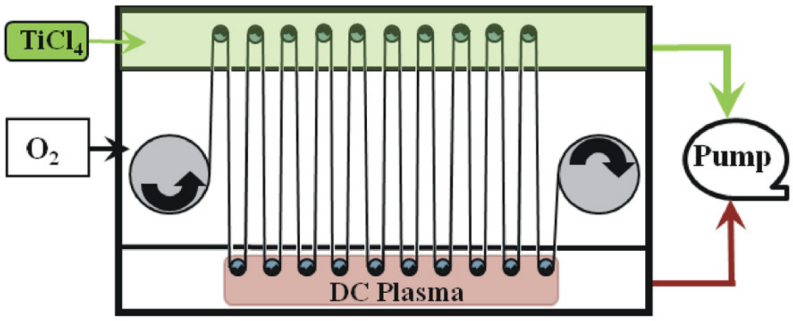

(a) *Lotus AT Transflex [11].*

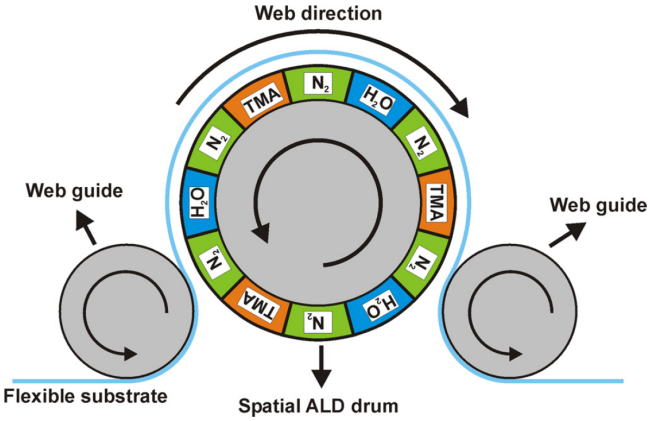

(b) *TNO R2R concept [91].*

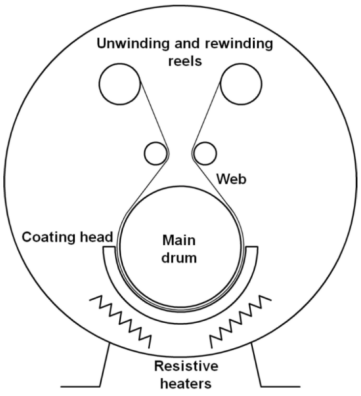

(c) *Beneq Oy WCS 600 [58].*

Figure 9: *Different R2R SALD reactor concepts . Figure (a) presents the Transflex R2R tool by Lotus AT. Figure (b) presents a R2R concept by TNO. In Figure (c) a schematic of the WCS 600 tool be Beneq Oy is presented.*

rate SALD tool which had the possibility to coat glass substrates with an area of 370 mm × 470 mm using an ozone based Al_2O_3 process [53]. The tool is shown in Figure 10b. In their study they reported of a coating speed of 7 nm/min with a substrate moving speed of 48 m/min, and demonstrated the thin films grown with the tool as effective OLED moisture barriers. Process temperatures ranged from 60 to 100°C and the gap between the substrate and the precursor injection systems was in 1-4 mm, up to 100 times higher than the gap in close proximity ALD. These longer distances between the head and the substrate are preferred in many industrial applications, as tool design and maintenance are easier than with micrometer-scale gaps that ought to be constant over a length of a few meters. The study published by Choi and co-workers is the first demonstration of industrial-sized glass coating with SALD. Also Beneq Oy has developed a SALD tool, presented in detail in Chapter 3.1, for the coating of rigid metal and glass substrates.

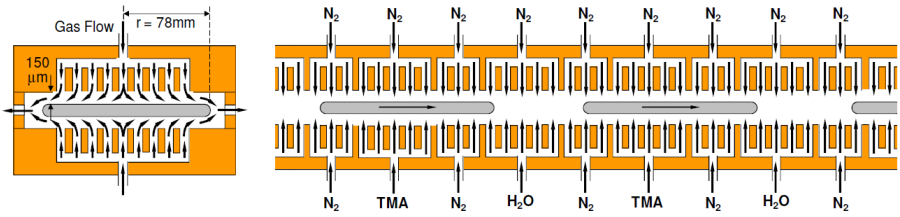

(a) *Levitech SALD concept [105].*

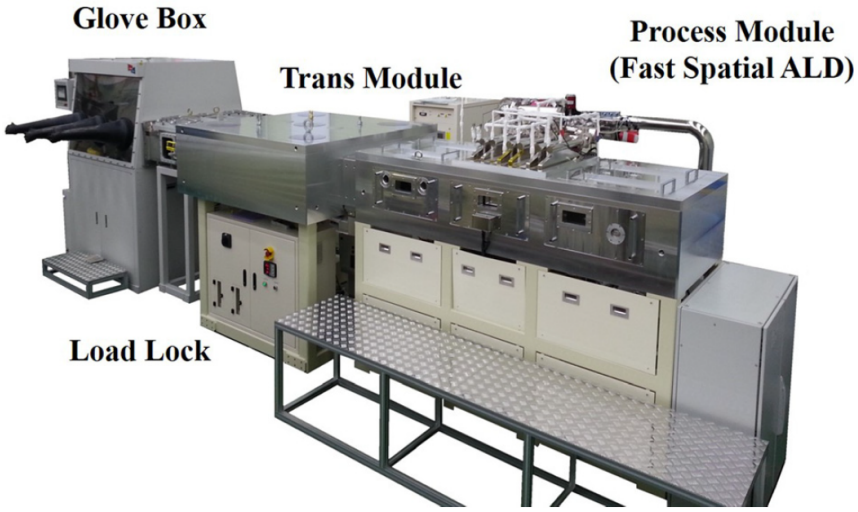

(b) *SALD tool capable of high deposition rates by Hanyang University and LIG INVENIA Co Ltd [53].*

Figure 10: *(a) SALD concept by Levitech Netherlands for the passivation of Si solar cells. The wafers move on gas bearings and are coated with* Al_2O_3*. (b) Large-area SALD tool by Hanyang University and LIG INVENIA Co Ltd designed for the deposition of protective coatings on OLEDs.*

2.3.4 Atmospheric and High Pressure Spatial ALD

An important goal for SALD is to develop concepts which would enable high-speed processing of ultra-high quality thin films and function in normal ambient pressures. Illiberi *et al.* have used the term Atmospheric Spatial ALD to describe SALD devices that do not necessarily need vacuum chambers, but in which the precursors are separated from the ambient air with efficient inert gas curtain flows [11]. Atmospheric processing would provide significant savings in industrial scale, as no vacuum chambers would be needed. Also maintenance would be very simple, as the SALD tool would effectively consist of just the coating head. The concept of atmospheric thin film processing has already been realized with *e.g.* PECVD [92], but the development of atmospheric ALD processing has had various challenges. In atmospheric pressures the uniformity and conformality could be an issue as the flow of precursor molecules towards the surface can be hindered by other molecules. The lack of a vacuum chamber can also expose the substrate to contaminations, which can lead to defects and pinholes in the deposited films.

Despite the challenges that atmospheric processing faces, atmospheric SALD has already been realized for small area substrates. Poodt, Illiberi *et al.* have reported successful atmospheric SALD processing of Al_2O_3 passivation layers and various Zn-containing materials using a research-scale rotary reactor operating in ambient pressures [74, 79, 82, 87, 96, 97, 107]. Scaling up the deposition area for atmospheric SALD is a significant research interest [19], and it is close to its industrial breakthrough.

ALD processing in higher pressures might have other advantages too, due to the fact that precursor partial pressure and concentration is a parameter that can affect the ALD process. The physical properties such as conductivity and elemental distributions as well as the growth rate of the deposited thin films can be drastically altered by different precursor partial pressures [74, 108]. Precursor partial pressure is also important in the coating of HAR structures, which contain long and narrow channels. Usually long precursor pulses in pulsing ALD are employed to facilitate the coating of HAR structures, but the higher the precursor partial pressure, the shorter the time that is needed for the precursor molecule to diffuse into these structures [109].

In this thesis the term High Pressure ALD is defined as ALD performed in significantly higher pressures than conventional pulsing ALD, in which pressure is usually in the mbar range. Elevated process pressure, achieved by tuning the flow balance in the reaction chamber, can be used to increase the absolute precursor pressure. Absolute precursor pressure can also be increased by increasing the carrier gas flows while keeping the flow through the exhaust line constant. In SALD the control of the precursor partial pressure in a continous flow can be achieved, for example, by heating the precursor source, which leads to higher vapor pressure and dose. Through the increase of precursor partial and absolute pressures SALD could thus be used in the coating of HAR structures embedded on planar substrates.

One of the major interests for the scope of this thesis was to study the feasibility of high pressure processing with an SALD reactor as a roadmap towards understanding the mechanisms of gas-surface reactions in atmospheric spatial ALD. Ultimately, the work conducted in this thesis aims for the application of SALD in the fast deposition of ZnO for many TCO applications, the deposition of Zn(O,S) buffer layers with easily controllable sulfur content on CIGS solar cells, as well as the deposition of ZnS for optical structures in elevated pressures.

3 Materials and Experiments

In this section a technical overview of the SALD tool SCS 1000 is given and substrates, precursors and sample fabrication methods are described. Also the process conditions and different precursor application configurations are presented in detail.

3.1 SCS 1000 Spatial ALD Tool

The Sheet Coating System SCS 1000 is a pilot spatial ALD tool designed by Beneq Oy for the fast and large-area coating of rigid substrates, such as glass and metal plates. A photograph of the installed tool and a schematic describing the position of the coating head and the substrate carrier are presented in Figure 11. The maximum line speed of the SCS 1000 tool is 30 m/min, with a deposition rate in the order or 12 nm/min for an Al_2O_3 process on an area of 400 mm × 500 mm.

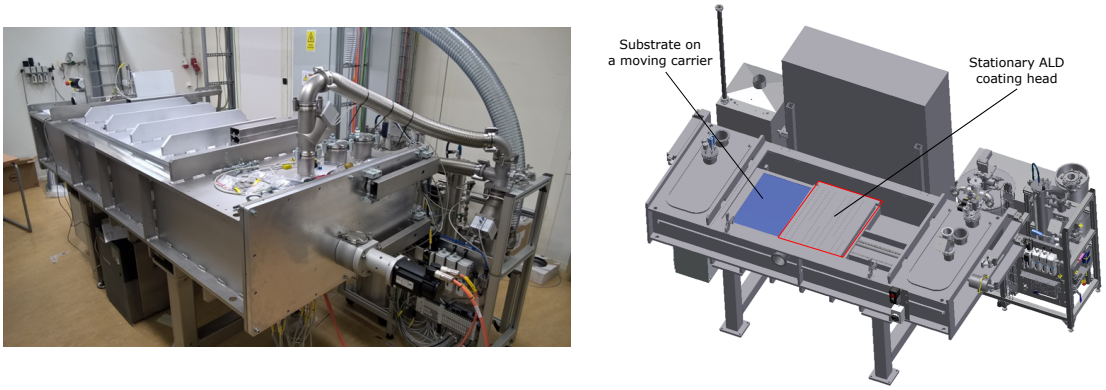

Figure 11: *Left: SCS 1000 sheet-to-sheet spatial ALD tool installed at the Beneq production facilities in Espoo. Right: model image of SCS 1000 without the vacuum chamber door. ©Beneq Oy 2016.*

The coating mechanism of SCS 1000 is based on the principle described in Figure 4. Gases are ejected from the separate nozzles towards a rigid substrate, which is positioned on a moving substrate carrier. The gap between the coating head and the substrate is fixed to approximately 1 mm. Precursor zones are separated from each other by N_2 curtain flows, and the whole coating area is isolated from the vacuum chamber with similar N_2 barriers. The substrate plate is moved back and forth under the coating head, which replicates the ALD cycle sequence. The area that is fully covered by all the precursor nozzles, called the active area, is 400 mm × 500 mm. A zone of gradually reducing film thickess occurs at the horizontal edges of the deposition area due to partial exposure of the substrate to the coating head. In the initial ramp-up of the tool stainless steel plates with dimensions of 0.8 mm × 1540 mm × 670 mm were used as substrates, but in later process tests similar sized stainless steel plate adapters with slots to fit in glass substrates and Si wafers were used.

The coating head of the tool had a total capacity of 11 nozzles: 5 for the metal and 6 for the nonmetal precursor. In this thesis only 3 metal and 4-5 nonmetal nozzles were used to achieve a desired nominal mixing ratio in the deposition of Zn(O,S) [67]. Liquid precursor (DEZ and H_2O) bottles were situated in a precursor bottle holder equipped with a water cooling system in the precursor cabinet. The dose of the liquid precursors was controlled with needle valves. H_2S bottle was positioned inside a separate cabinet designed to contain toxic gases. Precursors were supplied and distributed to the coating head with a specifically designed feed line system, which enabled simple changing of the precursor nozzle configuration.

3.2 Sample Fabrication

Polished Si wafers (100 mm in diameter) were used as sample substrates for ellipsometry and EDX measurements. Boron silicate glasses (dimensions 0.3 mm × 100 mm × 100 mm) were used as substrates for samples fabricated for UV-Vis measurements to study the optical properties of the deposited films. The Si wafers were used without wet etching, which was deemed suitable for the characterization of ALD-deposited films. The glass substrates were washed and dried in the Beneq Oy clean room facilities with a glass cleaning process. Compressed air was used to clean both substrates of particles prior to the deposition.

Samples were positioned on the substrate plate in the sample slots of the substrate adapter on dummy glass plates. The positions of the slots relative to the active area are presented and a photograph of the deposition area is shown in Figure 12. Sample slots L, M, and R refer the Si wafer positions, and LG as well as RG refer to glass substrates on left and right edges of the active area. Only sample positions M and LG were used to study the deposited materials. Uniformity studies of the whole active area, while essential in process development, were beyond the reach of this thesis.

3.2.1 Precursors and Surface Reactions

Well-known ALD chemicals were employed in the SALD reactor. ZnO, ZnS and Zn(O,S) thin films were fabricated using DEZ ($Zn(C_2H_5)_2$, Volatec Oy), H_2S (AGA Oy), and deionized H_2O purified in the Beneq facilities as precursors. DEZ is a spontaneously combustible organometallic compound and H_2S is a highly toxic gas with an LC_{50} of approximately 700 ppm, and thus safe chemical handling was of utmost importance [38,54]. These precursors were selected as they are affordable and readily available from industrial distributors, which is suitable for easily scalable fast SALD processing. DEZ and H_2O precursors were kept at a temperature of 20°C. The vapor pressure of DEZ at this temperature was 16.3 mbar, and the vapor pressure of H_2O was 23.3 mbar. The temperature of H_2S was not regulated, as H_2S was stored in a pressurized container.

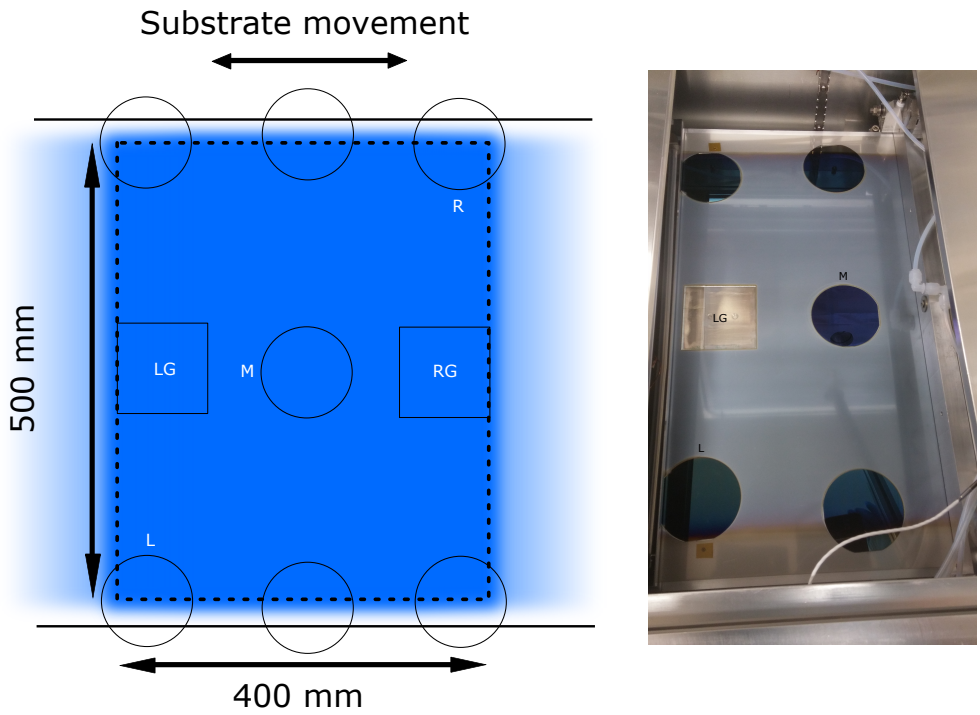

Figure 12: *The active area of the coating is 400 mm × 500 mm. At the horizontal edges of the substrate there is a sacrificial area, which is only partially exposed to the coating head. Only the Si wafer in the M position and the glass substrate in LG position were studied. Photograph on the right: ©Beneq Oy 2016.*

The ALD of ZnO from DEZ and H_2O can be described with the following half-reactions [26, 43, 76]:

$$\begin{aligned} &\text{I} \quad \text{OH*}\ (\text{s}) + \text{Zn}(\text{C}_2\text{H}_5)_2\ (\text{g}) \rightarrow \text{O–Zn–C}_2\text{H}_5\text{*}\ (\text{s}) + \text{C}_2\text{H}_6\ (\text{g}) \\ &\text{II} \quad \text{Zn–C}_2\text{H}_5\text{*}\ (\text{s}) + \text{H}_2\text{O}\ (\text{g}) \rightarrow \text{Zn–OH*}\ (\text{s}) + \text{C}_2\text{H}_6\ (\text{g}), \end{aligned}$$

in which * describes the surface species and (s) and (g) refer to solid and gas phases of the materials. The deposition of ZnS occurs rather similarly as that of ZnO via the following chemical reactions of DEZ and H_2S [35–37, 43]:

$$\begin{aligned} &\text{I} \quad \text{SH*}\ (\text{s}) + \text{Zn}(\text{C}_2\text{H}_5)_2\ (\text{g}) \rightarrow \text{S–Zn–C}_2\text{H}_5\text{*}\ (\text{s}) + \text{C}_2\text{H}_6\ (\text{g}) \\ &\text{II} \quad \text{Zn–C}_2\text{H}_5\text{*}\ (\text{s}) + \text{H}_2\text{S}\ (\text{g}) \rightarrow \text{Zn–SH*}\ (\text{s}) + \text{C}_2\text{H}_6\ (\text{g}), \end{aligned}$$

where * denotes the surface species. Zn(O,S) can be deposited by alternating between ZnO and ZnS reactions described above, but often the sulfur content in the films is higher than the ratio of the ZnO and ZnS sequences. This dominating ZnS growth can occur due to the fact that H_2S etches away ZnO [42, 43]. Therefore, tuning the sulfur content in Zn(O,S) thin films requires careful calibration, especially at varying process temperatures [48].

3.2.2 Run Parameters

ZnO and ZnS films as well as Zn(O,S) films with varying sulfur content were deposited using the SCS 1000 tool. The precursor nozzle configuration for each deposited material is presented in Figure 13. The precursors were separated from each other and other parts of the reaction chamber by N_2 flows. ZnO was deposited by moving the substrate below 4 H_2O and 3 DEZ nozzles. For the deposition of ZnS the H_2S line was connected to the nonmetal nozzles, thus the setup was similar to the ZnO configuration. Therefore, each full sweep under the coating head provided three ALD cycles in these setups. DEZ was injected with a concentration of 0.068 mmol/l in the carrier gas, while the concentration of H_2O in the carrier gas was 1.08 mmol/l. In the deposition of ZnS the H_2S concentration in the carrier gas was approximately 0.22 mmol/l, and in $Zn(O,S)_x$ processing the H_2S concentration was varied.

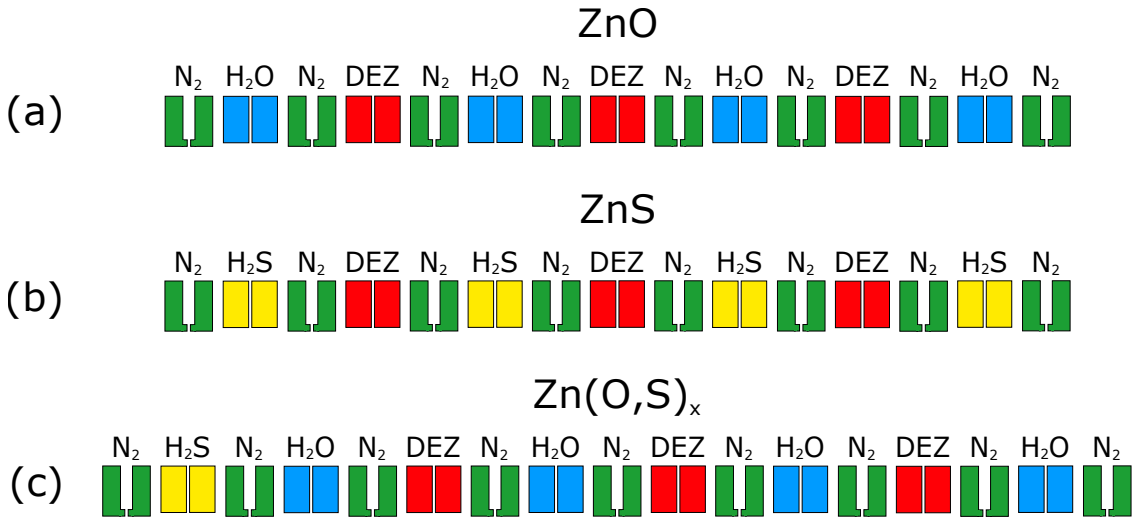

Figure 13: *Different nozzle configurations for the deposition of ZnO, ZnS, and $Zn(O,S)_x$. One full sweep under the coating head equaled three ALD cycles.*

In the case of Zn(O,S) deposition the ZnO setup was used, but an extra H_2S nozzle situated at the edge of the coating head was taken into use. Therefore, a sweep from left to right terminated the surface with H_2S, and afterwards 3 cycles of ZnO were deposited. When the substrate was moved back from right to left 3 cycles of ZnO were deposited, followed by a H_2S doping step. The H_2S nozzle was situated next to a H_2O nozzle to ensure that H_2S was always applied on a H_2O terminated surface, which regulated the rate at which H_2S etched away already deposited ZnO [43]. The sulfur content in the Zn(O,S) films was controlled by tuning the concentration of H_2S in the carrier gas flow with a mass flow controller (MFC) situated in the H_2S line. Values for the H_2S concentration x were 0.27, 0.45, 0.89 and 4.46 mmol/l, and throughout this thesis the deposited oxysulfides are differentiated from each other by x. The deposited films are referred to as $Zn(O,S)_x$, which means $Zn(O,S)_{0.45}$ refers to a film deposited with a H_2S concentration of 0.45 mmol/l. This nozzle configuration could be a viable option for an industrial buffer layer

deposition process, as the configuration potentially offer a simple way of tuning the sulfur content in the deposited films. There are also other viable methods in tuning the elemental ratios of the deposited thin films processed by SALD, discussed in Chapter 6, but in the scope of this thesis the flow-controlled side-feed of H_2S was focused on due to its simple installation procedure.

The process parameter combinations for the different experimental series, labeled ALD-like growth, T, τ and P series, are presented in Table 1. In the experiments the first step was to verify that ZnO and ZnS exhibit ALD-like growth *i.e.* film thickness increased linearly as a function of coating cycles. After this the effects of three process parameters on the deposition of the thin films were studied in separate experimental series. In the first series the temperature dependence of deposition parameters and film properties was studied by growing ZnO, ZnS and $Zn(O,S)_x$ at 110°C, 130°C, and 150°C. These temperatures were studied as the structural temperature limit for SCS 1000 is 150°C. In this thesis process temperature was referred to as the setpoint of the thermal elements which heated the coating head and substrate carrier.

Table 1: *The matrix for the design of experiments. Between different experimental series one parameter was varied, while others were kept constant.*

Experimental series	T [°C]	τ [ms]	P [mbar]
ALD-like growth	110	157	50
	110	157	50
T	130	157	50
	150	157	50
	130	157	50
τ	130	94	50
	130	67	50
	130	157	50
P	130	157	180
	130	157	380

The second experimental series focused on increasing the line speed of the SALD processing and studying how it affected the quality of the films. The deposition rate of SALD processing can be increased by moving the substrate faster under the precursor zones. It is beneficial to maximize the line speed of the process, but it is also essential to ensure that the chemical reactions have enough time to function in ALD mode, and that the movement of the substrate plate does not induce intermixing of precursors due to dragging molecules from one zone to another [101]. The ALD cycle time depended on the susceptor speed *i.e.* the speed at which the substrate was moved back and forth under the coating head. The susceptor speed determined

the time of precursor exposure, called the residence time τ, which was essentially the precursor pulsing length. The utilized susceptor speeds corresponded to τ values of 157, 94, and 67 ms, which corresponded to shorter cycle times than in conventional ALD reactors. Process temperature and pressure were kept constant.

The third altered process parameter was the vacuum chamber pressure in which the deposition occurred. Process pressure P is an important parameter in SALD processing, as close to atmospheric processing pressures would enable the SALD concept to be easily used in atmospheric in-line applications, and P also influences the precursor partial pressures in processing with SCS 1000. In these experiments P was controlled by adjusting the balance of precursor, inert gas and exhaust flows. With initial flow settings P was in the order of 50 mbar with normal process flows, and pressures of 180 and 380 mbar were also studied. In the scope of this thesis the effect of increased pressure was only characterized as a function of total process pressure, and line speed and process temperature were kept constant.

4 Characterization Methods

The deposited thin films were characterized using single-wavelength ellipsometry, UV-Vis spectrophotometry, and Energy Dispersive X-Ray (EDX) spectrocopy. The studied deposition and material characteristics of the films were growth per cycle (GPC), non-uniformity $d_{\%}$, refractive index n and optical band gap E_g for all materials. For $Zn(O,S)_x$ also molar elemental ratios S/Zn were determined.

GPC is a meaningful parameter for the study of ALD processes, since information about the saturation of the surface half-reactions can be deduced from the GPC value. Unusually low GPC values could be an indication of too low or too high thermal energy for the ALD process, or precursor dose might be insufficient [10,15]. Especially in SALD nonuniformity $d_{\%}$ describes how precursor gasses are spread from the nozzle to the substrate. If $d_{\%}$ increases heavily, it might be an indication that some areas of the substrate are exposed to different concentrations or partial pressures of the precursor. n and E_g are important optical parameters in many applications, as they describe the interactions between light and the material. The elemental ratios in films are directly related to many physical properties of the materials, such as refractive index and absorption properties.

4.1 Single-Wavelength Ellipsometry

Ellipsometry is an optical measurement technique in which changes in the polarization of light are measured when light is reflected or transmitted from a material. Changes in the polarization of light are characterized by the amplitude ratio Ψ and the phase difference Δ between p- and s-polarized light. The name 'ellipsometry' is derived from the measurement process: linearly polarized light often becomes elliptically polarized upon reflection. Ellipsometry data analysis is based on measuring Ψ and Δ of an optical signal reflected of the studied material and solving the equation

$$\tan\Psi \ \mathrm{e}^{i\Delta} = \rho(n_0, n_1, n_2, d, \theta_0), \tag{1}$$

in which ρ is the reflectance ratio of p- and s-polarized light, n_0 is the refractive index of air, n_1 the index of the studied thin film, n_2 that of the substrate, d the film thickness, and θ_0 the incidence angle of the light [110]. In the measurement process a light beam, in this case a laser beam with a wavelength of 633 nm, is directed to a polarizer and reflected from the sample with θ_0 being 70°. The reflected beam goes through an analyzer with a known polarization axis and is directed to a detector. The measurement can be done using multiple values for θ_0, which increases the data that can be used to solve the equation and can yield a more reliable result. The measurement parameters as well as a schematic of the measurement components are presented in Figure 14.

Ellipsometry is a versatile, fast, and non-destructive measurement method and most materials, such as dielectrics and metals, can be measured with minimal modification of measurement conditions. A major advantage is that the technique can be used in measuring *e.g.* a thin film deposition process *in-situ*. The main restrictions of the technique are that the surface roughness of the studied sample needs to be

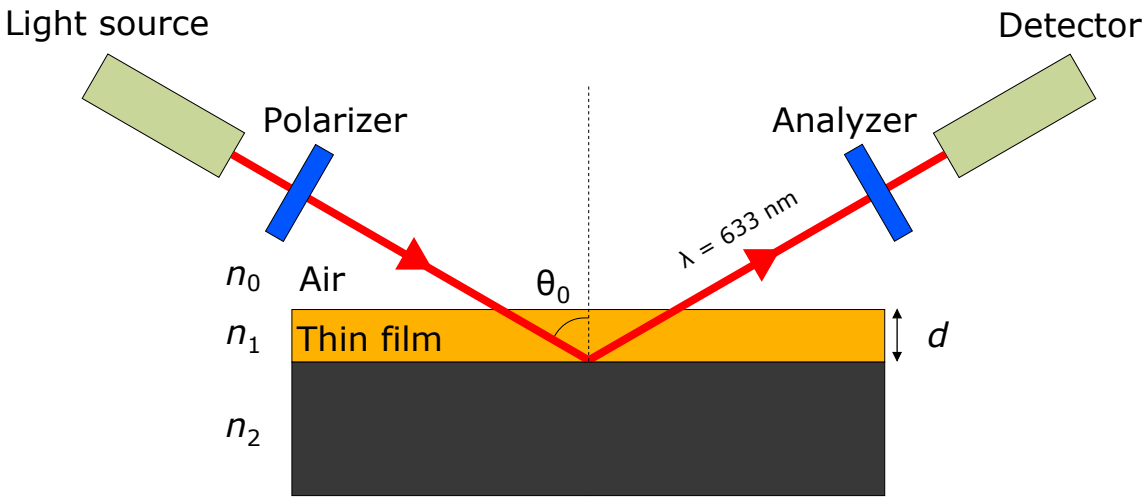

Figure 14: *Schematic of the single-wavelength ellipsometry measurement. Adapted from [110].*

small, and that the measurement needs to be performed at an oblique incidence angle, which depends on the optical properties of the sample. The ellipsometry method is inherently indirect, which means that an optical model containing estimates for n and d needs to be constructed prior to the measurement. [110] Data analysis of the measurement results is often complicated, but usually ellipsometry instruments are provided with in-built analysis software. Spatial resolution of the measurement is small, as laser beams with a mean diameter of millimeter scale are often used, but the fast measurement process makes multi-point mapping of sample surfaces feasible. Also, the numerical methods that are used to solve Equation 1 have a sensitivity regime, which means that they can not solve certain combinations of n and d. In the case of an unoptimal combination of n and d the aforementioned multiple angle measurement can be used.

Ellipsometry can be used to probe many material characteristics, such as crystallinity and composition, but it is often used in determining the thickness d and refractive index n of deposited thin films [110]. In this thesis, in addition to d and n, ellipsometry was used to study the uniformity of the deposited films on a 100 mm Si wafer. Thick films of ZnO, ZnS, and $Zn(O,S)_x$ were difficult to analyze with the ellipsometer software, so a three-angle measurement with θ_0 being 50, 60 and 70° was used to obtain more data of Ψ and Δ for these samples. The n obtained from this measurement was used as an estimate in mapping the sample substrates. A parameter called non-uniformity $d_{\%}$ defined with the following formula was studied:

$$d_{\%} = \frac{d_{max} - d_{min}}{2 \cdot \frac{1}{j} \sum_{i=1}^{j} d_i} \cdot 100\%, \tag{2}$$

in which d_{max} and d_{min} were the maximum and minimum thicknesses of a certain sample and j was the number of measurement points.

4.2 UV-Vis Spectroscopy

When light hits a surface there are three physical phenomena which can occur: the light flux can be transmitted or reflected from the interface or absorbed in the material [111]. Transmittance $T(\lambda)$ is a quantity which describes the amount of light which goes through the studied thin film as a function of the wavelength of light λ, while reflectance R is defined as the amount of the reflected light compared to the intensity of the incident light flux. Absorption coefficient α describes the amount of photons which are absorbed into the material, and it can be calculated from T and R spectra.

Transmittance and reflectance spectra of the samples were measured in a wavelength range of 350-1050 nm with a HunterLab Ultrascan PRO spectrophotometer using a 0.19 inch aperture for incident light. All substrates were measured in the same area, and only one measurement per sample was conducted. Therefore, variations in the optical properties of the thin films at different areas of the samples were not considered in the reach of this thesis.

4.2.1 Refractive Index

Refractive index n is a physical material property which is fundamentally related to the electronic properties of the atoms in a material. n describes light-electron interactions, and it is defined with the following equation

$$n = 1 + \frac{Nq_e^2}{2\epsilon_0 m(\omega_0^2 - \omega^2)}, \tag{3}$$

where N is the number of charges per unit volume, q_e the charge of an electron, ϵ_0 is the permeability of vacuum, m the mass of an electron, ω_0 the resonant frequency of an electron bound in an atom and ω is the angular frequency of the incident light [112]. N is directly proportional to the number of electrons in an atom, but it is also proportional to the density of the material: the higher the density is, the higher also N is. This information can be used in approximately comparing the properties of a material deposited with varying process parameters, as changes in the film composition and density can be seen as changes in n.

The refractive index n usually decreases as the wavelength is increased. Cauchy's relation is a simple empirical model which describes the relationship between n and λ:

$$n(\lambda) = B + \frac{C}{\lambda^2} + \frac{D}{\lambda^4} \ldots, \tag{4}$$

in which B, C and D are constants [113]. Often using the first two terms of the relation yields an accurate approximation of $n(\lambda)$.

The refractive indices of ZnO, ZnS, and $Zn(O,S)_x$ films were determined from their transmittance spectra by finding the parameters B and D in Equation 4 using OptiChar software (OptiLayer GmbH). Also the physical thickness d of the films deposited on glass were determined with the same software.

4.2.2 Absorption Coefficient and Optical Bandgap

The optical band gap E_g of semiconducting materials can be determined graphically from Tauc plots. The absorption coefficient α of a material is determined from transmittance and reflectance and the quantity $(\alpha h\nu)^2$, in which h is the Planck constant and ν the photon frequency, is plotted as a function of photon energy E. This method has been widely used in literature to determine the optical band gaps of ZnO, Zn(O,S) and ZnS films grown by ALD [38,43,45,48]. The absorption coefficient α can be calculated from $T(\lambda)$ and $R(\lambda)$ spectra with the following formula:

$$\alpha = \frac{1}{d} \cdot \ln \frac{1 - R(\lambda)}{T(\lambda)}, \tag{5}$$

in which d is the film thickness [114]. E_g can be determined from the Tauc plots by fitting a line in the linear regime of $(\alpha h\nu)^2$ plotted against E. The optical band gap E_g approximately corresponds to the photon energy at the intersection point of the fitted linear curve and the energy axis. An example of the graphical evaluation of the optical band gap is presented in Figure 15. This method of determining the optical band gaps of the deposited films is not very accurate, but it offers a simple way of characterizing changes in the absorbing properties of the films.

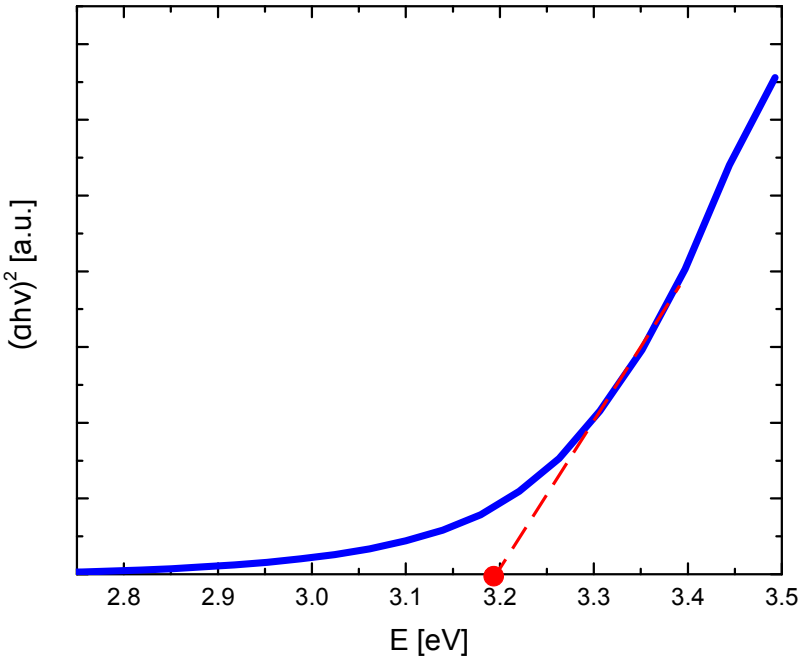

Figure 15: *Approximating the optical band gap for a Zn(O,S)$_{0.45}$ sample deposited at 150°C from a Tauc plot. E_g was determined to be 3.19 eV.*

4.3 Energy Dispersive X-Ray Analysis

Energy Dispersive X-Ray Analysis (EDX) can be used to study the elemental composition of samples. The technique is based on identifying characteristic X-rays that

are emitted from the studied sample due to the bombardment of the sample with high-energy electrons. The high-energy electrons kick out electrons from the inner energy shells, which are referred to as secondary electrons, of the target atoms. These vacancies in the inner shells are filled with an electron from an outer shell. As a result an X-ray photon γ with an energy defined by the energy difference ΔE of the inner and outer shells is emitted and collected to a detector [115, 116]. An EDX setup is often mounted to a Scanning Electron Microscope (SEM). The principle of EDX operation and the used equipment in the Aalto University OtaNano Nanomicroscopy Center as well as an example EDX spectrum are presented in Figure 16.

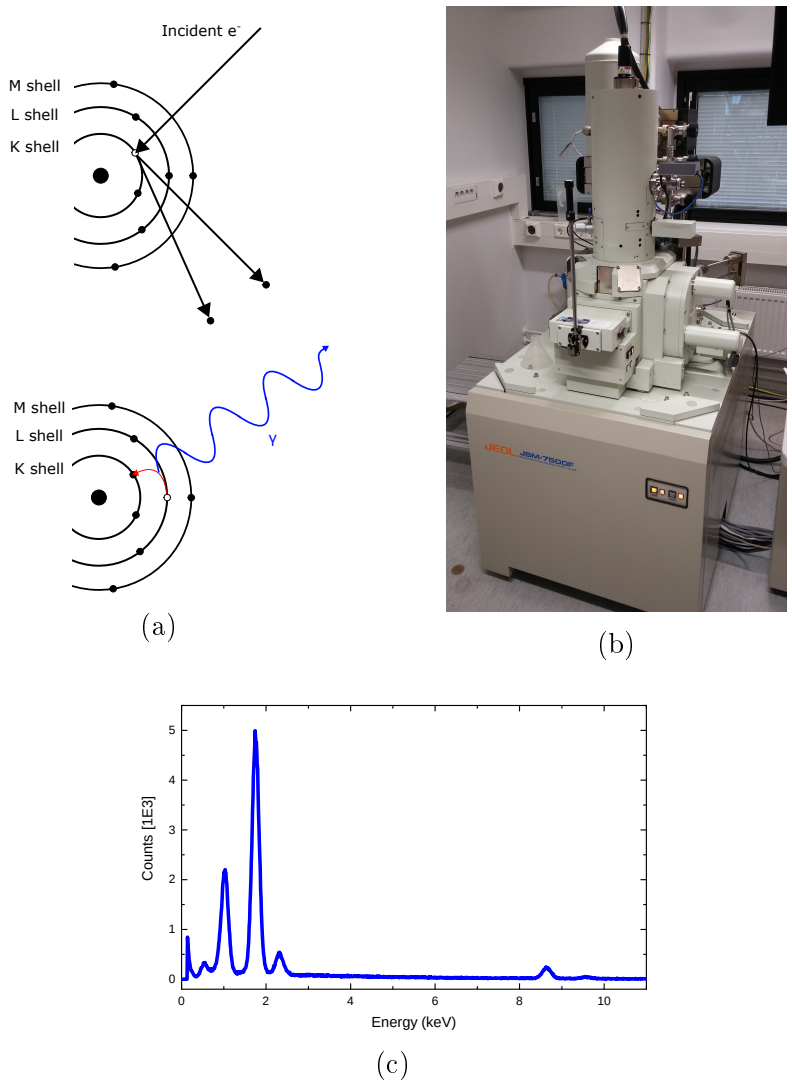

Figure 16: *(a) Formation of a characteristic X-ray photon γ due to secondary electron emission and the relaxation of a higher energy electron. (b) JEOL-SEM 7500F SEM equipped with EDX at the Aalto University Nanomicroscopy Center, part of OtaNano. c) An example of an EDX energy spectrum, measured from a $Zn(O,S)_{0.45}$ sample.*

Different energies of the X-ray photons correspond to different elements in the sample, and by studying the energy spectrum of the characteristic X-rays the elements can be identified. Elemental distributions can also be calculated based on the counts of characteristic X-ray photons obtained. In this thesis EDX analysis was used to probe the molar ratios of Zn, O, and S in the studied oxysulfide films, but also to observe whether the films contained carbon, which might have been an indication of reaction by-products or ligands of DEZ being incorporated into the films.

5 Results and Discussion

ZnO, ZnS, and Zn(O,S)$_x$ films were deposited with the process parameter combinations described in Table 1. Initial tests were performed to demonstrate that the films grew in the ALD mode. Next, the growth rate, uniformity, refractive index and optical band gap of the films grown at different temperatures were studied. For Zn(O,S)$_x$ also the S/Zn elemental ratios were researched. In the third experimental series precursor residence time and process pressure were varied. Thickness d of thin films deposited on Si substrates was measured with ellipsometry, and this data was used to determine the GPC of thin samples (d $<$ 100 nm) and $d_{\%}$ of all samples. The GPC of thicker samples ($d >$ 200 nm) was determined from samples deposited on boron silicate glass. Refractive index spectra and optical band gap values were determined from films deposited on glass substrates. S/Zn ratios of oxysulfide samples were measured from films with d over 200 nm deposited on Si substrates.

For all samples in T, τ and P series film thickess was in the order of 220 nm, which enabled an accurate optical analysis. Transmittance and reflectance spectra measured from all samples are presented in Appendix A. Films this thick were, however, not optimal for measuring with ellipsometry, but reliable approximate results of the film uniformity were obtained nonetheless. The influence of the Si substrate was visible in the EDX spectra, which slightly complicated the quantitative analysis. This meant that elemental distributions obtained from the data were not absolute, but relative changes in the elemental distributions of the samples could be identified. Elemental ratios and EDX graphs measured from all samples are presented in Appendix C.

5.1 Basic Parameters Tested in the Spatial ALD Concept

In ALD mode deposition the film thickness increases linearly and the growth rate per cycle (GPC) remains approximately constant as a function of ALD cycles [15]. In preliminary process tests the growth of ZnO and ZnS thin films deposited by SCS 1000 was confirmed to occur in the ALD mode at a temperature of 110°C, precursor residence time being 157 ms and process pressure 50 mbar. After this the growth rate, uniformity, optical properties, and elemental composition were studied as a function of increasing process temperature.

5.1.1 Confirmation of the ALD-Like Growth

ZnO and ZnS were grown on 100 mm Si wafers as well as boron silicate glass substrates at a process temperature of 110°C. The number of ALD cycles was 51, 102, 300 and 1002 for ZnO and 51, 102, 300 and 1542 for ZnS. Table 2 shows d and the GPC of both materials. Thickness of the films deposited on Si substrates was measured with ellipsometry with the exception of the thickest ZnS film, for which the thickness was determined from a film deposited on boron silicate glass using OptiChar analysis software. The thickness of the films varied from 5 to 120 nm for ZnO and 7 to 240 nm for ZnS. GPC values were calculated from the d values by

Table 2: *Film thickness d and GPC as a function of ALD cycles for ZnO and ZnS deposited at 110°C.*

Material	ALD cycles	d [nm]	GPC [Å/c]
ZnO	51	4.7	0.92
	102	11.6	1.14
	300	36.1	1.20
	1002	118.5	1.18
ZnS	51	7.2	1.42
	102	14.8	1.45
	300	44.8	1.49
	1542	234.8	1.52

dividing the film thickness with the number of cycles. Thicknesses of the deposited films as well as growth rates are visualized in Figure 17.

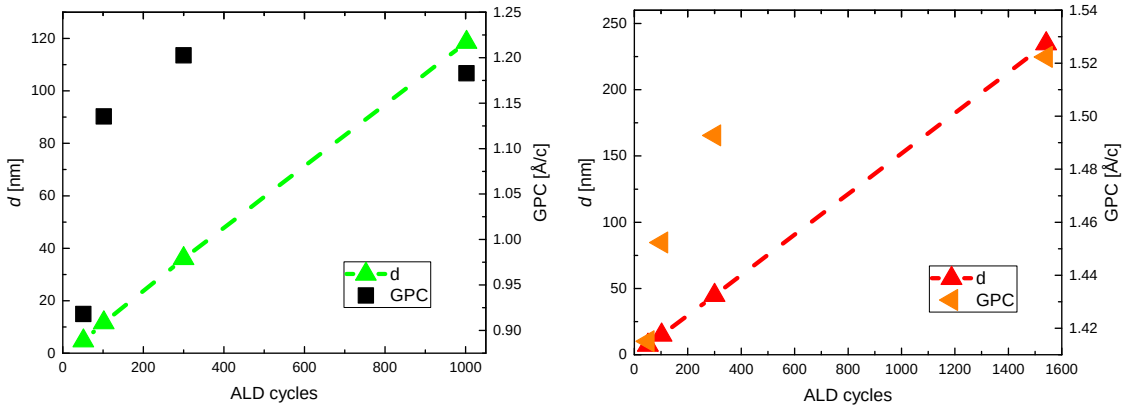

(a) *ZnO* (b) *ZnS*

Figure 17: *d and GPC of (a) ZnO and (b) ZnS films deposited with an increasing number of ALD cycles.*

For both materials the film thickness increased approximately linearly as a function of ALD cycles, which indicated that the film growth occurred in close to optimal ALD mode. This was supported by the GPC values: with a higher number of ALD cycles GPC was approximately constant. For very thin films with a thickness below 10 nm GPC was rather low, which indicated that a certain number of ALD cycles was initially required to fully cover the substrate surface with a monolayer of the material. This was identified as a substrate-inhibited growth mode [15]. GPC started to stabilize after approximately 100 ALD cycles. At a temperature of 110 °C the growth rates of ZnO and ZnS were approximately 1.2 Å/c and 1.5 Å/c, respectively. The growth rate of ZnO was rather low compared to processing done with pulsing ALD [26], which might have been caused by the rather low process temperature. The GPC of ZnS was also slightly below the growth rate of films deposited by pulsing

ALD using the same precursors at similar temperatures [37]. The low GPC values could be explained by underdoses of DEZ, H_2O or H_2S, but it was very likely that the dose of H_2S was sufficient due to it being stored in a pressurized container. Therefore, DEZ and H_2O doses were speculated to be insufficient to achieve completely saturated surface reactions.

As the film thickness of ZnO and ZnS increased linearly and the GPC values were approximately constant as a function of ALD cycles, we could confirm that the films deposited using the SCS 1000 SALD tool grew in the ALD mode.

5.1.2 Deposition of ZnO, ZnS, and Zn(O,S)$_x$ at Various Process Temperatures

After it was confirmed that the basic processes functioned in the ALD mode ZnO, ZnS, Zn(O,S)$_x$ with d above 200 nm were deposited at 110°C, 130°C, and 150°C on Si wafers and glass substrates. d as well as n spectra were determined for all materials from their transmittance spectra using OptiChar software. A Cauchy refractive index dispersion model was used. Non-uniformity was determined from ellipsometry measurements by mapping the 100 mm Si wafer measuring d in 49 data points. Before the mapping the refractive index of the deposited thin film at a wavelength of 633 nm was defined with a three-angle measurement, and this n value was autofixed. It should be noted that the autofixing of n combined the non-uniformity of the film thickness with the non-uniformity in the refractive index, meaning that $d_{\%}$ could have also described the non-uniformity of n. The ellipsometer software calculated the $d_{\%}$ value for each sample using Equation 2.

Growth rate and uniformity

GPC and non-uniformity values for all materials at all process temperatures are presented in Table 3 and visualized in Figure 18.

Table 3: *GPC [Å/c] of ZnO, ZnS, and Zn(O,S)$_x$ films deposited at 110°C, 130°C and 150°C on a glass substrate.*

	GPC [Å/c]					
T [°C]	ZnO	Zn(O,S)$_{0.27}$	Zn(O,S)$_{0.45}$	Zn(O,S)$_{0.89}$	Zn(O,S)$_{4.46}$	ZnS
110	1.27	1.24	1.09	1.09	1.16	1.52
130	1.59	1.46	1.48	1.46	1.26	1.44
150	1.89	1.57	1.57	1.60	1.56	1.34

	$d_{\%}$[%]					
T [°C]	ZnO	Zn(O,S)$_{0.27}$	Zn(O,S)$_{0.45}$	Zn(O,S)$_{0.89}$	Zn(O,S)$_{4.46}$	ZnS
110	1.7	6.7	3.7	4.7	5.7	1.1
130	1.8	1.0	1.7	6.9	1.6	1.8
150	1.4	1.1	1.0	0.9	1.7	1.9

When T was increased from 110 to 150°C the GPC of ZnO increased linearly from 1.27 to 1.89 Å/c, while the GPC of ZnS decreased linearly from 1.52 to 1.34 Å/c. The GPCs of ZnO and ZnS did not stabilize to constant values in the temperature range employed in these measurements. The GPCs indicated that higher process temperatures were more optimal for ZnO, while for the surface reactions of ZnS lower temperatures were advantageous. At 150°C the GPC of ZnO was close to values reported in literature, ranging from 1.4 to 2.5 Å/c [26], while the GPC of ZnS was below the reported values (from 1.9 Å/c at 100°C to 1.85 Å/c at 150°C) at all temperatures [37]. In the deposition of $Zn(O,S)_x$ the GPC was lower than that of ZnO for all H_2S concentrations at all temperatures. The GPC of $Zn(O,S)_x$ followed a similar trend for all H_2S concentrations, increasing rapidly from 110 to 130°C and moderately from 130 to 150°C, with the exception of $Zn(O,S)_{4.46}$. At 110°C the growth rates of $Zn(O,S)_x$ were the lowest for all concentrations, with $Zn(O,S)_{0.27}$ having the highest GPC of 1.24 Å/c and $Zn(O,S)_{0.45}$ the lowest of 1.09 Å/c. At 130°C the highest GPC for oxysulfides was that of $Zn(O,S)_{0.45}$, 1.48 Å/c, while the GPC of $Zn(O,S)_{4.46}$ was the lowest, 1.26 Å/c. For $Zn(O,S)_{4.46}$ the GPC was similar at 150°C as with lower concentrations, but significantly lower at 130°C. Overall, at 150°C only small deviations were observed in the GPC of oxysulfides, the values of which were close to the average GPC of ZnO and ZnS. The GPC of $Zn(O,S)_{4.46}$ suggested that the H_2S treatment etched away the deposited ZnO film more efficiently than with lower concentrations at 130°C, while at 150°C the already deposited film was etched away less effectively even with higher x [43].

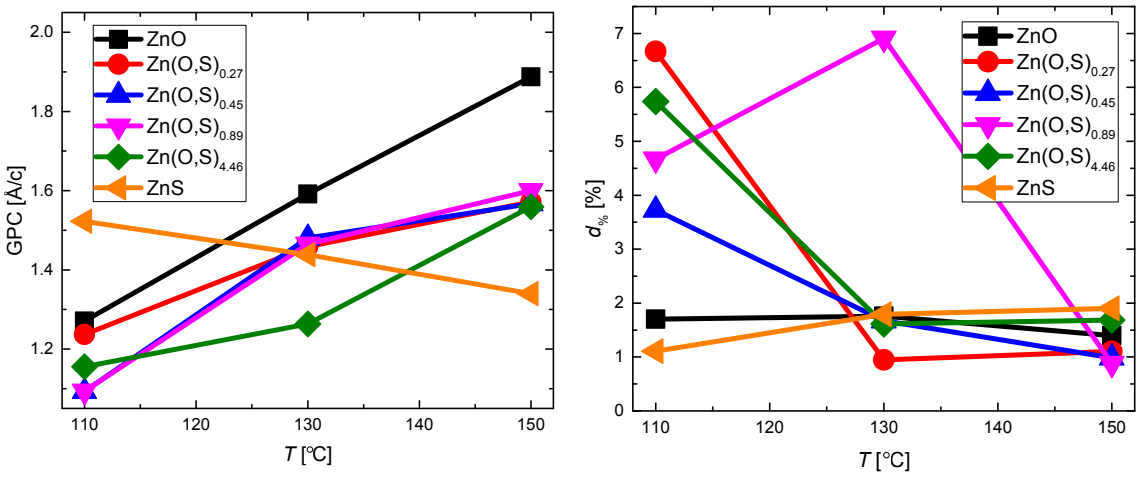

Figure 18: *Growth rates in Å/c and non-uniformity values in percentages for all deposited materials as a function of T.*

ZnO and ZnS films were uniform throughout the whole temperature range with $d_{\%}$ ranging from 1.4 to 1.7 % for ZnO and 1.1 to 1.9 % for ZnS. However, there were significant changes in the uniformity of $Zn(O,S)_x$ as T increased. Oxysulfide thin films deposited at 110°C were significantly less uniform than those grown at higher temperatures with minor exceptions. For example, by increasing T from 110 to 130°C the non-uniformity of $Zn(O,S)_{0.27}$ dropped from 6.7 to 1.0 %. Overall,

oxysulfides were very non-uniform when deposited at 110°C, but at 130 and 150°C their uniformity was similar as or even better than that of ZnO and ZnS. Only $Zn(O,S)_{0.89}$ deposited at 130°C was very non-uniform with a $d_{\%}$ of 6.9%, but at 150°C its non-uniformity was the lowest of the series, 0.9%. The uniformity development of the oxysulfide thin films suggested that the H_2S introduced from the nozzle situated at the edge of the coating configuration was spread more evenly on the surface when T was higher than 110°. Also, as ZnS had the highest GPC at 110°C, the applied H_2S pulses might have siphoned oxygen away from the surface more efficiently than at higher temperatures, which might have led to significant non-uniformity not only in thickness but also in the refractive index of the deposited thin films.

Refractive index

The refractive index spectra of all samples are presented in Figure 19, and n values at a wavelength of 633 nm are collected in Table 4. This wavelength was chosen as the comparison point due to it being close to the middle of the spectral range, as well as because it was the same probing wavelength used by the ellipsometer. At all temperatures the refractive index of ZnS was the highest (2.40 at 633 nm at all T) and that of ZnO was the lowest (1.96 at 633 nm at 110°C) of the studied materials. The n spectra of $Zn(O,S)_x$ were situated in between the spectra of ZnO and ZnS at all wavelengths. At 110°C the refractive indices of the oxysulfides increased systematically as a function of H_2S concentration throughout the whole spectral range. At 633 nm the n of $Zn(O,S)_{0.27}$ was 2.15, while for $Zn(O,S)_{0.45}$ the refractive index was 2.17, and for $Zn(O,S)_{0.89}$ and $Zn(O,S)_{4.46}$ the indices were 2.18 and 2.19, respectively. This systematic increase of the refractive index at all wavelengths was accounted to the increase of sulfur in the thin films. The refractive index spectra of ZnO and ZnS were similar as reported in literature [108, 117].

Table 4: *Refractive indices at a wavelength of 633 nm for $Zn(O,S)_x$ thin films deposited at 110°C, 130°C and 150°C.*

T [°C]	ZnO	$Zn(O,S)_{0.27}$	$Zn(O,S)_{0.45}$	$Zn(O,S)_{0.89}$	$Zn(O,S)_{4.46}$	ZnS
110	1.956	2.152	2.168	2.179	2.192	2.401
130	1.970	2.184	2.186	2.184	2.213	2.395
150	1.977	2.180	2.183	2.207	2.202	2.399

At 130°C the oxysulfide n spectra did not behave as systematically as at 110°C. At short wavelengths the n of $Zn(O,S)_{0.27}$ was the highest, but when λ was above approximately 520 nm, the highest refractive index was that of $Zn(O,S)_{4.46}$. The refractive index of $Zn(O,S)_{0.89}$ was the lowest at 450 nm, but at longer wavelengths its n was higher than that of the lower H_2S concentrations. Interestingly, the n spectra of $Zn(O,S)_{0.27}$, $Zn(O,S)_{0.45}$ and $Zn(O,S)_{0.89}$ intersected approximately at 630 nm. At 130°C the refractive index of ZnO at 633 nm was 1.97, which was slightly higher than in 110°C. For ZnS n at 130°C was approximately the same as in 110°C.

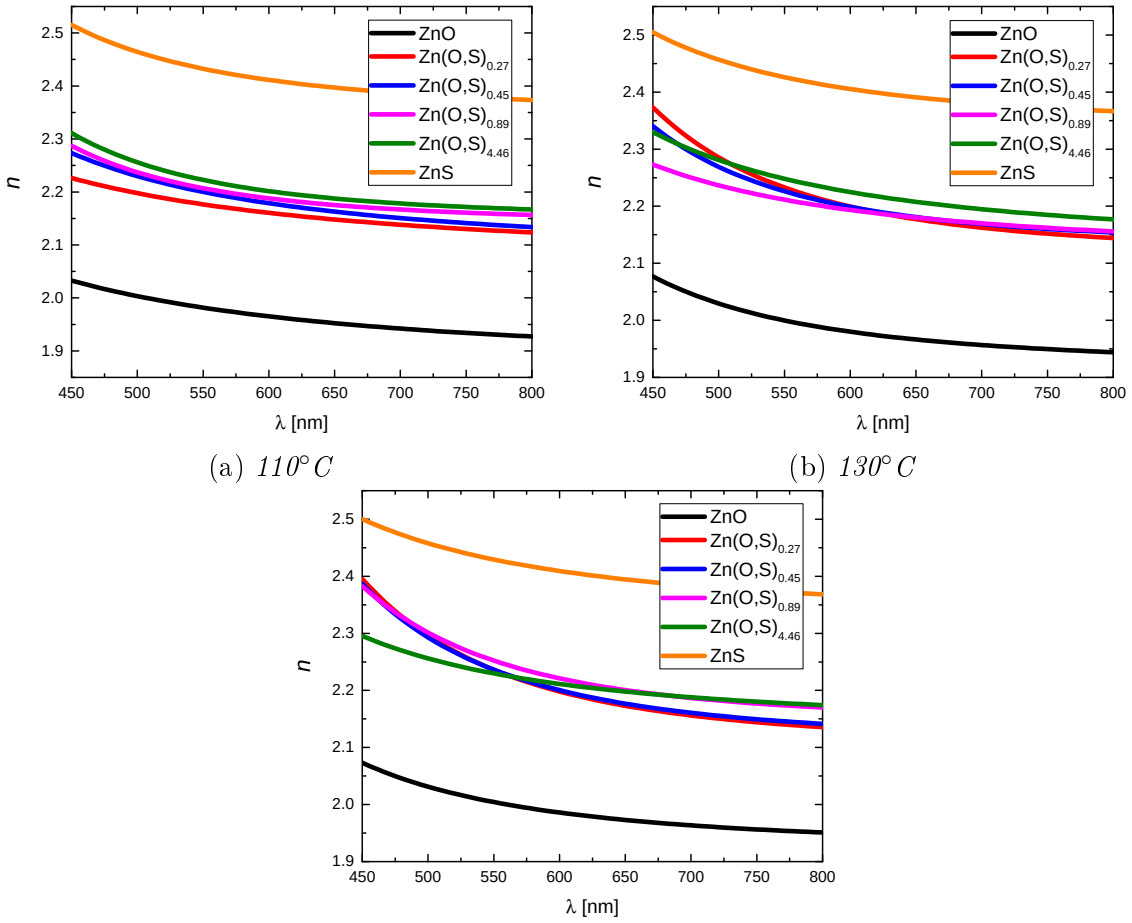

(a) *110°C* (b) *130°C*

(c) *150°C*

Figure 19: *Refractive index n with a spectral range of 450 to 800 nm for all materials deposited at all process temperatures.*

The refractive index of ZnO at 633 nm was the highest at 150°C, 1.977, which further indicated that higher process temperatures were more optimal for the growth of ZnO. For ZnS n at 150°C was similar as at lower temperatures. The refractive index spectra of $Zn(O,S)_{0.27}$ and $Zn(O,S)_{0.45}$ were almost identical in the whole spectral length at this temperature. For $Zn(O,S)_{0.89}$ the refractive index spectrum at wavelengths below 525 nm was similar to the spectra of films fabricated with lower H_2S concentration, but at longer wavelengths the n spectra of $Zn(O,S)_{0.89}$ and $Zn(O,S)_{4.46}$ were almost identical.

The changes in the refractive index spectra of the oxysulfides as a function of temperature led to a deduction that the rate at which sulfur was chemisorbed into the thin film significantly affected the refractive index, as the GPC of ZnO increased and that of ZnS decreased as a function of temperature. Also the balance of the exchange reaction between oxygen and H_2S might have had an effect on the density of the films and the nature of the bonding of sulfur to the surface species, as described by Equation 3. In these cases n could have also been affected by different ratios of oxygen and sulfur in the films, but also possible contaminants such as reaction by-

products might have been left in the deposited films. The differences in the shapes of the refractive index spectra might have also been influenced by possible changes in the crystalline structure of the thin films as a function of x. The measurement process might have also affected the results, as measurements might not have been conducted exactly at the same areas of different samples. This could have led to slightly different transmittance spectra. In addition, there might have been particle contaminants on the substrates as processing was not done in a clean room environment, which could have caused scattering. Also, as at all temperatures the refractive index spectra of oxysulfides behaved systematically as a function of the H_2S doping above approximately 650 nm, the accuracy of the optical analysis software could be disputed.

Optical band gap and elemental ratios

The optical band gaps for all samples were resolved from Tauc plots, which were determined from the thickness and transmittance and reflectance spectra of the samples. The absorption coefficient α was calculated using Equation 5, and the band gaps were determined by performing a linear curve fit to the region in which $(\alpha h\nu)^2$ was linear and calculating its intersection with the E-axis. The Tauc plots of all samples are presented in Appendix B. The optical band gap of ZnS could not be determined: according to literature E_g of ZnS is approximately 3.5-3.7 eV [38, 45], which correspond to a wavelength in the range of 335-354 nm. The wavelength range of the spectrophotometer was not sufficient to analyze optical band gaps in these enegy scales. E_g of ZnO and Zn(O,S)$_x$ as a function of T are presented in Figure 20a and Table 5.

The band gaps of ZnO and Zn(O,S)$_x$ were close to values reported in literature (3.25 eV for ZnO, 2.85 to 3.29 eV for Zn(O,S)), so this approximation method for the optical band gap was considered valid [43, 45, 48]. E_g of ZnO remained almost constant as T was increased, with band gap increasing slightly from 3.260 eV at 110°C to 3.270 eV at 150°C. For Zn(O,S)$_{4.46}$ the band gap decreased from 3.320 to 3.246 eV when T was increased from 110 to 150°C. For all other oxysulfides deposited at 110°C the band gaps were very close to each other, approximately 3.29 eV. At higher temperatures significant differences between the oxysulfides started to appear. At 130°C Zn(O,S)$_{0.27}$ had the lowest E_g of 3.196 eV, and at this temperature the band gap increased as a function of x. At 130 and 150°C the band gap of Zn(O,S)$_{4.46}$ was higher than E_g of oxysulfides deposited with lower H_2S concentrations. The band gap of Zn(O,S)$_{4.46}$ was closest to the band gap of ZnO of all the oxysulfides. The obtained optical band gaps of oxysulfides were lower than values reported by Bugot *et al.* [48], but still within the values reported for Zn(O,S) [44]. These results showed that the optical band gap of SALD-deposited Zn(O,S)$_x$ depend on the process temperature, and that tuning the E_g of Zn(O,S)$_x$ by altering the H_2S concentration require a higher process temperature than 110°C. At 130°C the optical band gaps of the oxysulfides followed a distinct trend: the higher the H_2S concentration in the precursor flow was, the higher were the optical band gaps. The optical band gap of ZnO showed only minor changes as a function of T, which meant that the absorbing

properties of ZnO were relatively independent of the process temperature.

Changes in the S/Zn ratios of $Zn(O,S)_x$ as a function of process temperature were analyzed by EDX. An EDX spectrum was recorded from samples deposited on Si substrates with an acceleration voltage of 15 kV, and collection time was 4 minutes. The ratios of sulfur and zinc were studied, and the S/Zn of oxysulfide samples are presented in Figure 20b and Table 5.

S/Zn ratios of the samples behaved systemically as a function of increasing H_2S concentration: $Zn(O,S)_{4.46}$ had the highest and $Zn(O,S)_{0.89}$ the second highest S/Zn ratio at all temperatures. $Zn(O,S)_{0.45}$ had the lowest S/Zn ratio at 110°C (0.178), while at 130°C the S/Zn ratios of $Zn(O,S)_{0.27}$ and $Zn(O,S)_{0.45}$ were similar. At 150°C $Zn(O,S)_{0.27}$ had the lowest S/Zn ratio of 0.117. When T increased the S/Zn ratio dropped for all H_2S concentrations with the exception of $Zn(O,S)_{4.46}$, which increased from 0.223 at 110°C to 0.246 at 150°C.

Generally the S/Zn ratio was noticed to decrease as temperature increased. The observed elemental ratios correlated with the changes in the refractive index spectra and the optical band gaps of the materials: the higher the sulfur content was, the higher were the refractive index and the optical band gap with the exception of $Zn(O,S)_{4.46}$. Therefore, these results supported the hypothesis that n and E_g were connected to the actual elemental properties of the thin films. It was also noteworthy that ZnO deposited at 110°C and ZnS deposited at 150°C both contained trace amounts of carbon, which was a further indication that higher process temperatures were more suited for ZnO growth and lower temperatures were more optimal for ZnS growth. For oxysulfide films no carbon was detected at any process temperature.

Table 5: *Optical band gaps of ZnO and $Zn(O,S)_x$ and S/Zn ratios of $Zn(O,S)_x$ films deposited at 110°C, 130°C and 150°C.*

	E_g [eV]				
T [°C]	ZnO	$Zn(O,S)_{0.27}$	$Zn(O,S)_{0.45}$	$Zn(O,S)_{0.89}$	$Zn(O,S)_{4.46}$
110	3.260	3.285	3.293	3.285	3.320
130	3.262	3.196	3.207	3.242	3.270
150	3.270	3.188	3.189	3.204	3.246

	S/Zn			
T [°C]	$Zn(O,S)_{0.27}$	$Zn(O,S)_{0.45}$	$Zn(O,S)_{0.89}$	$Zn(O,S)_{4.46}$
110	0.188	0.178	0.195	0.223
130	0.149	0.147	0.167	0.217
150	0.117	0.131	0.163	0.246

Based on the results obtained from the experiments conducted at various process temperatures, the processing of ZnO, ZnS, and $Zn(O,S)_{0.45}$ at 130°C was chosen to study the effects of decreased residence time τ and increased process pressure P. 130°C was chosen as the process temperature because the overall uniformity of the thin films was considered acceptable at approximately 2% and at 130°C GPC was

higher for ZnO and $Zn(O,S)_{0.45}$ than at 110°C. Processing at 150°C was not considered feasible as industrial processing is preferred to be done at low temperatures, though a higher T yielded better results in terms of lower S/Zn ratio, GPC and uniformity. Therefore, 130°C was considered the lowest process temperature at which processing could be applied in large-scale use. $Zn(O,S)_{0.45}$ was chosen as the oxysulfide material as at 130°C it exhibited the lowest S/Zn ratio at 110 and 130°C. The optical band gap of $Zn(O,S)_{0.45}$ also changed more than the E_g of $Zn(O,S)_{0.27}$ when T was increased from 130 to 150°C. Due to these reasons it was hypothesized that $Zn(O,S)_{0.45}$ was the optimal material to probe possible changes in the properties of the films due to differences in residence time and process pressure.

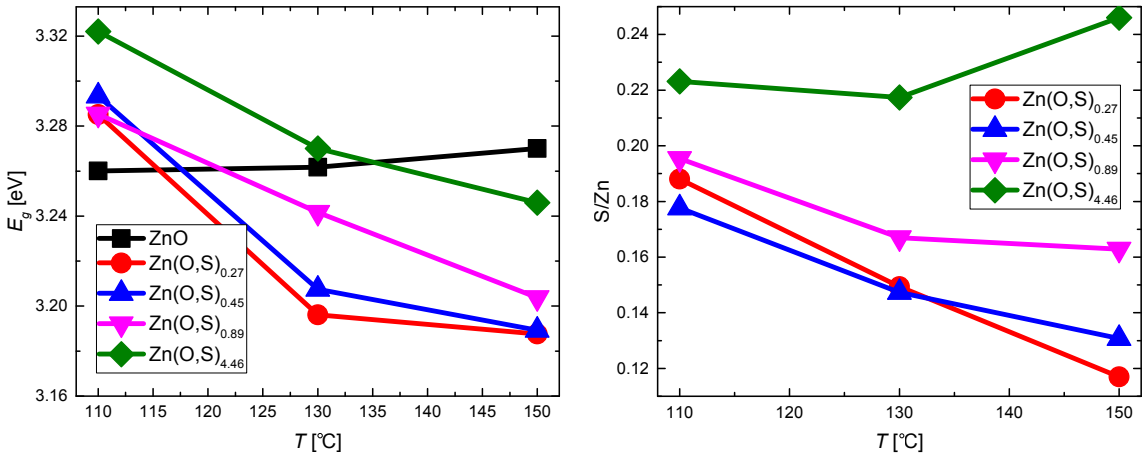

Figure 20: *(a) E_g for ZnO and $Zn(O,S)_x$ as a function of T. (b) S/Zn ratios for $Zn(O,S)_x$ deposited in the studied process temperatures.*

5.2 The Effect of Increased Line Speed on Film Growth

ZnO, $Zn(O,S)_{0.45}$ and ZnS were grown at 130°C with increasing susceptor speed to investigate whether the deposition rate of processing with the SCS 1000 could be increased while maintaining high film quality. Increased susceptor speed led to decreased precursor residence time, as the width of the precursor zones was constant. However, the deposition rate D measured in nm/min increased significantly. The employed line speeds corresponded to residence times of 157, 94 and 67 ms, and the deposition rates for each residence time are presented in Table 6.

Table 6: *Deposition rate D of ZnO, ZnS, and Zn(O,S)$_{0.45}$ films deposited at 130°C.*

	D [nm/min]		
τ [ms]	ZnO	Zn(O,S)$_{0.45}$	ZnS
157	4.6	4.2	4.1
94	6.7	6.6	7.1
67	7.9	8.2	9.8

For ZnO D increased from 4.6 nm/min to 7.9 nm/min when τ was shortened from 157 to 67 ms. Similarly the deposition rate of Zn(O,S)$_{0.45}$ increased from 4.2 to 8.2 nm/min. The increase in deposition rate was the most pronounced for ZnS, as D increased from 4.1 to 9.8 nm/min.

Growth rate and uniformity

The viability of increasing deposition rate was studied by looking at the effect of decreased residence time τ on the growth, properties and structure of the deposited thin films. GPC and $d_{\%}$ as a function of τ are presented in Figure 21 and Table 7. When τ was shortened from 157 to 67 ms the GPC of ZnO and Zn(O,S)$_{0.45}$ decreased, but for ZnS the growth rate remained almost constant. The GPC of ZnO dropped the most, from 1.59 to 1.20 Å/c, and the GPC of Zn(O,S)$_{0.45}$ followed a similar trend, decreasing from 1.48 to 1.23 Å/c. For ZnS GPC varied from 1.44 to 1.48 Å/c, reaching the maximum value with a residence time of 94 ms. It should be noted that the precursor dose was kept constant when residence time was decreased. Maydannik *et al.* observed a drop of GPC with shorter residence times in a TMA + H_2O process [100,101], and accounted the drop in GPC to incomplete coverage of the surface due to insufficient precursor dose. In the deposition of ZnO and Zn(O,S)$_{0.45}$ an insufficient H_2O dose for the short residence times might have been the reason for the significant drop in GPC, as the GPC of ZnS remained almost constant as a function of τ. Thefore, it was deduced that DEZ and H_2S doses were sufficient for all residence times.

Table 7: *GPC and $d_{\%}$ of ZnO, ZnS, and Zn(O,S)$_{0.45}$ films deposited at 130°C with decreasing residence time τ on a glass substrate.*

	GPC [Å/c]			$d_{\%}$ [%]		
τ [ms]	ZnO	Zn(O,S)$_{0.45}$	ZnS	ZnO	Zn(O,S)$_{0.45}$	ZnS
157	1.59	1.48	1.44	1.8	1.7	1.8
94	1.38	1.35	1.48	1.6	7.4	2.1
67	1.20	1.23	1.46	1.6	9.6	2.9

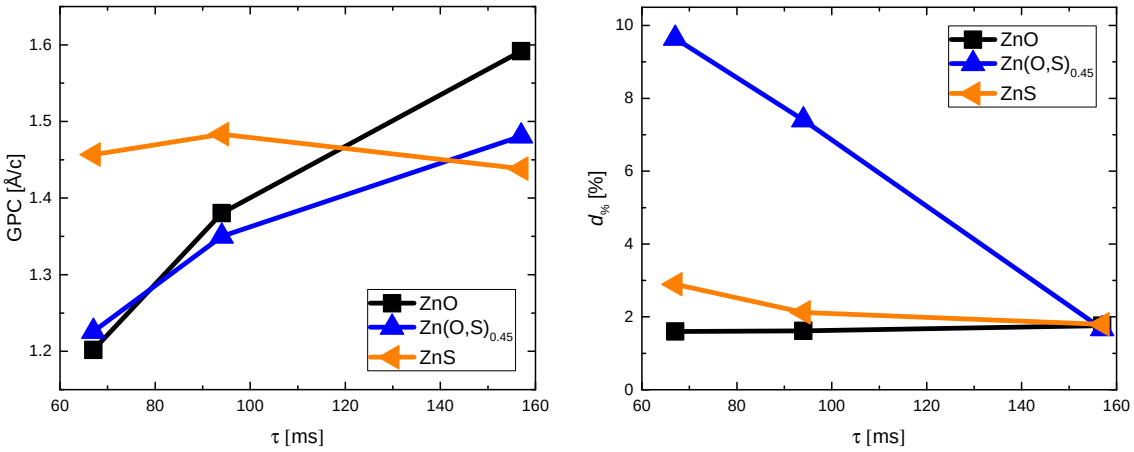

Figure 21: *GPC and $d_{\%}$ for films deposited with decreasing τ.*

The uniformity of ZnO remained good even when τ was decreased: $d_{\%}$ decreased from 1.8 to 1.6 % when the residence time was shortened from 157 to 67 ms. Therefore, it was likely that DEZ and H_2O were ejected from their nozzles in such a way that precursor concentration and pressure were similar under the whole nozzle along its whole length. For ZnS $d_{\%}$ increased from 1.8 to 2.9 % with shortened τ. The non-uniformity of $Zn(O,S)_{0.45}$ increased dramatically with decreased residence time. The $d_{\%}$ of the oxysulfide increased from 1.7 to 7.4% when τ was shortened from 157 to 94 ms, and when τ was 67 ms a non-uniformity of 9.6 % was obtained. As the non-uniformity of ZnS and $Zn(O,S)_{0.45}$ increased with shorter τ, H_2S might not have been optimally spread under the whole nozzle. The significant increase in the non-uniformity of $Zn(O,S)_{0.45}$ could be explained, however, by different reaction kinetics and timeframe of the S-O exchange reactions compared to the gas-surface reactions of the non-mixed materials. It was also possible that the refractive index of the $Zn(O,S)_{0.45}$ thin film was not entirely uniform across the whole substrate, as the ellipsometry measurement relies on finding out both d and n.

Refractive index

The refractive index spectra of all materials deposited with decreased residence time are presented in Figure 22 and n values at a wavelength of 633 nm are shown in Table 8. For ZnO the refractive index spectra were very close to each other at wavelengths in the middle of the spectrum, but with shorter residence times n dropped slightly at short and long wavelengths. The shape of the n spectra of $Zn(O,S)_{0.45}$ spectra changed with residence time: a longer τ yielded higher n at wavelengths below 630 nm and lower n above 630 nm. For ZnS n of the film deposited with a residence time of 67 ms was lower throughout the whole spectrum than the spectra of samples deposited with longer τ.

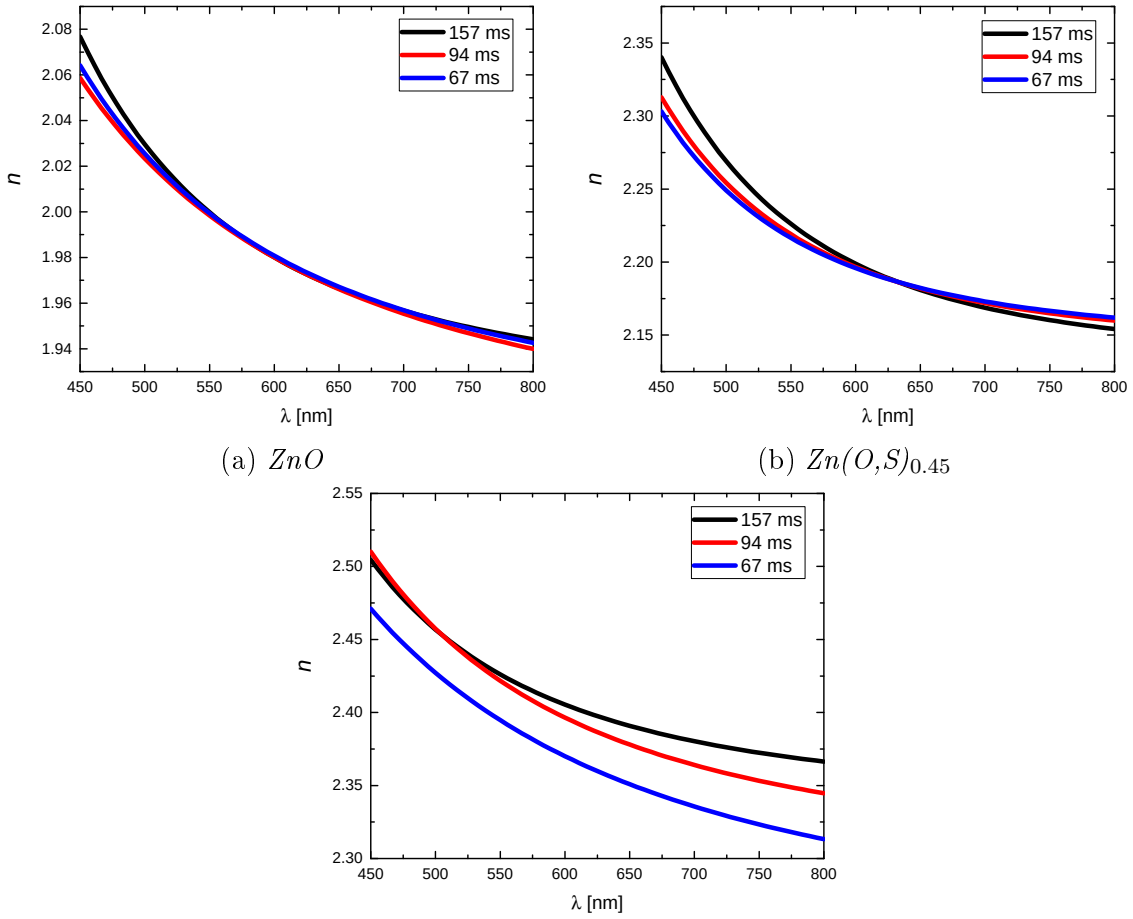

(a) *ZnO* (b) $Zn(O,S)_{0.45}$

(c) *ZnS*

Figure 22: *Refractive index spectra of ZnO,* $Zn(O,S)_{0.45}$ *and ZnS deposited at 130°C with decreasing residence time.*

Table 8: *Refractive index at 633 nm of films deposited at 130°C with decreasing* τ.

τ [ms]	ZnO	$Zn(O,S)_{0.45}$	ZnS
157	1.970	2.186	2.395
94	1.970	2.186	2.384
67	1.971	2.186	2.357

At 633 nm the refractive indices of ZnO and $Zn(O,S)_{0.45}$ were identical regardless of residence time, approximately 1.97 for ZnO and 2.19 for $Zn(O,S)_{0.45}$. The refractive index of ZnS dropped significantly, from 2.395 with a τ of 157 ms to 2.357 with 67 ms. This was considered an indication of too short residence time for the chemical reaction between DEZ and H_2S to take place at this temperature, especially as precursor doses were considered sufficient in the deposition of ZnS. The too short reaction time might have resulted in decreased film density, which affected the

refractive index as described by Equation 3. Also changes in the crystalline structure of the deposited thin films as a function of τ could explain the shapes of the n spectra. The changes in the n spectra of ZnO and $Zn(O,S)_{0.45}$ were very minor compared to the differences in the spectra of ZnS. This could be explained a minor CVD component in the growth of ZnS with the shortest residence times.

Optical band gap and elemental ratios

The optical band gaps of ZnO and $Zn(O,S)_{0.45}$ films as a function of τ are presented in Figure 23a and Table 9. With a residence 67 ms the E_g of ZnO was the lowest, 3.222 eV, while with longer residence times the band gaps were 3.268 eV (94 ms) and 3.262 eV (157 ms). The band gap of $Zn(O,S)_{0.45}$ was lowest with a value of 3.207 eV with the longest residence time, but with shorter τ the band gaps were determined to be only slightly higher: 3.227 eV for 94 ms and 3.217 eV for 67 ms.

The S/Zn ratios of $Zn(O,S)_{0.45}$ are presented in Figure 23b and Table 9. The S/Zn ratio increased with shortened τ, from 0.147 with 157 ms to 0.192 with 67 ms. These changes in ratios might arise from the insufficient H_2O dose which led to incomplete surface reactions, also observed in the dropping of GPC with shorter residence times for ZnO and $Zn(O,S)_{0.45}$. However, the changes in S/Zn ratios did not correlate with the changes in the optical band gap as a function of τ. Speculatively the increased share of sulfur showed in the refractive index spectra of $Zn(O,S)_{0.45}$, as n slightly decreased at shorter wavelengths and increased at longer wavelengths with shortened τ. No trace amounts of carbon were detected for any samples when the residence time was decreased, which indicated no significant amounts of undesired reactions by-products were incorporated into the films. This signified that the drop in GPC might have occurred due to the fact that some surface reaction sites had not reacted with the precursors, which further supported the theory of insufficient precursor dose for H_2O.

Table 9: *Optical band gaps of ZnO and $Zn(O,S)_{0.45}$ and S/Zn ratios of $Zn(O,S)_{0.45}$ thin films as a function of residence time.*

	E_g [eV]		S/Zn
τ [ms]	ZnO	$Zn(O,S)_{0.45}$	$Zn(O,S)_{0.45}$
157	3.262	3.207	0.147
94	3.268	3.227	0.169
67	3.222	3.217	0.192

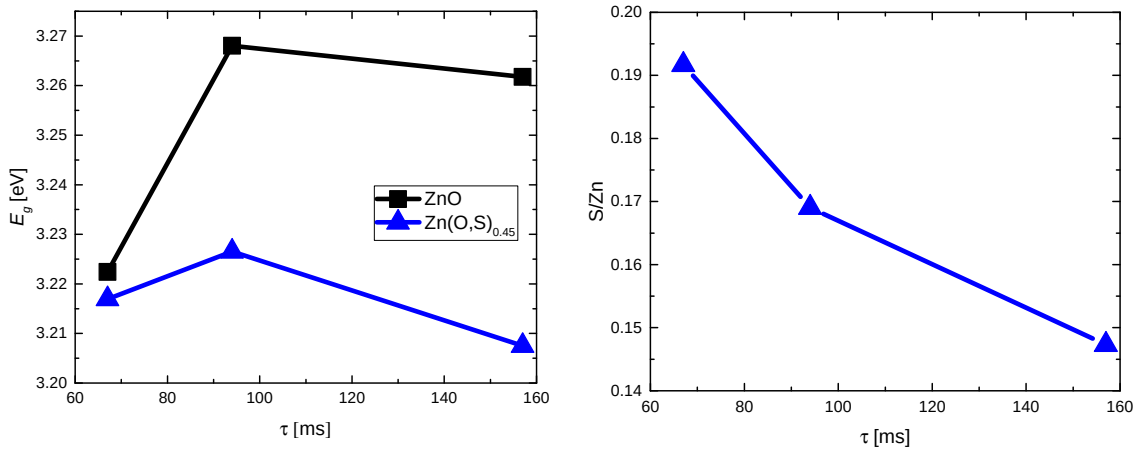

Figure 23: *(a) E_g of ZnO and Zn(O,S)$_{0.45}$ as a function of τ. (b) S/Zn ratios for Zn(O,S)$_{0.45}$ deposited with shortened residence time τ.*

5.3 Towards Atmospheric Spatial ALD through Increased Process Pressure

The deposition of ZnO, ZnS and Zn(O,S)$_{0.45}$ was studied in increased process pressure to test the feasibility of high pressure and ultimately atmospheric processing with the SCS 1000. The growth rate and uniformity were studied similarly as before, and films were deposited at 130°C with a τ of 157 ms. Process pressures studied were 50, 180 and 380 mbar, which were sufficient for studying the effects of High Pressure SALD.

Growth rate and uniformity

GPC and $d_{\%}$ for all materials as a function of P are presented in Figure 24 and summarized in Table 10. The GPC of ZnO and ZnS increased when P was increased from 50 to 180 mbar and dropped slightly when P increased to 380 mbar. The highest GPC for ZnO was approximately 1.65 Å/c and for ZnS 1.55 Å/c, both reached in 180 mbar. Also for Zn(O,S)$_{0.45}$ the GPC increased when P was 180 mbar, but in 380 mbar the drop in growth rate was more pronounced than with ZnO or ZnS. For all materials maximum GPC was reached in 180 mbar, and GPC in 380 mbar was higher than the GPC in basic process pressure of 50 mbar. The higher process pressure led to an increased precursor concentration under the nozzle, which in turn speculatively increased the GPC [109]. When process pressure was 380 mbar, the amount of precursor molecules which reached the surface might have dropped due to an increased amount of molecules in the deposition zone, which blocked the motions of precursor molecules. Also reaction products and non-reactive molecules could have hindered the movement of precursor molecules above the surface of the substrate due to inefficient purging to the exhaust lines.

There were no distinct trends in how P affected the uniformity of the studied

materials: for ZnO $d_{\%}$ dropped from 1.76 to 0.89% when P increased from 50 to 180 mbar but increased to 3.54% in 380 mbar. The non-uniformity of ZnS increased steadily from 1.79 to 2.55% when P increased from 50 to 380 mbar. For $Zn(O,S)_{0.45}$ $d_{\%}$ behaved differently, as it was first increased from 1.67% in 50 mbar to 4.07% in 180 mbar and decreased to 2.82% in 380 mbar. This development of non-uniformity as a function of P might have been influenced by the same mechanisms as the growth rate. The significant increase in non-uniformity of $Zn(O,S)_{0.45}$ processed in 180 mbar might have been caused by the interplay of increased precursor partial pressure and hindered precursor spreading. The precursor flow from the solitary H_2S nozzle might not have been uniformly distributed under the active length of the nozzle, which could have led to variations in refractive index and thickness of the deposited film. ZnO was most uniform in 180 mbar and ZnS in 50 mbar, for in these pressures the balance of the process flows and exhaust flow was speculatively optimal for the spreading of precursors for each material.

Table 10: *GPC and $d_{\%}$ of ZnO, $Zn(O,S)_{0.45}$ and ZnS films deposited on glass substrates deposited in increasing P.*

	GPC [Å/c]			$d_{\%}$ [%]		
P [mbar]	ZnO	$Zn(O,S)_{0.45}$	ZnS	ZnO	$Zn(O,S)_{0.45}$	ZnS
50	1.59	1.48	1.44	1.8	1.7	1.8
180	1.65	1.62	1.55	0.9	4.1	2.2
380	1.63	1.48	1.55	3.5	2.8	2.6

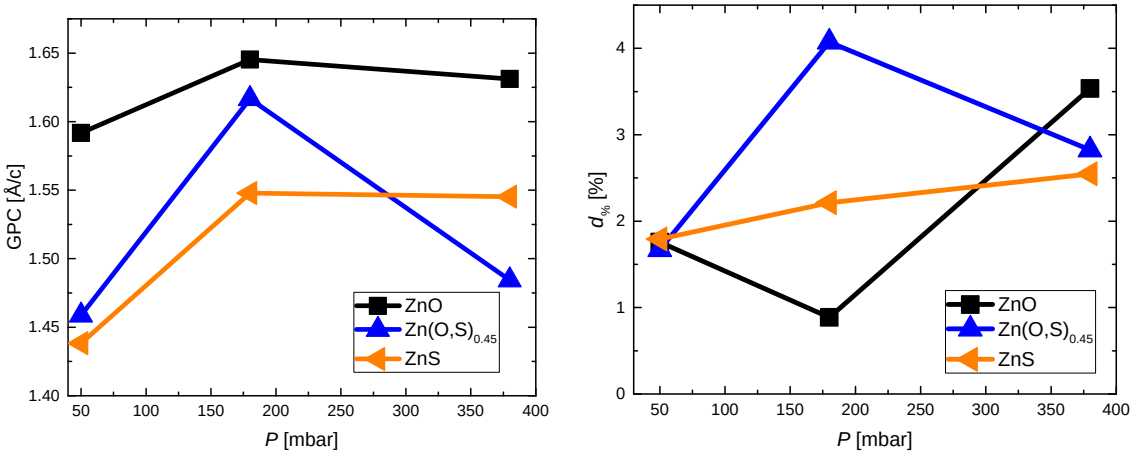

Figure 24: *GPC and $d_{\%}$ as a function of P. Maximum GPC for all materials was reached in a process pressure of 180 mbar. Non-uniformity results varied from material to another.*

Refractive index

The influence of P on the refractive index of ZnO, ZnS and $Zn(O,S)_{0.45}$ is visualized in Figure 25 and n values at a wavelength of 633 nm are presented in Table 11. Changes in n were observed for all materials as a function of P. The refractive index of ZnO dropped marginally but systematically at all wavelengths when process pressure was increased, while for ZnS the highest n values were obtained in 180 mbar. For ZnS also processing in 380 mbar yielded a higher refractive index compared to the base pressure of 50 mbar. For $Zn(O,S)_{0.45}$ n dropped at all wavelengths when P was increased.

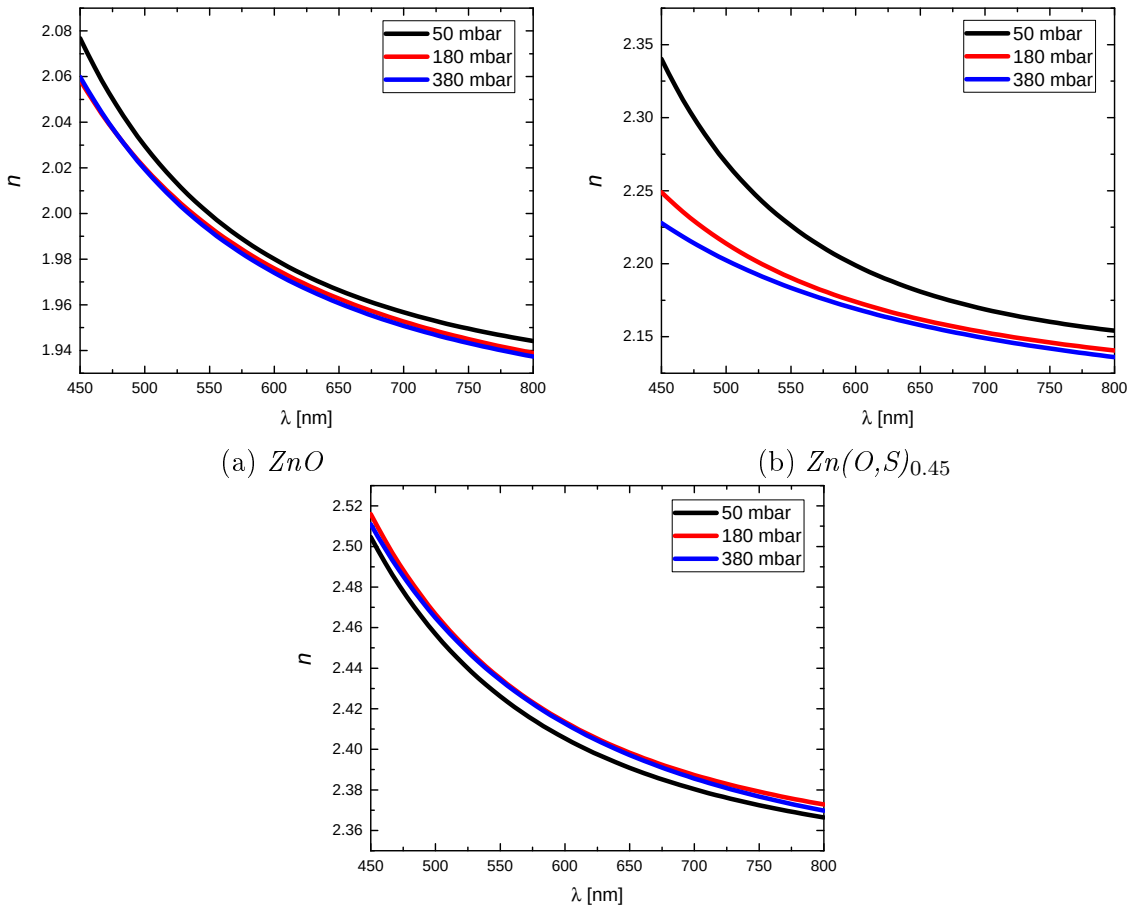

(a) *ZnO* (b) $Zn(O,S)_{0.45}$

(c) *ZnS*

Figure 25: *n spectra of ZnO, $Zn(O,S)_{0.45}$ and ZnS deposited in the studied process pressures.*

At a wavelength of 633 nm the refractive index of ZnO dropped from 1.970 to 1.967 when P was increased from 50 to 180 mbar, and in a pressure of 380 mbar n was 1.965. For $Zn(O,S)_{0.45}$ n dropped abrubtly from 2.186 to 2.166 when process pressure was elevated from 50 to 380 mbar, which could have been caused by changes in the elemental distribution of the films or by altered density. Only the refractive index of ZnS was observed to slightly increase with heightened process pressure, from 2.395

in 50 mbar to 2.403 in 180 mbar. In 380 mbar the n of ZnS was marginally lower than that of the film deposited in 180 mbar. The changes in the refractive index might have indicated that the density of ZnO and $Zn(O,S)_{0.45}$ decreased when the process pressure was elevated due to the same reasons that affected the uniformity. Reactant molecules might not have reached the substrate as efficiently as in lower pressures, but also less efficient purging of reaction products might have caused a minor CVD component in the growth.

Table 11: *n of ZnO, $Zn(O,S)_{0.45}$ and ZnS at 633 nm as a function of P.*

P [mbar]	ZnO	$Zn(O,S)_{0.45}$	ZnS
50	1.970	2.186	2.395
180	1.967	2.166	2.403
380	1.965	2.161	2.402

Optical band gap and elemental ratios

Optical band gaps of the samples deposited in the studied process pressures are visualized in Figure 26a and presented in Table 12. The band gap of ZnO decreased slightly, from approximately 3.23 eV to 3.20 eV when P was increased from 50 mbar to 380 mbar. On the other hand, the optical band gap of ZnS increased from 3.16 eV in 50 mbar to 3.19 eV in 380 mbar. Of the studied materials the E_g of $Zn(O,S)_{0.45}$ changed the most, hiking from 3.04 eV in 50 mbar to 3.21 eV in 380 mbar. The band gap of $Zn(O,S)_{0.45}$ was the highest of all materials deposited in 380 mbar, even higher than that of ZnO in the same pressure.

S/Zn ratios of $Zn(O,S)_{0.45}$ deposited in the studied process pressures are presented in Figure 26b and Table 12. The S/Zn ratio increased with higher values for P, climbing from 0.15 in 50 mbar to 0.19 in 380 mbar. There were no signs of carbon impurities in any of the deposited films, but the ZnS sample processed in 380 mbar showed minor amounts of oxygen. This was most likely caused by oxygen contamination as the sample was exposed to air. Also, ZnO samples were found out to contain minor but observable amounts of sulfur, which might have been transferred to the ZnO films in the deposition process inside the reactor or during the storaging of the samples.

Table 12: *Optical band gaps of ZnO and Zn(O,S)$_{0.45}$ and S/Zn ratios of Zn(O,S)$_{0.45}$ films as a function of P.*

P [mbar]	E_g [eV] ZnO	E_g [eV] Zn(O,S)$_{0.45}$	S/Zn Zn(O,S)$_{0.45}$
50	3.262	3.207	0.147
180	3.309	3.263	0.178
380	3.225	3.307	0.189

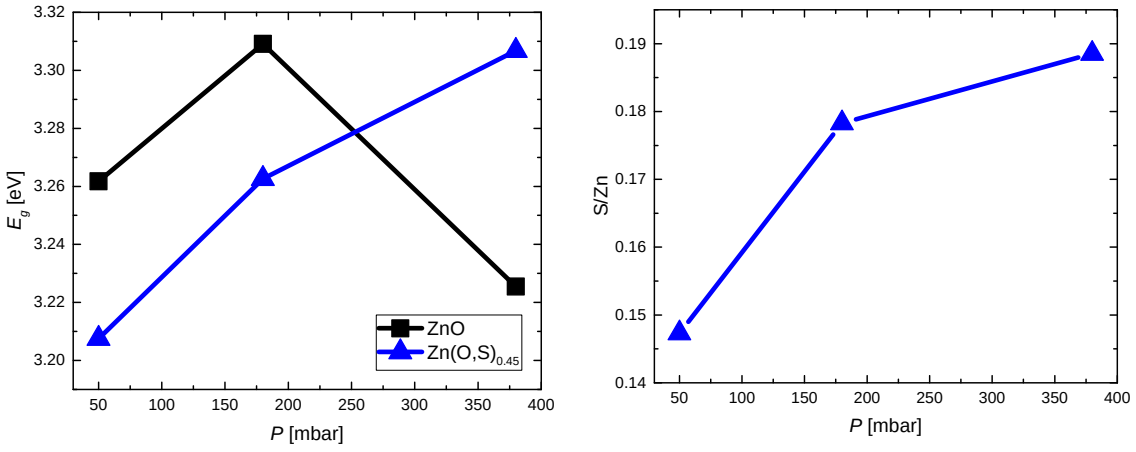

(a) (b)

Figure 26: *(a) E_g of ZnO and Zn(O,S)$_{0.45}$ as a function of P. (b) S/Zn ratios for Zn(O,S)$_{0.45}$ as a function of process pressure.*

The optical band gap of Zn(O,S)$_{0.45}$ correlated with the S/Zn ratio and, therefore, the sulfur content of the film. The higher the S/Zn ratio was, the higher also the optical band gap climbed. These results suggested that reaction conditions, such as precursor partial pressure, impurities in the films and purging efficiency significantly affected the optical properties of the films. However, film growth was observed in all process pressures, which indicated that the SALD tool functioned even in higher pressures. The data from the P series also indicated that film growth in an SALD reactor is strongly influenced by the flow balance of the precursor flows, barrier flows and purging zones, and that the optimal run parameters might vary from material to another.

6 Conclusions and Future Interests

The goals of this thesis included reviewing spatial ALD, proving that the SCS 1000 SALD tool functions in the ALD mode, performing process tests for ZnO, ZnS and Zn(O,S), and determining future steps for the process development. In this section the experimental results are reviewed and process development prospects are discussed.

The measurements conducted in this thesis confirmed that SALD processing of ZnO, ZnS and Zn(O,S) was viable with the SALD tool SCS 1000. Film growth of ZnO and ZnS was confirmed to occur in the ALD mode at the lowest deposition temperature of 110°C. As the deposition of ZnO and ZnS was feasible in 110°C, it was concluded that their deposition also at higher temperatures was ALD-like, as these temperatures were close to feasible process temperatures reported in literature [26, 37]. Process temperature T had a major effect on the growth rate, uniformity, optical properties and elemental distribution of the films. Also reduced residence time and increased process pressure generated differences in the properties of the films.

The growth rates of the deposited films were determined quite accurately, but the optical properties of the samples were measured only in one area of the substrate. Observing the film properties throughout the whole active area of the tool is vital in the industrial-scale process development of the SALD processing. Also, depositing ZnS films on sapphire substrates and measuring their transmittance and reflectance with a spectrophotometer capable of reaching wavelengths below 300 nm would enable the studying of the optical band gap of ZnS. Films with a thickness in the order of 50 nm should be deposited on Si wafers to measure the non-uniformity of not only the thickness but also of the refractive index with the ellipsometer, as with this film thickness there would be no need to autofix the refractive index. This measurement would further shed light on the growth characteristics of the zinc oxide and sulfide thin films.

The measurement method used to determine the elemental properties of the films, EDX, had significant sources of uncertainty. Especially the oxygen content of the films was only used as an approximate value, as samples were stored in air which could have led to oxygen contamination of all films. Also, as polished unetched Si wafers were used and the thickness of the native oxide on the Si substrates could not be determined, the amount of oxygen detected by the EDX detector might have varied from substrate to another. The ratio of S and Zn was considered a moderately reliable quantity to observe.

The results presented in this thesis provide an important reference for the SALD development at Beneq. There have been numerous reports concerning ZnO, both undoped and doped, fabricated by SALD [74, 79, 80, 82], but the deposition of Zn(O,S) by SALD has so far not been studied extensively. The only report of Zn(O,S) processed by SALD was issued by Illiberi *et al.* in 2015 [96]. So far no academic studies nor reports on the SALD of ZnS have been published, thus this thesis represents the first results of ZnS films fabricated by SALD.

Process Temperature

All materials were successfully deposited at process temperatures of 110, 130 and 150°C. Transmittance spectra showed that the transparency of all samples was relatively high, as would be needed for optical applications and in CIGS. The growth rate of ZnO increased while the GPC of ZnS decreased as a function of process temperature. At the lowest deposition temperature, 110°C, the growth rate of ZnS was higher than that of ZnO, but at higher temperatures the GPC of ZnO was higher than that of ZnS. This was a demonstration of how the characteristics of film growth in the ALD mode are unique for each process: even though DEZ was used as the metal reactant in the deposition of both materials, the different chemical properties of H_2O and H_2S affected the film growth process. However, the observed GPC values were slightly below those reported in literature, which might have been an indication of insufficient precursor dose for both materials [26,37]. An important notion was to consider the reaction kinetics of H_2S in the deposition of Zn(O,S), as the rate of the exhange reaction between H_2S and oxygen speculatively depended on the temperature. This was indicated by how the GPC of oxysulfides developed as a function of temperature: at 150°C the GPC of $Zn(O,S)_x$ was almost the same regardless of x. The uniformity of the deposited films was considered good with process temperatures above 110°C.

The refractive index at a wavelength of 633 nm increased as a function of T for ZnO while for ZnS n remained almost constant. This was considered an implication that higher temperatures produced denser ZnO films, but the density of ZnS was almost unaffected by the deposition temperature. At 110°C changes in the refractive index spectra of $Zn(O,S)_x$ were attirubuted to changes in density, but at higher temperatures also differences in the elemental ratios of the films could have been the reason for these results. The crystalline structure of Zn(O,S) has been showed to change with sulfur content [43], and changes in the crystallinity of $Zn(O,S)_x$ might have caused changes in the refractive index. However, these assumptions would need to be studied further using X-Ray Reflectivity (XRR) analysis to investigate the density, Fourier Transform Infrared Spectroscopy (FTIR) or X-Ray Photoelectron Spectroscopy (XPS) to probe the bonding of the atoms, and accurate X-Ray Diffraction (XRD) measurements to confirm changes in the crystallinity. Results from preliminary XRD measurements are presented in Appendix D.

The optical band gap E_g of ZnO slightly increased as a function of temperature, and the obtained band gaps were close to values reported in literature, 3.25 eV for ALD-grown ZnO [43, 48]. The optical band gap of $Zn(O,S)_x$ decreased when x and T were increased. The changes in the optical band gaps of $Zn(O,S)_x$ generally correlated with the sulfur content of the films determined by studying the S/Zn molar ratios measured by EDX: E_g decreased as sulfur content decreased. However, in the residence time experimental series the correlation between S/Zn and E_g was less pronounced. The optical band gap was successfully tuned by altering the H_2S concentration in the carrier gas: at 130°C a band gap range of 3.196 to 3.270 eV was achieved. However, as the band gap of Zn(O,S) has been reported to be in the order of 2.8 to 3.6 eV [46], the obtained band gap tuning range was quite narrow. Also,

the accuracy of the method used to determine the optical band gap of all materials was debatable, which signified that the results obtained in this thesis should be confirmed using more accurate measurement methods.

The Effect of Increased Line Speed on Film Quality

The deposition rate of SALD processing could be significantly increased by increasing the velocity at which the substrate is moved under the coating head. The effect of increased line speed on film quality was studied by observing changes in the growth rate, uniformity, optical properties of all films and the elemental composition of $Zn(O,S)_{0.45}$ films as a function of residence time τ, measured in ms. The deposition of all the materials was technically successful: the deposited films were highly transparent, and the inert gas barriers had successfully prevented the intermixing of precursors in the active coating area. Also, no parasitic deposition occurred in other parts of the vacuum chamber. However, the reduced residence time had a major effect on the quality of the deposited $Zn(O,S)_{0.45}$ and ZnS films.

The GPC of ZnS remained high even at higher line speeds, but the growth rate of ZnO and $Zn(O,S)_{0.45}$ plummeted when τ was decreased from 157 ms to 67 ms. This was attributed to the reactivity of H_2O and an insufficient H_2O dose [100, 101], as the GPC of ZnS was not noticeably affected by the decreased residence times. The deposition of ZnO and $Zn(O,S)_{0.45}$ with these residence times would be beneficial to be investigated with a significanty larger H_2O dose, but also deposition at higher temperatures would need to be studied to gain further understanding of the kinetics of the surface chemical reactions. Too high concentrations of H_2O might, however, lead to inefficient purging and ultimately to the mixing of precursors in the gas phase.

The non-uniformity of ZnO remained below 2% at all residence times, and the non-uniformity of ZnS increased slightly when τ was shortened. However, the non-uniformity of $Zn(O,S)_{0.45}$ increased dramatically at higher line speeds. This was attributed to an uneven H_2S concentration under the nozzle and the different reaction kinetics of the H_2S-oxygen exchange reactions compared to the film growth of ZnO and ZnS. The uniformity of deposited oxysulfide materials could be enhanced by applying a different mechanical solution to spreading the precursors under the whole length of the nozzle or by tuning the H_2S process flow to see whether higher pressure in the precursor line could enhance the uniformity even with faster line speeds. Also, different H_2S concentration in the carrier gas would be interesting to test to see if this effect would be amplified by higher precursor concentrations.

The refractive index spectra of ZnO and $Zn(O,S)_{0.45}$ remained rather similar as a function of τ, but pronounced changes in the n of ZnS were observed. At reduced residence times the refractive index of ZnS dropped, which could have been an indication of reduced film density. This might have been caused by the desorption of deposited surface species due to more rapidly changing pressure gradients when the substrate was moved under the coating head from one end to another. This hypothesis could be confirmed by measuring the density of the deposited thin films with XRR. Also studying the possible changes in the crystallinity of the deposited

materials would shed light on the growth processes.

The optical band gap of ZnO dropped from 3.262 to 3.222 eV when residence time was shortened from 157 to 67 ms. These changes could be caused by residual reaction products that were embedded into the films, but this would need to be confirmed with more accurate methods to determine the elemental composition, such as Time-Of-Flight Elastic Recoil Detection Analysis (TOF-ERDA). The sulfur content of $Zn(O,S)_{0.45}$ was noticed to increase with decreasing residence time, as the S/Zn ratio increased. The changes in the sulfur content correlated slighly with the optical band gap of $Zn(O,S)_{0.45}$, as the band gap increased from 3.207 to 3.227 eV when residence time was shortened from 157 to 94 ms. It was speculated that impurity atoms that were possibly embedded into the films with the shortest residence time reduced the optical band gap of the material.

High Pressure Spatial ALD

Industrially promising atmospheric SALD processing was tested by depositing ZnO, $Zn(O,S)_{0.45}$ and ZnS with the SCS 1000 in elevated pressures. Again, deposition in all process pressures was technically successful, but small precursor leaks outside the active coating area were observed. This was an indication of insufficient N_2 curtain flow, and higher inert gas flows would be required if the SCS 1000 would be operated in even higher process pressures.

The GPC of all materials rose from the GPC in the base pressure of 50 mbar when process pressure was elevated to 180 and 380 mbar. The GPC of ZnO and $Zn(O,S)_{0.45}$ reached their maxima in 180 mbar, while the GPC of ZnS was approximately the same in 180 and 380 mbar. The increase in GPC could be explained by elevated precursor partial pressure under the coating head which increased the rate at which precursor molecules collided with the substrate, leading to higher reactivity. The drop in the GPC of ZnO and $Zn(O,S)_{0.45}$ at 380 mbar was possibly caused by an excess of inert molecules and reaction by-products, which hindered the movement of precursor molecules. The validity of this theory could be studied by installing a mass spectrometer into the exhaust channel to study which molecules in which concentrations are ejected into the exhaust. Studying the reaction products would also enable the accurate tuning and optimization of the precursor dose.

Uniformity of the deposited films did not follow a distinct trend. ZnO films were most uniform when deposited in 180 mbar but $Zn(O,S)_{0.45}$ and ZnS films were the most uniform in 50 mbar. Thus, it was deduced that the optimal balance of process flows is unique for each process, and this equilibrium is influenced by the precursor reactivity, process flow rate and the pumping speed.

The mechanisms that affected the growth rate of the deposited films were also speculated to affect their density, as was indicated by the changes of the refractive indices of ZnO, $Zn(O,S)_{0.45}$ and ZnS. The refractive index of ZnO dropped sligthly and systemicatically when process pressure was increased, while the drop in the refractive index of $Zn(O,S)_{0.45}$ was much more pronounced. The hindrance of the precursor molecules by the reaction by-products might have led to a lower density in the films, despite the higher precursor pressure. The refractive index of ZnS, on

the other hand, slightly increased reaching its maximum at a pressure of 180 mbar, which was considered an indication of increased density. Again, measurements with XRR would be needed to confirm these hypotheses of film densities.

E_g of ZnO slightly decreased with increasing process pressure. This observation indicated that processing in lower pressures was more optimal for ZnO with the employed process parameters, and that the elemental composition might have slightly changed with the increasing pressure. The changes in the band gap were, however, only in the order of 0.04 eV, so measurement accuracy could also explain these deviations. The band gap of $Zn(O,S)_{0.45}$, on the other hand, increased from 3.207 to 3.307 eV when pressure was increased from 50 to 380 mbar. This change in band gap was significant, and it correlated with the sulfur content in the oxysulfide film. Changes in the sulfur content as a function of process pressure were in the same order as with decreasing residence time, but significant changes in the band gap were observed only as a function of the process pressure. Therefore, it was deduced that sulfur content was not the only property which affected the optical band gap of the film, but that also impurity atoms might play a major role in determining the absorption properties of the deposited films. Again, more accurate measurements concerning the elemental composition and optical properties of the films would be required to confirm this conclusion.

Process Development Prospects

ZnO, $Zn(O,S)_x$ and ZnS were deposited successfully in all process conditions using the SCS 1000 SALD tool. Based on the results of this thesis, the greatest challenges in the SALD process development are related to enhancing the uniformity and refractive index of $Zn(O,S)_x$. In industrial applications the non-uniformity of the deposited thin films should be as small as possible over a significantly larger area than studied in this thesis. Also, the sulfur content of the $Zn(O,S)_x$ thin films ought to be controlled within a wider range in order to achieve better industrial process tunability.

In the deposition of $Zn(O,S)_x$ H_2S was introduced into the reaction area from a separate precursor nozzle, and the sulfur content of the films was controlled by altering the concentration of H_2S in the carrier gas. This method of H_2S treatment proved to function quite well at the tested process temperatures. The S/Zn ratio ranged from 0.15 to 0.25 at all process temperatures, which meant that some control of the sulfur content was achieved. However, the optical band gaps of $Zn(O,S)_x$ varied only from 3.188 to 3.320 eV, which was a very narrow range compared to values reported in literature, from 2.6 to 3.6 eV [45]. Therefore, it was deduced that the sulfur content in the oxysulfide films was quite high with the employed deposition setup. This could have signified that the absolute S/Zn values obtained in the EDX measurements were inaccurate, but the observed trends in the evolution of sulfur content were still considered plausible. Therefore, more research is needed to confirm whether $Zn(O,S)_x$ films deposited with this nozzle setup could actually be applied, for example, as buffer layers on CIGS solar cells.

Also alternative methods for the H_2S introduction would need to be considered. If

a similar nozzle configuration would be employed in the industrial coating of Zn(O,S) films, lower concentrations of H_2S would be required, or the H_2S nozzle could be positioned in the middle of the coating head. This would change the cycling of H_2S pulses, as H_2S would be applied more often on the surface, but H_2S pulses would always be followed by H_2O and DEZ pulses. In the setup used H_2S was always applied at the start and the end of the SALD supercycle.

Another viable option for the H_2S injection would be the mixing and co-injection of H_2O and H_2S from the same precursor nozzle, which would reduce the coating head dimensions as no extra nozzles would be needed. This approach has been used by Illiberi *et al.* in the atmospheric SALD processing of various materials with promising results [96]. The sulfur content of the Zn(O,S) films could also be tuned by two-step laminate processing, which would consist of separate ZnO and $Zn(O,S)_x$ sweeps. This processing mode would be similar to the better-known pulsing ALD processing of Zn(O,S).

The deposition of ALD films with the SCS 1000 SALD tool was proved to be feasible, and the goals of the thesis were met. Process tests for deposition of other materials, such as Al_2O_3 and TiO_2, have already been conducted. Further research interests include testing ALD films deposited with the SCS 1000 as gas permeation barriers and depositing nanolaminate structures for optical applications. Worldwide, accelerated development of spatial ALD has only started, and the implementation of SALD in industrial scale is waiting for its realization. A revolution of ALD process technology might just be around the corner waiting to leap forward in huge steps.

References

[1] M. Leskelä and M. Ritala, *Angew. Chem. Int. Ed.*, 2003, **42**, 5548-5554

[2] J. Niinistö, K. Kukli, M. Heikkilä, M. Ritala and M. Leskelä, *Adv. Eng. Mater.*, 2009, **11**, 4, 223-234

[3] H. Kim, H.-B.-R. Lee and W.-J. Maeng, *Thin Solid Films*, 2009, **517**, 2563-2580

[4] T. Alasaarela: *Atomic layer deposited titanium dioxide in optical waveguiding applications*, Doctoral thesis, 2011, Aalto University, School of Electrical Engineering, Department of Micro- and Nanosciences, Espoo, Finland.

[5] T. Pilvi: *Atomic Layer Deposition for Optical Applications: Metal Fluoride Thin Films and Novel Devices*, Doctoral thesis, 2008, University of Helsinki, Faculty of Science, Department of Chemistry, Helsinki, Finland.

[6] M. Knez, K. Nielsch and L. Niinistö, *Adv. Mater.*, 2007, **19**, 3425-3438

[7] X. Meng, X.-Q. Yang and X. Sun, *Adv. Mater.*, 2012, **24**, 3589-3615

[8] C. Marichy, M. Bechelany and N. Pinna, *Adv. Mater.*, 2012, **24**, 1017-1032

[9] R. W. Johnson, A. Hultqvist and S. F. Bent, *Mater. Today*, **17**, 5, 236-246

[10] S. M. George, *Chem. Rev.*, **110**, 111-131

[11] P. Poodt, D. C. Cameron, E. Dickey, S. M. George, V. Kuznetsov, G. N. Parsons, F. Roozeboom, G. Sundaram and A. Vermeer, *J. Vac. Sci. Technol. A*, 2012, **30**, 010802

[12] D. Muños-Rojas and J. MacManus-Driscoll, *Mater. Horiz.*, 2014, **1**, 314

[13] R. L. Puurunen, *Chem. Vap. Deposition*, 2014, **20**, 1-13

[14] G. N. Parsons, J. W. Elam, S. M. George, S. Haukka, H. Jeon, W. M. M. Kessels, M. Leskelä, P. Poodt, M. Ritala and S. M. Rossnagel, *J. Vac. Sci. Technol. A*, 2013, **31**, 050818

[15] R. L. Puurunen, *J. Appl. Phys.*, 2005, **97**,121301-121301-52

[16] T. S. Suntola, J. Antson, U.S. Patent No. 4,058,430, 15.11.1977

[17] V. Miikkulainen, M. Leskelä, M. Ritala and R. L. Puurunen, *J. Appl. Phys.*, **113**, 021301-1

[18] T. S. Suntola, A. J. Pakkala and S. G. Lindfors, U.S. Patent No. 4,413,022, 28.6.1983

[19] P. Poodt, J. van Lieshout, A. Illiberi, R. Knaapen, F. Roozeboom and A. van Asten, *J. Vac. Sci. Technol. A*, 2013, **31**, 01A108

[20] A. Yamada, B. Sang, M. Konagai, *Appl. Surf. Sci.*, 1997, **112**, 216-222

[21] E. B. Yousfi, J. Fouache, D. Lincot, *Appl. Surf. Sci.*, 2000, **153**, 223-234

[22] P.-Y. Lin, J.-R. Gong, P.-C. Li, T.-Y. Lin, D.-Y. Lyu, D.-Y.- Lin, H.-J. Lin, T.-C. Li, K.-J. Chang and W.-J. Lin, *J. Cryst. Growth*, 2008, **310**, 3024-3028

[23] S. J. Lim, S. Kwon and H. Kim, *Thin Solid Films*, 2008, **516**, 1523-1528

[24] K. Kopalko, M. Godlewski, J. Z. Domagala, E. Lusakowska, R. Minikayev, W. Paszkowicz and A. Szczerbakow, *Chem. Mater.*, 2004, **16**, 1447-1450

[25] M. Godlewski, E. Guziewicz, G. Luka, T. Krajewski, M. Lukasiewicz, L. Wachnicki, A. Wachnicka, K. Kopalko, A. Sarem and B. Dalati, *Thin Solid Films*, 2009, **518**, 1145-1148

[26] T. Tynell and M. Karppinen, *Semicond. Sci. Technol.*, 2014, **29**, 043001

[27] D. Saha, A. K. Das, R. S. Ajimsha, P. Misra and L. M. Kukreja, *J. Appl. Phys.*, 2013, **114**, 043703

[28] E. Guziewicz, M. Godlewski, T. Krajewski, L. Wahnicki, A. Szczepani, K. Kopalko, A. Wojcik-Glodowska, E. Przezdziecka, W. Paszkowicz, E. Lusakowska, P. Kruszewski, N. Huby, G. Tallarida and S. Ferrari, *J. Appl. Phys*, 2009, **105**, 122413

[29] J.-Y. Hwang, S. Y. Park, J.-H. Park, J.-N. Kim, S. M. Koo and C. H. Ko, *Thin Solid Films*, 2012, **520**, 1832-1836

[30] L. Wahnicki, T. Krajewski, G. Luka, B. Witkowski, B. Kowalski, K. Kopalko, J. Z. Domagala, M. Guziewicz, M. Godlewski and E. Guziewicz, *Thin Solid Films*, 2010, **518**, 4556-4559

[31] H. Misano, A. Miyake, T. Yamada, N. Yamamoto, T. Yamamoto, *Thin Solid Films*, 2009, **517**, 3138-3142

[32] Y.-Y. Lin, C.-C. Hsu, M.-H. Tseng, J.-J. Shyue, F.-Y. Tsai, *ACS Appl. Mater. Interfaces*, 2015, **7**, 22610-22617

[33] T.-H. Jung, J.-S. Park, D.-H. Kim, Y. Jeong, S.-G. Park and J.-D. Kwon, *J. Vac. Sci. Technol. A*, 2013, **31**, 01A124

[34] J. T. Tanskanen, J. R. Bakke, T. A. Pakkanen and S. F. Bent, *J. Vac. Sci. Technol. A*, 2011, **29**, 3, 031507-1

[35] G. Stuyven, P. De Visschere, A. Hikavyy and K. Neyts, *J. Cryst. Growth*, 2002, **234**, 690-698

[36] Y. S. Kim and S. J. Yun, *Appl. Surf. Sci.*, 2004, **229**, 105-111

[37] J. T. Tanskanen, J. R. Bakke, S. F. Bent and T. A. Pakkanen, *Langmuir*, 2010, **26**, 14, 11899-11906

[38] J. R. Bakke, J. S. King, H. J. Jung, R. Sinclair and S. F. Bent, *Thin Solid Films*, 2010, **518**, 5400-540

[39] T. B. Nasr, N. Kamoun and C. Guasch, *Mater. Chem. Phys.*, 2005, **96**, 84-898

[40] B. W. Sanders and A. Kitai, *Chem. Mater.*, 1992, **4**, 1005-1011

[41] C. Persson, C. Platzer-Björkman, J. Malmström, T. Törndahl and M. Edoff, *Phys. Rev. Lett.*, 2006, **97**, 146403

[42] C. Platzer-Björkman, T. Törndahl, D. Abou-Ras, J. Malmström, J. Kessler and L. Stolt, *J. Appl. Phys.*, 2006, **100**, 044506

[43] J. R. Bakke, J. T. Tanskanen, C. Hägglund, T. A. Pakkanen and S. F. Bent, *J. Vac. Sci. Technol. A*, 2012, **30**, 01A135

[44] H. H. Park, R. Heasley and R. G. Gordon, *Appl. Phys. Lett.*, 2013, **102**, 132110

[45] T. Kobayashi and T. Nakada, *Sol. Energ. Mat. Sol. Cells*, 2013, **117**, 526-530

[46] T. Kobayashi, T. Kumazawa, Z. J. L. Kao and T. Nakada, *Sol. Energ. Mat. Sol. Cells*, 2013, **119**, 129-133

[47] T. Kobayashi, Z. J. L. Kao and T. Nakada, *Sol. Energ. Mat. Sol. Cells*, 2015, **143**, 159-167

[48] C. Bugot, N. Schneider, M. Jubault, D. Lincot and F. Donsanti, *J. Vac. Sci. Technol. A*, 2015, **33**, 01A151

[49] A. Illiberi, P. Poodt, P.-J. Bolt and F. Roozeboom, *Chem. Vap. Deposition*, 2014, **20**, 234-242

[50] Process Line Implementation for Appliced Surface Nanotechnologies (PLIANT), European Union project. Home page available: `http://www.pliant.eu/`. Accessed 24.5.2016.

[51] S. Franssila: *Introduction to Microfabrication*, 1st Edition, 2010, John Wiley and Sons, Ltd., the UK.

[52] E. Salmi: *Atomic Layer Deposited Coatings for Corrosion Protection of Metals*, Doctoral thesis, 2015, University of Helsinki, Faculty of Science, Department of Chemistry, Helsinki, Finland.

[53] H. Choi, S. Shin, H. Jeon, Y. Choi, J. Kim, S. Kim, S. C. Chung and K. Oh, *J. Vac. Sci. Technol. A*, 2016, **34**, 01A121

[54] N. P. Dasgupta, J. F. Mack, M. C. Langston, A. Bousetta and F. B. Prinz, *Rev. Sci. Instrum.*, 2010, **81**, 044102

[55] P. Poodt, A. Lankhorst, F. Roozeboom, K. Spee, D. Maas and A. Vermeer, *Adv. Mater.*, 2010, **22**, 3564-3567

[56] D. M. King, X. Liang and A. W. Weimer, *Powder Technol.*, 2012, **221**, 13-25

[57] T. Hirvikorpi: *Thin Al_2O_3 barrier coatings grown on bio-based packaging material by atomic layer deposition*, Doctoral thesis, 2011, VTT Technical Research Centre of Finland, Espoo, Finland.

[58] P. Maydannik: *Roll-to-roll atomic layer deposition process for flexible electronics applications*, Doctoral thesis, 2015, Lappeenranta University of Technology, Lappeenranta, Finland.

[59] T. Hirvikorpi, M. Vähä-Nissi, T. Mustonen, E. Iiskola and M. Karppinen, *Thin Solid Films*, 2010, **518**, 2654-2658

[60] T. Hirvikorpi, M. Vähä-Nissi, A. Harlin and M. Karppinen, *Thin Solid Films*, 2010, **518**, 5463-5466

[61] T. Hirvikorpi, M. Vähä-Nissi, J. Nikkola, A. Harlin and M. Karppinen, *Surf. Coat. Tech.*, 2011, **205**, 5088-5092

[62] T. O. Kääriäinen, P. Maydannik, D. C. Cameron, K. Lahtinen, P. Johansson and J. Kuusipalo, *Thin Solid Films*, 2011, **519**, 3146-3154

[63] K. Lahtinen, P. Maydannik, P. Johansson, T. Kääriäinen, D. C. Cameron and J. Kuusipalo, *Surf. Coat. Tech.*, 2011, **205**, 3916-3922

[64] P. S. Maydannik, T. O. Kääriäinen, K. Lahtinen, D. C. Cameron, M. Söderlund, P. Soininen, P. Johansson, J. Kuusipalo, L. Moro and X. Zeng, *J. Vac. Sci. Technol. A*, 2014, **32**, 051603

[65] E. K. Baumert and O. N. Pierron, *Appl. Phys. Lett.*, 2012, **101**, 251901

[66] J. G. Lee, H. G. Kim and S. S. Kim, *Thin Solid Films*, 2013, **534**, 515-519

[67] J. R. Bakke, K. L. Pickrahn, T. P. Brennan and S. F. Bent, *Nanoscale*, 2011, **3**, 3482

[68] S. Bordihn, P. Engelhart, V. Mertens, G. Kesser, D. Köhn, G. Dingemans, M. M. Mandoc, J. W. Müller and W. M. M. Kessels, *Energy Procedia*, 2011, **8**, 654-659

[69] G. Dingemans and W. M. M. Kessels, *ECS Transactions*, 2011, **41**, 2, 293-301

[70] H. Savin, P. Repo, G. von Gastrow, P. Ortega, E. Calle, M. Garin, R. Alcubilla, *Nature Nanotech.*, 2015, **10**, 624-629

[71] Lumineq® Electroluminescent Displays. Beneq Oy, website, available: `http://lumineq.com/en/technology`. Accessed 16.6.2016.

[72] nSilver® Anti-Tarnishing Coatings. Beneq Oy, marketing material brochure, available: `http://beneq.com/nsilver-anti-tarnish-coating.html`. Accessed 16.6.2016.

[73] T. Tynell: *Atomic Layer Deposition of Thermoelectric ZnO Thin Films*, Doctoral thesis, 2013, Aalto University, School of Chemical Technology, Department of Chemistry, Espoo, Finland

[74] A. Illiberi, F. Roozeboom and P. Poodt, *ACS Appl. Mater. Interfaces*, 2012, **4**, 268-272

[75] P. Banerjee, W.-J. Lee, K.-R. Bae, S. B. Lee and G. W. Rubloff, *J. Appl. Phys.*, 2010, **108**, 043504

[76] T. Dhakal, D. Vanhart, R. Christian, A. Nandur, A. Sharma and C. R. Westgate, *J. Vac. Sci. Technol. A*, 2012, **30**, 021202

[77] T. Tynell, H. Yamauchi, M. Karppinen, R. Okazaki and I. Terasaki, *J. Vac. Sci. Technol. A*, 2013, **31**, 01A109

[78] M. Ruoho, V. Pale, M. Erdmanis and I. Tittonen, *Appl. Phys. Lett.*, 2013, **103**, 203903

[79] A. Illiberi, R. Scherpenborg, F. Roozeboom and P. Poodt, *ECS J. Solid State Sci. Technol.*, 2014, **3**, 5, 111-114

[80] R. L. Z. Hoye, D. Muños-Rojas, S. F. Nelson, A. Illiberi, P. Poodt, F. Roozeboom and J. L. MacManus-Driscoll, *APL Mater.*, 2015, **3**, 040701

[81] A. Illiberi, R. Scherpenborg, M. Theelen, P. Poodt and F. Roozeboom, *J. Vac. Sci. Technol. A*, 2013, **31**, 061504

[82] A. Illiberi, R. Scherpenborg, Y. Wu, F. Roozeboom and P. Poodt, *ACS Appl. Mater. Interfaces*, 2013, **5**, 13124-13128

[83] D. Hariskos, S. Spiering and M. Powalla, *Thin Solid Films*, 2005, **480-481**, 99-109

[84] K. Orgassa, U. Rau, Q. Nguyen, H. W. Schock and J. H. Werner, *Prog. Photovolt: Res. Appl.*, 2002, **10**, 457-463

[85] S. Siebentritt, *Solar Energy*, 2004, **77**, 767-775

[86] Z.-H. Li, E.-S. Cho and S. J. Kwon, *Appl. Surf. Sci.*, 2014, **314**, 97-103

[87] P. Poodt, A. Illiberi and F. Roozeboom, *Thin Solid Films*, 2013, **532**, 22-25

[88] D. H. Levy, D. Freeman, S. F. Nelson, P. J. Cowdery-Corvan and L. M. Irving, *Appl. Phys. Lett.*, 2008, **92**, 192101

[89] D. H. Levy and S. F. Nelson, *J. Vac. Sci. Tech. A*, 2012, **30**, 018501

[90] S. F. Nelson, D. H. Levy, L. W. Tutt and M. Burberry, *J. Vac. Sci. Technol. A*, 2012, **30**, 01A154

[91] P. Poodt, R. Knaapen, A. Illiberi, F. Roozeboom and A. van Asten, *J. Vac. Sci. Technol. A*, 2012, **30**, 01A142

[92] A. Illiberi, F. Grob, C. Frijters, P. Poodt, R. Ramachandra, H. Winands, M. Simor and P. J. Bolt, *Prog. Photovolt: Res. Appl.*, 2013, **21**, 1559-1566

[93] S-M. Lee, E. Pippel, U. Gösele, C. Dresbach, Y. Qin, C. V. Chandran, T. Bräuniger, G. Hause and M. Knez, *Science*, 2009, **324**, 488-492

[94] K. E. Gregorczyk, D. F. Pickup, M. G. Sanz, I. A. Irakulis, C. Rogreo and M. Knez, *Chem. Mater.*, 2015, **27**, 181-188

[95] J. S. Jur and G. N. Parsons, *Am. Ceram. Soc. Bull.*, 2012, **91**, 6, 24-27

[96] A. Illiberi, C. Frijters, J. E. Balder, P. Poodt and F. Roozeboom, *ECS Transactions*, 2015, **69**, 7, 31-37

[97] A. Illiberi, B. Cobb, A. Sharma, T. Grehl, H. Brongersma, F. Roozeboom, G. Gelinck and P. Poodt, *ACS. Appl. Mater. Interfaces*, 2015, **7**, 3671-3675

[98] Lotus Applied Technology, Vortex Rotary Batch ALD Technology. White paper, available: `http://lotusat.com/rotary-ald/`. Accessed 15.6.2016.

[99] Applied Materials, Inc. Olympia Rotary ALD tool. Technical briefing, available: `http://www.appliedmaterials.com/products/olympia-ald`. Accessed 16.6.2016.

[100] P. S. Maydannik, T. O. Kääriäinen and D. C. Cameron, *Chem. Eng. J.*, 2011, **171**, 345-349

[101] P. S. Maydannik, T. O. Kääriäinen and D. C. Cameron, *J. Vac. Sci. Technol. A*, 2012, **30**, 01A122

[102] Beneq Oy, WCS 600 R2R SALD reactor. Online marketing material, available: `http://beneq.com/wcs-600.html`. Accessed 15.6.2016.

[103] K. Ali, K.-H. Choi, J. Jo and Y. W. Lee, *Mater. Lett.*, 2014, **136**, 90-94

[104] B. Vermang, A. Rothschild, A. Racz, J. John, J. Poortmans, R. Mertens, P. Poodt, V. Tiba and F. Roozeboom, *Prog. Photovolt: Res. Appl.*, 2011, **19**, 733-739

[105] E. H. A. Granneman, V. I. Kuznetsov and P. Vermont, invited conference paper, *225th ECS Meeting*, Orlando, USA, May 12-16, 2014.

[106] SoLayTec, SALD products. Online product portfolio, available: `http://www.solaytec.com/products`. Accessed 16.6.2016.

[107] P. Poodt, V. Tiba, F. Werner, J. Schmidt, A. Vermeer and F. Roozeboom, *J. Electrochem. Soc.*, 2011, **158**, 9, H937-H940

[108] H. Kumagai, Y. Masuda, T. Shinagawa, *IOP Conf. Series: Materials Science and Engineering*, 2011, **24**, 012022

[109] J. W. Elam, D. Routkevich, P. P. Mardilovich and S. M. George, *Chem. Mater.*, 2003, **15**, 3507-3517

[110] H. Fujiwara: *Spectroscopic Ellipsometry: Principles and Applications*, 2003, John Wiley & Sons Ltd., the UK.

[111] R. P. Feynman, R. B. Leighton, M. L. Sands: *The Feynman Lectures on Physics*, Volume 2, Chapter 33. ©1963, 2006, 2010 by M. A. Gottlieb and R. Pfeiffer, California Institute of Technology, USA.

[112] R. P. Feynman, R. B. Leighton, M. L. Sands: *The Feynman Lectures on Physics*, Volume 1, Chapter 31. ©1963, 2006, 2010 by M. A. Gottlieb and R. Pfeiffer, California Institute of Technology, USA.

[113] M. Born and E. Wolf: *Principles of Optics*, 6th Edition, 1980, Pergamon, New York, USA.

[114] Y. Hishikawa, N. Nakamura, S. Tsuda, S. Nakano, Y. Kishi and Y. Kuwano, *Jpn. J. Appl. Phys.* , 1991, **30**, 1008-1014

[115] G. H. Michler: *Electron Microscopy of Polymers*, 2008, Springer, Germany.

[116] L. C. Sawyer, D. T. Grubb, G. F. Meyers: *Polymer Microscopy*, 3rd Edition, 2008, Springer, Germany.

[117] S. M. A. Durrani, A. M. Al-Shukri, A. Iob and E. E. Khawaja, *Thin Solid Films*, 2000, **379**, 199-202

[118] B. E. Warner: *X-Ray Diffraction*, 2nd Edition, 1990, Dover Publications, Inc., New York, USA.

A Transmittance and Reflectance Spectra

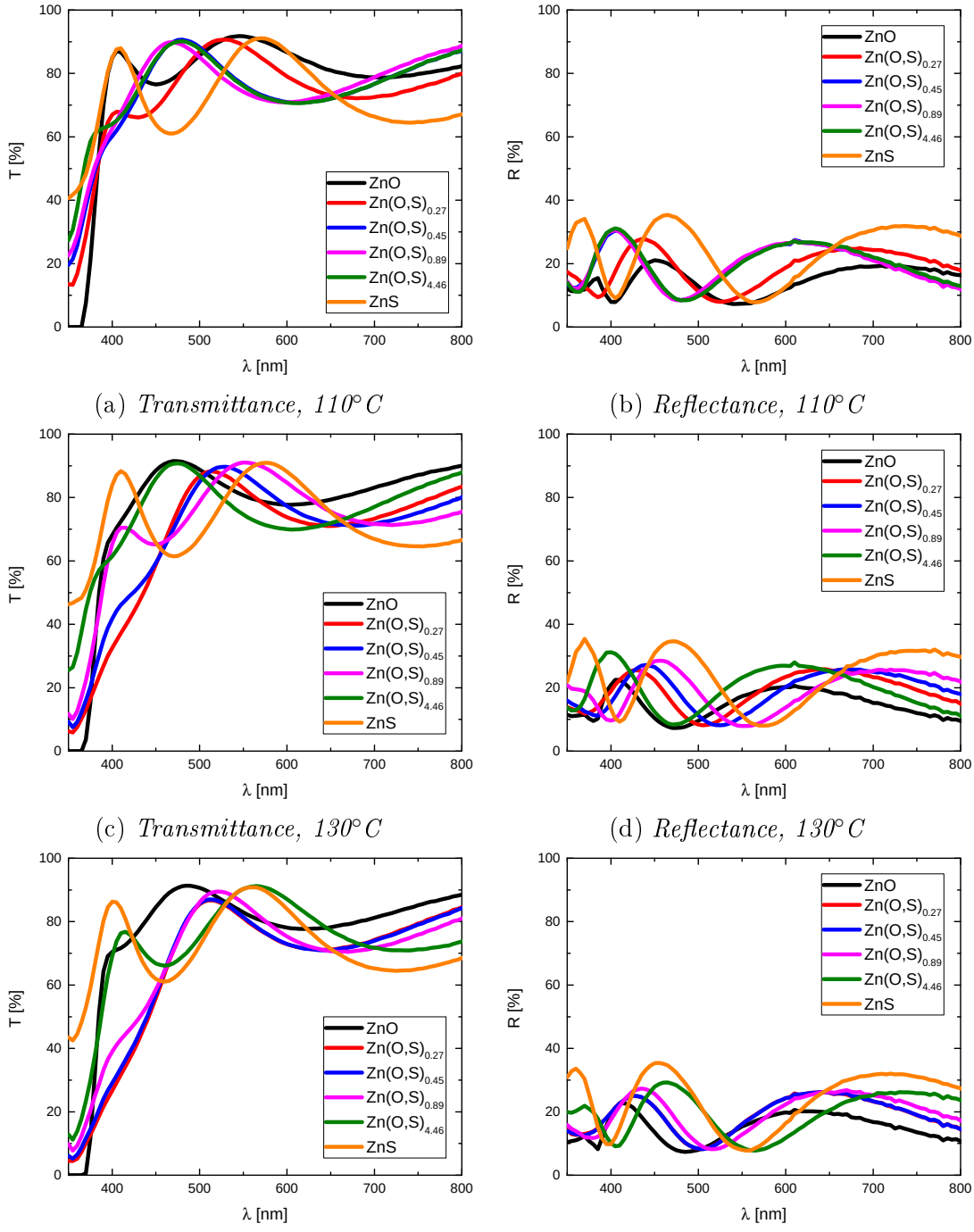

(a) *Transmittance, 110° C* (b) *Reflectance, 110° C*

(c) *Transmittance, 130° C* (d) *Reflectance, 130° C*

(e) *Transmittance, 150° C* (f) *Reflectance, 150° C*

Figure A1: *T(λ) and R(λ) spectra of the films deposited at the studied process temperatures.*

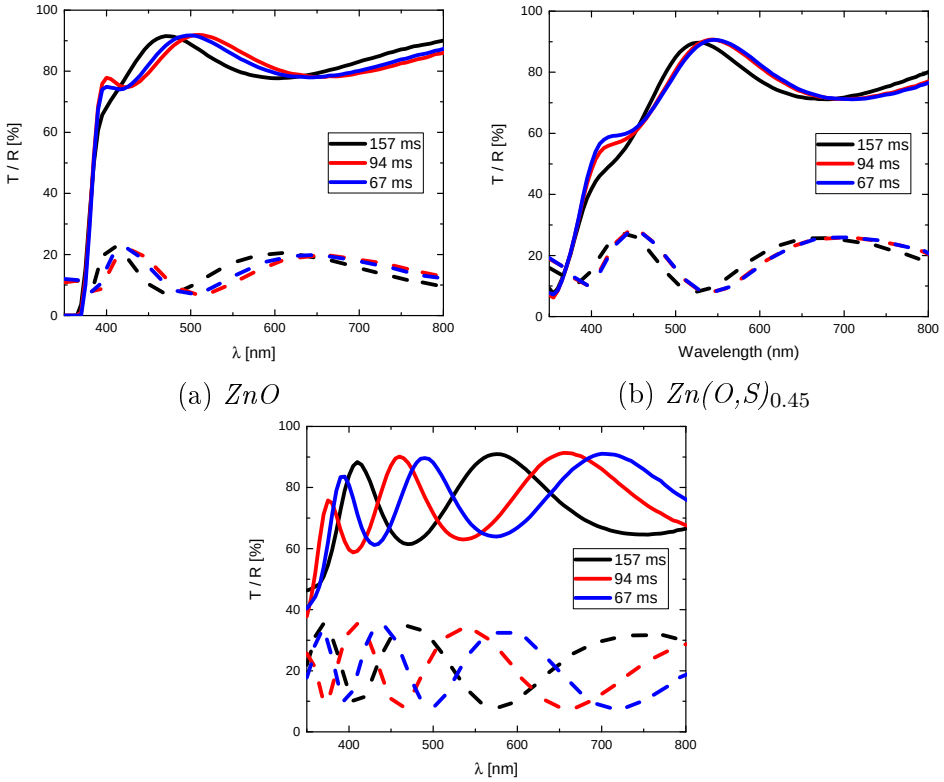

(a) *ZnO* (b) $Zn(O,S)_{0.45}$

(c) *ZnS*

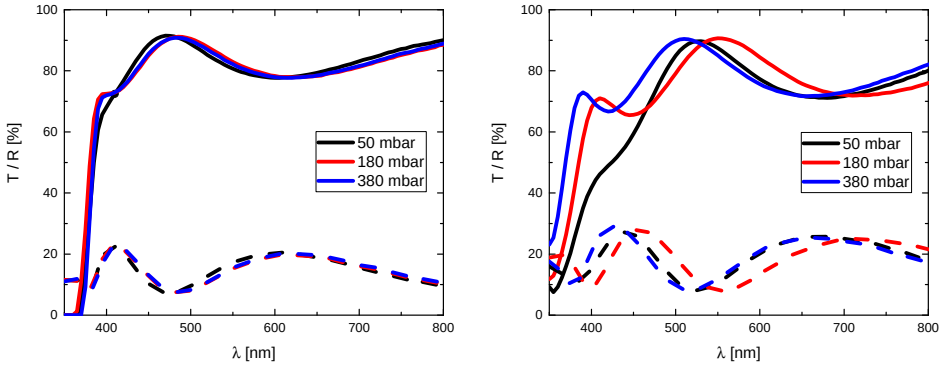

(d) *ZnO* (e) $Zn(O,S)_{0.45}$

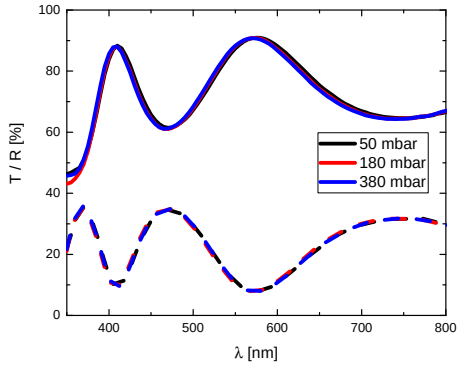

(f) *ZnS*

Figure A2: *T(λ) and R(λ) spectra of the films deposited with the studied residence times and process pressures. T(λ) spectra are presented by solid lines, R(λ) spectra with dashed lines.*

B Tauc Plots

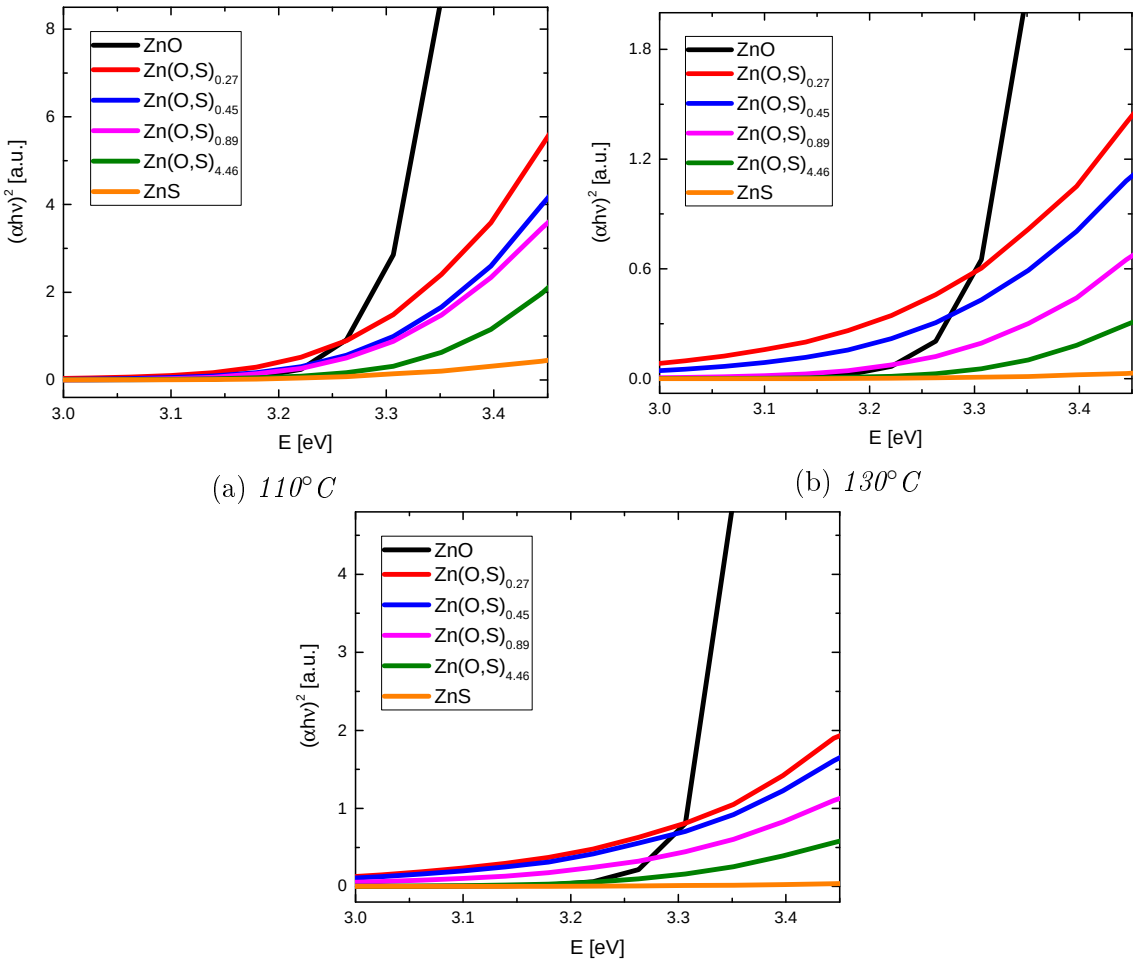

(a) *110° C* (b) *130° C*

(c) *150° C*

Figure B1: *Tauc plots of all materials deposited at the studied process temperatures.*

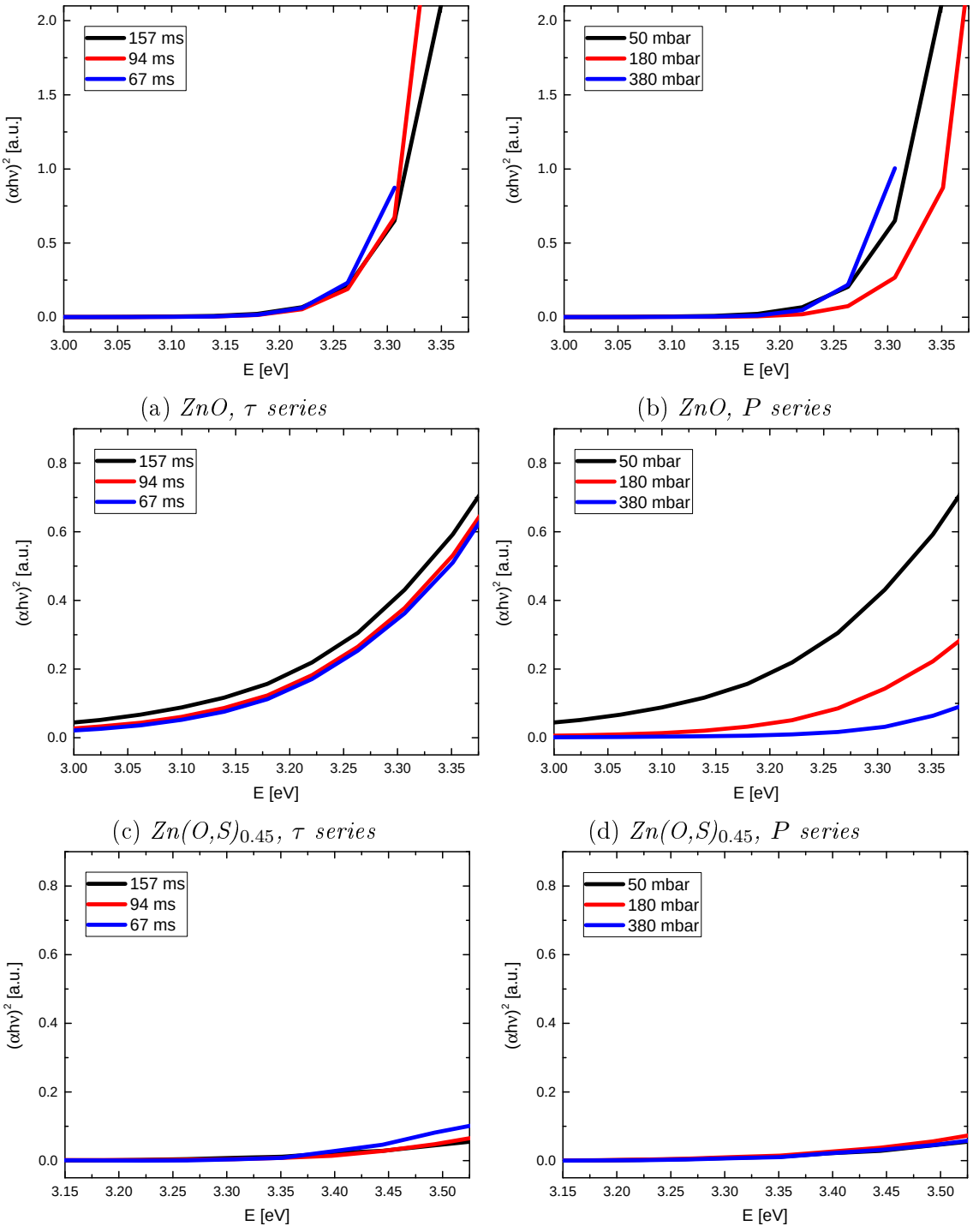

(a) *ZnO, τ series*

(b) *ZnO, P series*

(c) $Zn(O,S)_{0.45}$, *τ series*

(d) $Zn(O,S)_{0.45}$, *P series*

(e) *ZnS, τ series*

(f) *ZnS, P series*

Figure B2: *Tauc plots of all materials deposited with the studied residence times and process pressures.*

C EDX Data

In this appendix the EDX data is presented. The molar ratios in % given by the EDX measurement software are shown in Table C1 and the original EDX spectra are presented in Figures C1, C2, C3, C4, and C5. The EDX spectra were recorded with a 15 kV acceleration voltage, and the data collection time was 4 minutes.

Table C1: *Molar percentages [%] for different elements for all experimental series obtained from EDX data.*

	ZnO				$Zn(O,S)_{0.27}$				$Zn(O,S)_{0.45}$			
T [°C]	C	O	S	Zn	C	O	S	Zn	C	O	S	Zn
110	0.6	15.1	0.0	84.3	0.0	10.1	14.2	75.7	0.0	11.6	13.3	75.0
130	0.0	19.4	0.9	79.7	0.0	10.8	11.6	77.6	0.0	13.3	11.1	75.6
150	0.0	17.5	0.0	82.5	0.0	9.4	9.5	81.1	0.0	10.2	10.2	78.1

	$Zn(O,S)_{0.89}$				$Zn(O,S)_{4.46}$				ZnS			
T [°C]	C	O	S	Zn	C	O	S	Zn	C	O	S	Zn
110	0.0	13.5	14.1	72.4	0.0	9.2	16.6	74.2	0.0	0.0	23.7	76.3
130	0.0	5.1	13.6	81.3	0.0	10.3	16.0	73.7	0.0	0.0	24.9	75.1
150	0.0	12.1	12.3	75.6	0.0	7.8	18.2	74.0	1.6	3.1	25.0	70.3

	ZnO				$Zn(O,S)_{0.45}$				ZnS			
τ [ms]	C	O	S	Zn	C	O	S	Zn	C	O	S	Zn
157	0.0	19.4	0.9	79.7	0.0	13.3	11.1	75.6	0.0	0.0	24.9	75.1
94	0.0	15.1	0.4	84.5	0.0	10.7	12.9	76.4	0.0	0.0	25.1	74.9
67	0.0	14.1	0.0	85.9	0.0	9.4	14.6	76.0	0.0	0.0	24.4	75.7

	ZnO				$Zn(O,S)_{0.45}$				ZnS			
P [mbar]	C	O	S	Zn	C	O	S	Zn	C	O	S	Zn
50	0.0	19.4	0.9	79.7	0.0	13.3	11.1	75.6	0.0	0.0	24.9	75.1
180	0.0	15.2	0.3	84.5	0.0	4.4	14.5	75.0	0.0	0.0	25.0	75.0
380	0.0	18.0	0.0	82.0	0.0	14.1	13.6	73.4	0.0	1.1	25.4	73.4

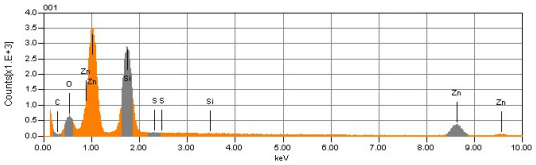

(a) ZnO

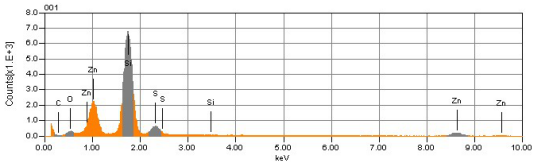

(b) $Zn(O,S)_{0.27}$

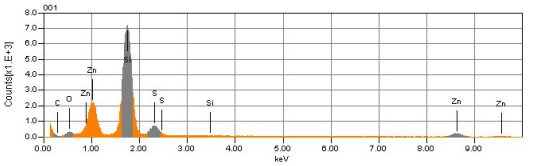

(c) $Zn(O,S)_{0.45}$

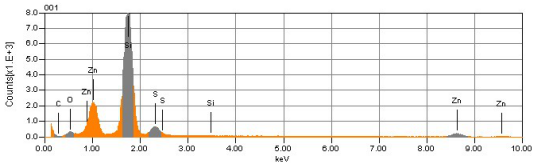

(d) $Zn(O,S)_{0.89}$

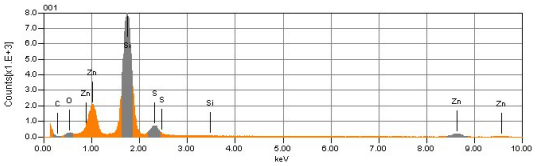

(e) $Zn(O,S)_{4.46}$

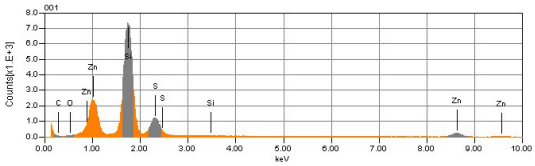

(f) ZnS

Figure C1: *EDX graphs of samples deposited at 110°C.*

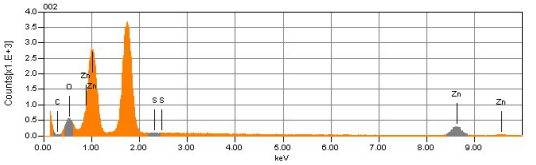

(a) ZnO

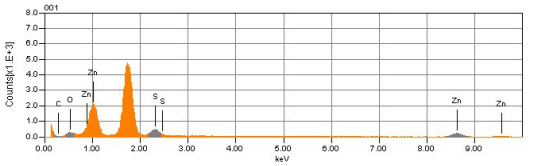

(b) $Zn(O,S)_{0.27}$

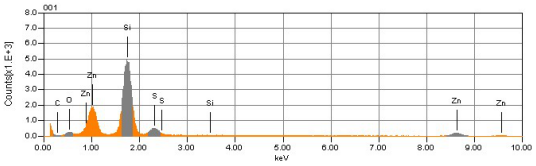

(c) $Zn(O,S)_{0.45}$

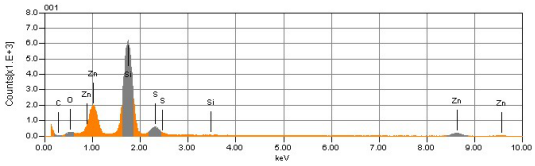

(d) $Zn(O,S)_{0.89}$

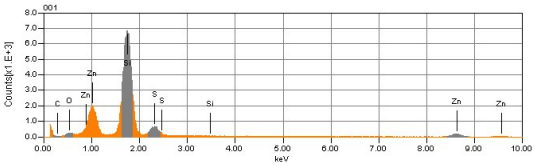

(e) $Zn(O,S)_{4.46}$

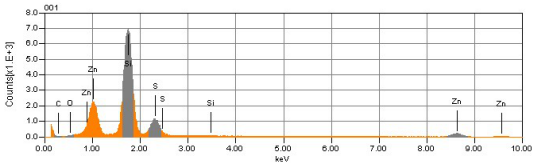

(f) ZnS

Figure C2: *EDX graphs of samples deposited at 130°C.*

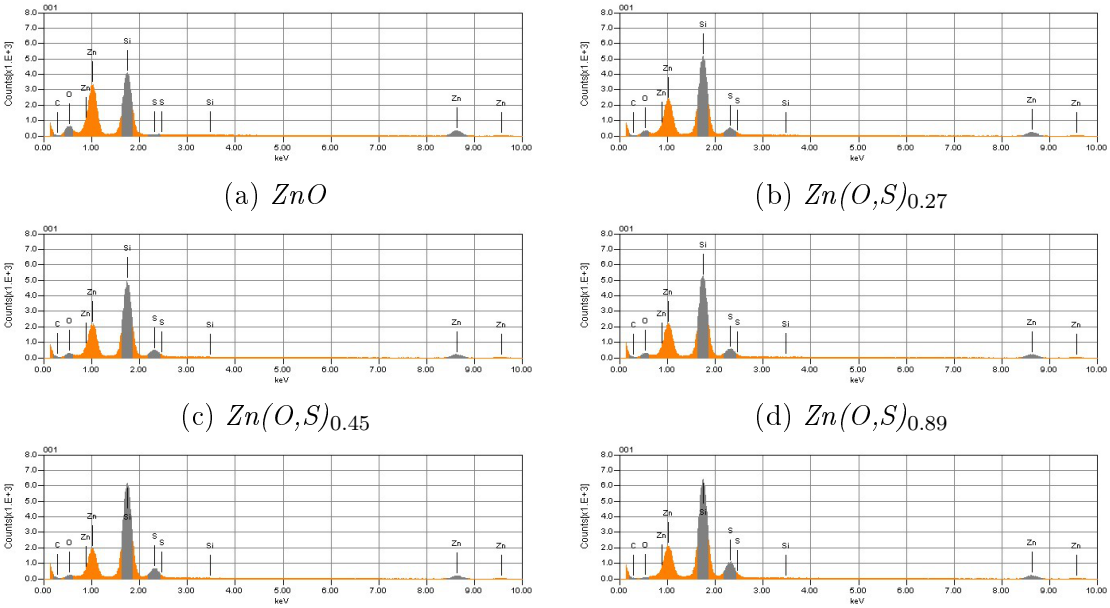

(a) *ZnO* (b) $Zn(O,S)_{0.27}$

(c) $Zn(O,S)_{0.45}$ (d) $Zn(O,S)_{0.89}$

(e) $Zn(O,S)_{4.46}$ (f) *ZnS*

Figure C3: *EDX graphs of samples deposited at 150°C.*

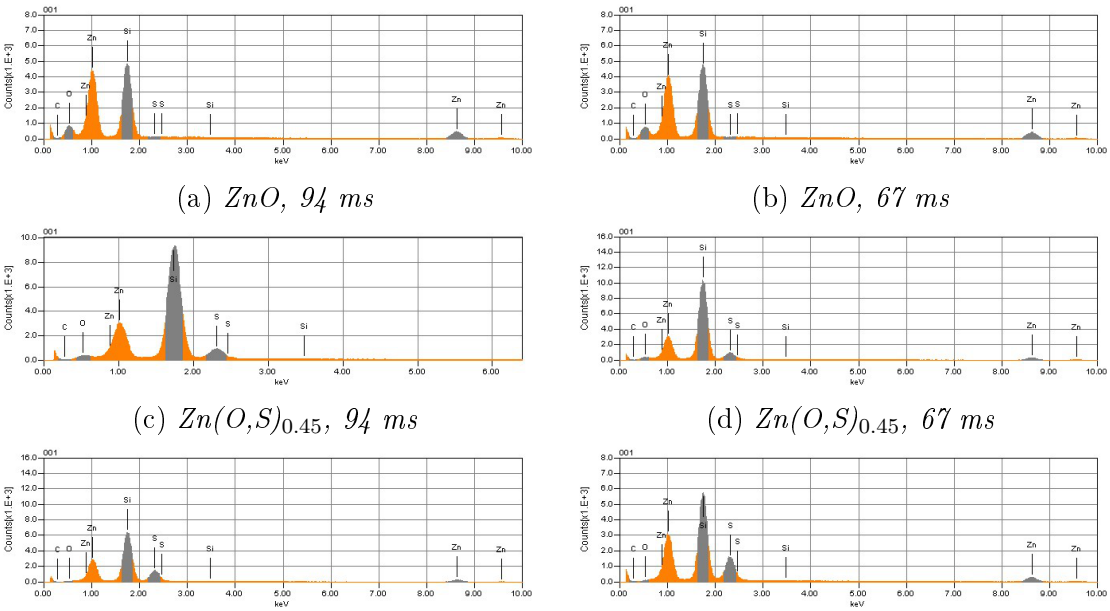

(a) *ZnO, 94 ms* (b) *ZnO, 67 ms*

(c) $Zn(O,S)_{0.45}$, *94 ms* (d) $Zn(O,S)_{0.45}$, *67 ms*

(e) *ZnS, 94 ms* (f) *ZnS, 67 ms*

Figure C4: *EDX graphs of samples deposited with decreasing* τ.

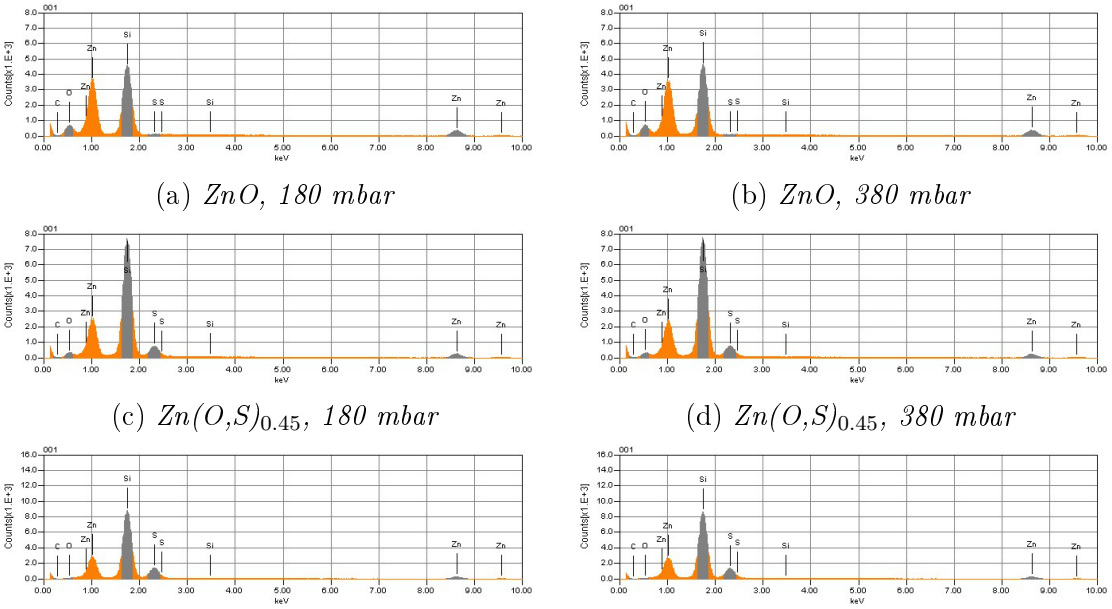

(a) *ZnO, 180 mbar*

(b) *ZnO, 380 mbar*

(c) *Zn(O,S)*$_{0.45}$*, 180 mbar*

(d) *Zn(O,S)*$_{0.45}$*, 380 mbar*

(e) *ZnS, 180 mbar*

(f) *ZnS, 380 mbar*

Figure C5: *EDX graphs of samples deposited in increasing P.*

D Preliminary XRD Analysis

ZnO and ZnS films were confirmed to be slightly crystalline by X-Ray Diffraction (XRD) analysis [118] performed with 2θ-ω scans using equipment at Aalto University Micronova. The angles of the scanning procedure are presented in Figure D1a. Using XRD to quantify the changes in the structure of the films was unfeasible, as the ZnO and ZnS peaks in the diffraction spectra obtained (Figures D1b and D1c) were barely distinguishable from background noise. It was observed that the deposited ZnO and ZnS thin films exhibited crystalline forms, but with such low deposition temperatures the crystalline structure was difficult to study with the XRD setup used. The positions of the peaks were in line with values reported in literature for ALD-grown films: for ZnO the peak at $2\theta = 33.1°$ corresponded probably to a hexagonal (1 0 0) structure [29, 77] and for ZnS the peak at $2\theta = 28.5°$ to a cubic (1 1 1) structure [34]. Further analysis of the crystallinity of thin films deposited with SALD with more accurate XRD analysis equipment would be justified.

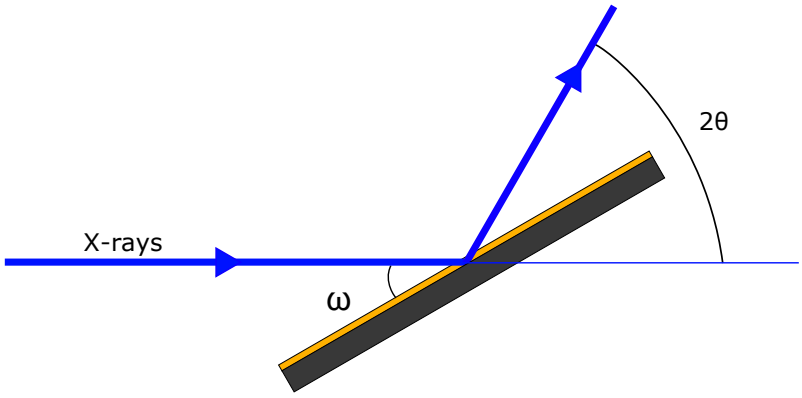

(a) *Angles in the XRD measurement.*

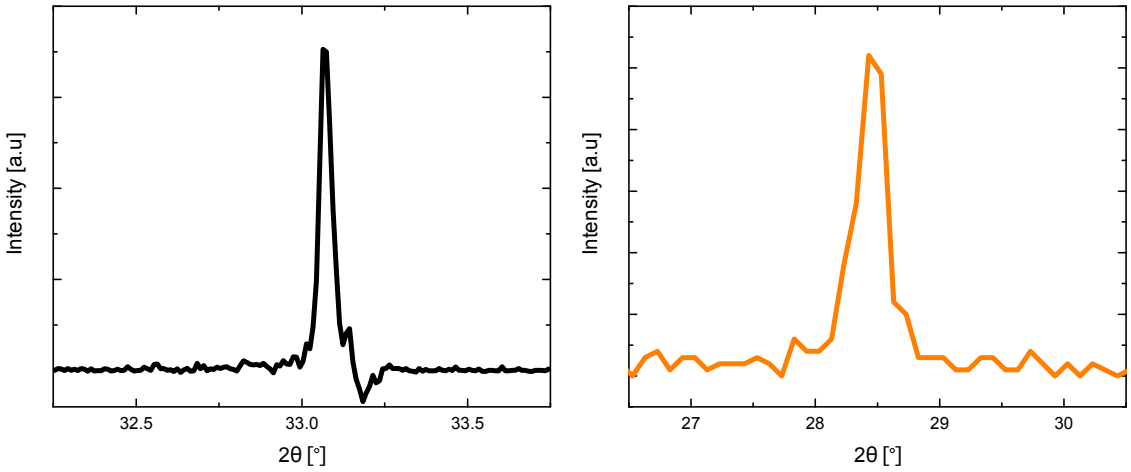

(b) *ZnO* (c) *ZnS*

Figure D1: *(a) Schematic of the angles in the XRD setup. XRD graphs measured from (b) ZnO and (c) ZnS deposited on Si wafers at 130°C.*